A NOVEL DESIGN TESTING THE EFFECTS OF STATIC AND DYNAMIC EQUIBIAXIAL STRETCH GRADIENTS ON FIBROBLAST CELL MIGRATION

A Thesis

by

SHIVA ANGELA YAZDANI-BEIOKY

Submitted to the Office of Graduate Studies of
Texas A&M University
in partial fulfillment of the requirements for the degree of

MASTER OF SCIENCE

December 2010

Major Subject: Biomedical Engineering

A Novel Design Testing the Effects of Static and Dynamic Equibiaxial Stretch Gradients on Fibroblast Cell Migration

A NOVEL DESIGN TESTING THE EFFECTS OF STATIC AND DYNAMIC EQUIBIAXIAL STRETCH GRADIENTS ON FIBROBLAST CELL MIGRATION

A Thesis

by

SHIVA ANGELA YAZDANI-BEIOKY

Submitted to the Office of Graduate Studies of
Texas A&M University
in partial fulfillment of the requirements for the degree of

MASTER OF SCIENCE

Approved by:

Chair of Committee,	James E. Moore Jr.
Committee Members,	Emily Wilson
	Roland Kaunas
	Michael Moreno
Head of Department,	Gerard L. Cote

December 2010

Major Subject: Biomedical Engineering

ABSTRACT

A Novel Design Testing the Effects of Static and Dynamic Equibiaxial Stretch Gradients on Fibroblast Cell Migration. (December 2010)
Shiva Angela Yazdani-Beioky, B.S., Texas A&M University
Chair of Advisory Committee: Dr. James E. Moore Jr.

The study of mechanobiology and the cellular response to the mechanical environment plays a vital role in the understanding of the atherogenesis and the treatment of the disease state through interventions such as stent placement. Cell migration in response to complex stresses also plays a critical role in wound healing. Modeling the mechanical environment as a circular membrane with a center defect can be an accurate representation of in vivo stress gradients.

In this study, we created a novel cell stretching device that exposed cells to both static and 1 Hz dynamic stretch. Using NIH 3T3 fibroblasts stained with DiI membrane stain, we were able to expose cells to the two stretch regimes for 48 hours and observe the cellular response via live cell imaging. Cells were observed at 0, 12, 24, and 48 hour time points, and analysis of the change in their radial position was used to determine if cell migration occurred.

Cell displacement was calculated using both the kinematic equation and the NeoHookean constitutive model. Uncertainty of the cell displacement calculation was used in determining whether or not there was cell migration.

In this study, we were able to prescribe successfully the stretch regimes and observe the cellular response to stretch. Within the bounds of our uncertainty based on the error in the hole radius estimation and our measurement of cell and membrane displacement, however, we cannot say conclusively that cell migration occurred. This study established the methods and protocols necessary for further investigation into

mechanobiology, in particular, the cell response to stress environments that more closely resemble the in vivo conditions.

DEDICATION

To my loving husband Hormozd and my family who have been so patient and understanding through this long process

ACKNOWLEDGEMENTS

I would like to begin by thanking my husband, Hormozd Bozorgchami, who has been so patient and given me more love and support through this entire process than I ever could have dreamed. I would also like to acknowledge the love and support of my parents Bob and Carolyn Yazdani-Beioky, who have instilled confidence in me and taught by example the meaning of hard work. I would also like to thank my sister Andia and brother Kamran who have kept me in check with the knowledge that I am their role model.

I would, of course, like to thank my advisor, Jimmy Moore, who has given me so many opportunities and been such a great help through this entire process and along the way become a great friend. Thank you also to Mike Moreno for his help getting this project off the ground and his friendship and wisdom through so many life changes. I would also like to acknowledge Peggy Moore, who let me lean on her when I was at my weakest and helped me get the courage to come back and finish what I started.

Thank you also to my committee whose time and understanding are invaluable, especially Dr. Wilson for providing me with the fibroblast cells used in my experiments. I would also like to acknowledge my best friend Josh Meisner who has seen me through all phases of my higher education and been there for support, opinions, and questions. I would like to extend a special thanks to Ellie Rahbar who has been my right hand woman and shoulder to cry on in all things. And last, but certainly not least, thank you to my lab mates over the years, Luke Timmins who helped machine the cell stretching device, Will Richardson who picked up the project after I left and was instrumental in the final writing process, Julian Bedoya, Clark Meyer, and Joao Soares.

NOMENCLATURE

FAK	Focal Adhesion Kinase
FA	Focal Adhesion
EC	Endothelial Cell
SMC	Smooth Muscle Cell
ECM	Extracellular Matrix
α-SMA	Alpha Smooth Muscle Actin
3T3	NIH 3T3 Fibroblast Cell
PBS	Phosphate Buffered Saline
PDGF	Platelet-Derived Growth Factor
TGF-β	Transformin Growth Factor-Beta
t	Time
P^t	Cell Radial Position at time, t
r_{inner}	Deformed Inner Radius
R_{inner}	Undeformed Inner Radius
D	Cell Displacement without Membrane Displacement
M	Membrane Displacement
C	Cell Displacement Taking into Account Membrane Displacement
λ_z	Stretch in the z-Direction
c	Material Constant Used in NeoHookean Constitutive Equation

TABLE OF CONTENTS

Page

LIST OF FIGURES

FIGURE Page

FIGURE Page

1. INTRODUCTION

The study of mechanically active tissues has long been at the forefront of biomechanics, particularly with emphasis on mechanobiology. The cell response to its mechanical environment plays a crucial role in the tissue response to injury thereby influencing the success of a variety of medical procedures as well as the pathogenesis of atherosclerosis. Medical technology has made great strides in the development of minimally invasive surgical techniques as well as the treatment of heart disease through interventional procedures such as stent implantation; these methods, however, still induce changes in the mechanical environment. Such changes cause adverse reactions that lead to prolonged hospital stays and procedural failures that necessitate repeated intervention. Consideration of cellular responses to their mechanical environment is vital to the development of new technologies that can improve the outcome of many procedures.

1.1 Application of Mechanobiology

Procedures that cause minimal tissue damage can still initiate an inflammatory cellular response. Holes are introduced into tissues through a wide variety of procedures, which lead to changes in the solid mechanical stress environment. This mechanical environment can be modeled as a circular membrane with a center hole in which radial stress increases from the inner boundary of the membrane to the outer edge (David and Humphrey, 2004). Interventional procedures producing holes yield a traction free boundary condition, and it has been found that material behavior determines the stress environment as the size of the center hole changes (David and Humphrey 2004). In particular, it was shown that for isotropic membranes with a small center hole there is a discernible stress gradient that increases as the size of the hole decreases (David and Humphrey 2004). Cells must then actively adapt to these stresses, and as there is a move

---

This thesis follows the style of the Journal of Biomechanics.

toward more minimally invasive surgical techniques producing small puncture wounds within tissue optimization of these stress gradients becomes more important as it can lead to greater procedural success. For example, punch biopsy is a minimally invasive procedure used to diagnose conditions such as melanoma not only in the skin but also in the iris; oral cancer, and cervical cancer, as well as small fiber neuropathy and neuromuscular disorders.

A hole is punched through the skin or tissue to obtain a diagnostic specimen, leaving a void in the tissue thus altering the mechano-environment. Possible complications of this include infection and puncture damage to nearby tissue or organs. It has been noted that although the punch biopsy sample is taken in circular specimens, most wounds take on an elliptical shape due to the stress in the skin (Bush et al., 2007). The current technique for performing diagnostic punch biopsies requires that the physician stretch the skin to ease skin tension and allow for easier wound closure of the elliptically shaped wound (Zuber, 2002).

The structure and properties of scars are influenced by the mechanical state during wound healing because of how cell migration and protein regulation are affected by stress (Balestrini and Billiar, 2006). In addition to altering the mechanical field this procedure like many others initiates the wound healing process. There are three known phases of wound healing; the inflammatory, proliferative, and remodeling phase. The wound healing process is initiated by the inflammatory phase; phagocytes ingest necrotic tissue and protect tissue from risk of infection. During the proliferative phase, fibroblasts migrate into the wound and form granulation tissue, which is composed of blood vessels and a collagen matrix (DiPietro and Burns, 2003). During this time, fibroblasts convert to myofibroblasts, which contain **α** smooth muscle actin; myofibroblasts initiate wound contraction during the remodeling phase of the healing process (Clark, 1996; Hinz and Gabbiani, 2003).

Successful wound healing is determined by three critical factors: 1) the closing tension of the wound which has been shown to cause increased wound strength for wounds closed under tension, 2) tensile strength of the scar once it has completely

formed and 3) the overall healing time of the wound (Pickett et al., 1996). With current techniques, wound strength levels off at 70-90% of unwounded skin strength values and wound failure can occur when wound strength is not adequately restored (DiPietro and Burns, 2003). With cell mobility being a primary component of the wound healing process; promoting cell motility could improve postoperative wound contraction. The mechanisms of cell migration have been the focus of many studies in the field of mechanobiology.

In addition to having implications to wound healing, mechanobiology plays a significant role in atherogenesis and stent restenosis. Circumferential stress distribution in relatively straight arterial segments is approximately uniform because of the presence of residual stress(Chuong and Fung, 1986). More complex arterial anatomy however, has greater non-uniformity of stress distribution which can lead to pathogenic reactions. Also, increased pressure due to hypertension can create greater intimal stress at the inner wall than at the outer wall; this combined with strain stiffening material properties can lead to stronger stress gradients (Delfino et al., 1998). In the end, the cell reaction to these stress gradients leads to a greater understanding of atherosclerosis. Likewise, heart disease treatment modalities such as graft and stent placement also create strong changes in the stress environment. Stent placement within the vessel creates high tensile circumferential stress at the intimal surface (Bedoya et al.,2006). Cellular response to the increased stress leads to intimal hyperplasia and restenosis which can warrant further intervention.

1.2 Cellular Response to Mechanical Enviornment

Though not completely understood, it is known that cell migration occurs as a stepwise process in which there is actin polymerization of the cytoskeleton in the direction of migration, this leads to protrusion of the leading edge and formation of new adhesions at the front of the cell. Next, there is contraction of the cell that causes the release of adhesions at the rear of the cell and thus, cell movement. (Silver et al., 2003). The directional migration of cells in response to their mechanical environment is known as mechanotaxis as noted by Li et al. (2002), such migration is often the result of

changes in stress fields. One example is the reaction of endothelial cells to shear stresses. Cells under static conditions migrate randomly while those exposed to shear stress migrate in the directions of flow (Li et al., 2002). Endothelial cells exposed to shear stress showed preferential migration in the direction of flow as well as increased migration speed over those cells under static condition. Remodeling of the cell at the protein level preceded this change in directional migration, where first there was lamellipodial protrusion in the flow direction and then focal adhesion kinase (FAK) was recruited to focal adhesions (FAs) inducing the complete directional change of the cell. It was also determined that Rho activation is increased and this in turn leads to increased traction force generation which as previously stated is an integral part of the migration process. Cells not only react to changes in the fluid mechanical environment, but also to those in the solid mechanical environment. The migratory response of cells to cyclic equiaxial strain is dependent on the cell type, in that migration is enhanced in endothelial cells (ECs) and smooth muscle cells (SMCs), but inhibited in epithelial cells (Hinz and Gabbiani, 2003). Also, cyclic equiaxial strain does not induce the same cell alignment response that is found when cells are exposed to cyclic uniaxial strain. Fibroblasts and myofibroblasts cultured on microgrooved surfaces aligned and migrated in the direction of the microgrooves, however for grooves that are smaller, mechanical loading may be the determining factor of cell alignment (Loesberg et al., 2005). It has also been shown that cells migrate primarily in the direction of principal strain (Raeber, et al. 2007). Furthermore, myofibroblast migration speed was slower than that of fibroblasts (Thampatty and Wang, 2007).

Cell motility and morphology vary based on different substrate rigidities (Pelham and Wang, 1997). Cells respond to substrate rigidity by exerting contractile forces and then interpreting substrate deformation to determine preferred direction of movement (Pelham and Wang, 1997, Sheetz et al., 1998). Cell motility and tissue formation are influenced by rigidity of the substrate as cells probe the substrate as well as cell-cell interactions (Guo, et al., 2006, Lo, C-M. et al., 2000). Bischofs and Schwarz (2003) used a linear elastic model to demonstrate that fibroblast alignment at borders of stiffer

regions allows cells to build up forces more efficiently. Specifically, the phenomenon known as “durotaxis” occurs when cells migrate preferentially towards more rigid substrates and migrate away from soft substrates in low cell density cultures (Lo, C-M., et al., 2000). However, the study that first demonstrated a pronounced pattern of durotaxis was conducted on membranes that were not stretched statically or dynamically, illustrating that cell movement was due to active sensing of the passive unstressed membrane. This was shown using a method in which the rigidity of the substrate was purposely varied by altering the chemical formulation of the substrate mixture. The more rigid section of the substrate was embedded with fluorescent microbeads in order to identify which direction cells were migrating while using standard fluorescent microscopy. It is thought that cells migrate to stiffer regions to strengthen contacts and cytoskeletal structures in stiffer areas of the substrate. Durotaxis can also be explained by the idea that more rigid surfaces can lead to stronger cell-ECM connections that lead to stronger traction forces which in turn lead to migration toward the more rigid surface.

Ohashi, T., et al. (2007) found that cells develop stress fibers in response to non-uniform strain and development of these stress fibers eventually leads to a shift in the location of the cell nucleus. Ohashi, T., et al. (2007) produced a monotonically increasing strain gradient by embedding glass within a silicone elastomer and stretching the substrate. They were able to produce a 0.2%/μm strain gradient across each cell from the border region where the glass was embedded to the region of 50% strain where the substrate consisted of elastomer only. The lowest strain region, which is near the glass-elastomer border showed no signs of cellular elongation or orientation; cells within the region of high strain acted as predicted by aligning perpendicular to the direction of stretch. They also found that cells develop stress fibers in response to non-uniform strain; the fibers were particularly developed in regions of high strain. They found that strain dependent formation of stress fibers exists and leads to cell remodeling due to the strain gradient (Ohashi, T., et al., 2007). It has been shown that fibroblasts change their alignment by orienting perpendicular to the direction of strain (Grymes and Sawyer,

1997). Cells also tend to have more pronounced alignment if microgrooves in the substrate are perpendicular to stretch than if they are parallel to the direction of stretch. Loesberg, W.A., et al. (2005) show that mechanical loading plays a secondary role in fibroblast phenotype modulation while substrate topography is the primary influence.

The most common 3D matrices currently in use are collagen gels and fibrin gels. Both materials are capable of supporting a variety of cell types, though collagen matrices are mechanically weaker than fibrin matrices whose mechanical properties can be altered more than collagen matrices. Brown, et al. (1998) described how fibroblasts alter their contractile forces based on their mechanical loading conditions within collagen gels in order to maintain an optimal "tensional homeostasis". The term tensional homeostasis describes how cells create tension in their extracellular matrix (ECM) to oppose external loading. Fibroblasts facilitate tensional homeostasis by taking on a smooth muscle-like phenotype. Alpha smooth muscle actin (α-SMA) plays a significant role in fibroblast force generation. Differentiated α-SMA myofibroblasts apply higher contractile forces on deformable silicone substrates than undifferentiated fibroblasts (Hinz and Gabbiani, 2003).

1.3 Current Techniques in Mechanobiology

Current techniques utilize various methods of testing cell response to stretch. Many of these methods are uniaxial or biaxial and do not allow for precise control of stretch and measurement of strain fields, and stretching regimes are uniform which is not relevant to in vivo situations. Various mechanical loading methods can have different spatial and temporal effects on cell motility. These techniques also use various substrates ranging from smooth cell seeded elastic membranes to microgrooved elastic membranes as well as 3D matrices such as collagen gels, double hydrogels, and PEG gels (Raeber et al., 2008, Beningo and Wang, 2007, Loesberg et al., 2005, Lo, C-M. et al., 2000). Cell migration studies have been conducted in both 2D and 3D. It is commonly believed that 3D models more accurately depict the in vivo environment; however the 2D environment has widely been used to model cell migration and in determining cell-ECM interactions. The primary requirements of any cell matrix,

whether 2D or 3D are that it provides a region for cell adhesion along with some structural integrity. It has been noted that cell morphology and the type of cell adhesions vary not only between 2D and 3D matrices, but also vary based on the structure and composition of 3D matrices. Cells alter their migration strategy depending on dimensionality by responding to differences in the extracellular matrix. This is evidenced by the fact that cell migration in 2D is adhesion dependent while cell migration in 3D is adhesion independent.

For both 2D and 3D studies the Flexcell (Flexcell International, Cary, NC) system is a method currently used to apply stresses to cells. In this system, a circular flexible-bottom cell culture device to which a vacuum is applied to deflect the bottom surface. The device applies a non-uniform stretch environment to cells; however the stretch is not controllable and non-uniformity is due to the geometry of the wells. The Flexcell system has not been used to study the effects of spatially varying physiologic strain on cells. The system has been adapted to produce more uniform strain fields (Vande Geest et al., 2004). Though understanding of the role of cellular mechanics and mechanobiology has increased with the advent of improved cell culture and imaging techniques, the precise manipulation of the mechanical environment remains an imperfect science, which if improved could lead to more in depth knowledge of cellular response to mechanical stresses and matrix rigidity.

Studies have shown that cells respond to their mechanical environment in a variety of ways including cell migration. Alterations to the mechanical environment introduced by procedures and interventions often leave wounds that result in stress gradients. These stress gradients can be modeled as a circular membrane with either a center hole or fixation. It is thought that a center hole can represent a wound site and initiate the cellular response in wound healing. During the wound healing process fibroblasts migrate toward the wound in response to biochemical signals such as platelet derived growth factor (PDGF) and transforming growth factor-beta (TGF-β) (Martin, 1997) as well as mechanical signals.

To further examine the cell response to mechanical signals we believe that the stress gradients would be a mechanical cue that could stimulate migration toward the wound. A hole created at the center of the membrane results in high stress with a high gradient at the edge of the hole, and low stress with a low gradient at the outer edge of the membrane. I propose that fibroblasts will migrate in response to stress gradients, i.e. that mechanical cues stimulate fibroblasts to migrate toward wound sites.

In order to investigate stress gradient effects on fibroblasts, we will design and build a device that simulates the mechanical environment surrounding a wound. Fibroblasts will be cultured on a membrane and observed to determine if they migrate toward the mock wound. This study will use NIH 3T3 fibroblast cells because they are a widely accepted standard fibroblast cell line. A small stretch will be applied to the membrane, which will result in stress gradients that vary radially from the perforation. As an example, cells will be stretched statically to simulate simple perforations in skin. In order to simulate wounds in arteries or other cyclically loaded tissues, cells will be exposed to cyclic stretch. My hypothesis is that fibroblast cells migrate toward the center hole in response to stress gradients. If the cells migrate toward the hole (wound) then it will be evident that mechanical cues, specifically stress gradients, drive fibroblast migration toward wound sites. If the cells do not migrate towards the hole, then perhaps some additional biochemical cue is responsible for fibroblast behavior in wound healing.

2. METHODS

In order to observe the cellular response to a complex mechanical environment, cells were stained and then seeded onto a silicone membrane with a center hole. The membrane was stretched statically and dynamically and the presence of the center hole created a stretch gradient. We applied live cell imaging using fluorescence microscopy that allowed for the observation of the migratory response of cells over a 48 hour time period.

2.1 Cell Culture

An integral part of this project was the proper growth and maintenance of cells, in order to ensure that the cells were able to survive the stretching protocols to which they were exposed. The live cell imaging aspect of this project required that cells were properly stained and were robust enough to survive transfer from culture to experimentation. This was accomplished through proper sterile technique and previously established cell culture methods. Briefly, 3T3 fibroblasts were cultured in cell culture media consisting of Dulbecco's Modified Eagle's Medium (Gibco, Invitrogen, Carlsbad,CA) , 5% fetal bovine serum (Atlas Biologicals, Fort Collins,CO) and 1% antibiotic-antimycotic (Gibco, Invitrogen, Carlsbad,CA). Cells were grown to approximately 80% confluence in 75cm^2 cell culture flasks in humidified 37°C incubators with 5% CO_2. The cells were removed from culture flasks using 2 mL of trypsin-EDTA(Lonza, Basel, Switzerland) and neutralized in 4 mL trypsin neutralizing solution (Lonza, Basel, Switzerland), then centrifuged at 1500RPM and resuspended in growth medium.

Cells were stained using Vybrant CM-DiI cell labeling solution (Molecular Probes, Invitrogen, Carlsbad, CA). Cells were stained according to manufacturer's instructions for staining adherent cells. Adherent cells were stained as subconfluent monolayers in cell culture flasks. Serum free media (7mL) was mixed such that there was 5µL DiI for every 1mL media. Cells were incubated for 30 minutes to ensure uniform staining. Cells were then rinsed 3 times with growth serum and incubated for

10 minutes between each wash. DiI is a lipophilic membrane stain whose absorption and emission lines are at 549 and 565 nm, respectively.

One requirement was that once cells were cultured they have a stable substrate to which they could adhere and undergo stretch. In this case, preliminary 2D experiments were carried out with surface cell cultures on elastomeric membranes. Circular isotropic membranes were constructed from 0.02 inch non-reinforced vulcanized gloss/gloss 40D silicone sheeting that had a Young's Modulus E=375 psi, which was determined by the manufacturer [Specialty Manufacturing, Saginaw, MI]. Disks with a diameter of 7 cm were cut from the silicone sheeting; the center hole representative of the defect has a diameter of approximately 0.5 cm and was made using a dye punch. The membrane was autoclaved at 121°C for 1 hour to guarantee sterility and then treated with fibronectin to ensure cellular adhesion. The membranes were incubated with bovine fibronectin diluted in phosphate buffered saline (PBS) (Gibco, Invitrogen, Carlsbad, CA) to a concentration of 50μL/mL for a period of 1 hour. The membranes were then rinsed with PBS and incubated with culture media for 1 hour. Membranes were then seeded with stained cells in fresh culture media on a specially designed culturing device (Appendix A) that allowed the membrane to remain taut, but not stretch throughout the culture process and transfer to the stretch device. The device was partially disassembled and parts were rearranged for attachment to the stretching device for experimentation.

Low passage (P5-P9) NIH 3T3 fibroblasts were used for cell culture experiments. Cells were seeded at a density of approximately 20000 cells/cm^2 i.e. 1,000,000 cells total across the entire membrane, and then allowed to proliferate for at least 24 hours and no longer than 36 hours in order to form their own cell-matrix connections and cell to cell contacts.

2.2 Equibiaxial Cell Stretching Device

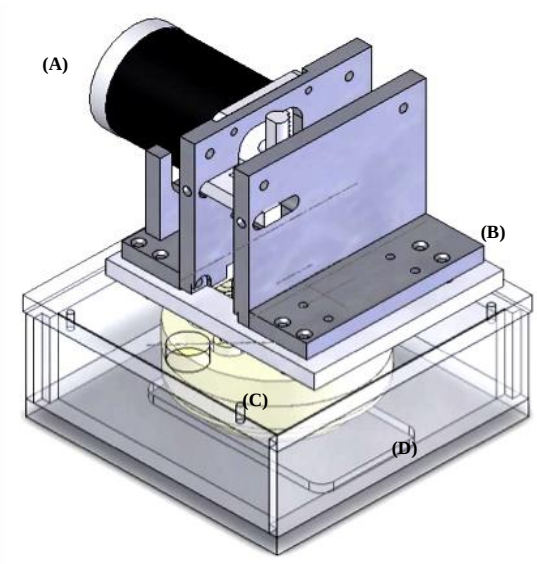

Fig. 1. Equibiaxial stretch device. a. Isometric view of equibiaxial stretch device (A) stepper motor attaches to (B) lid and controls (C) cell stretch contained within (D) box with viewing window on bottom for imaging via inverted microscopy.

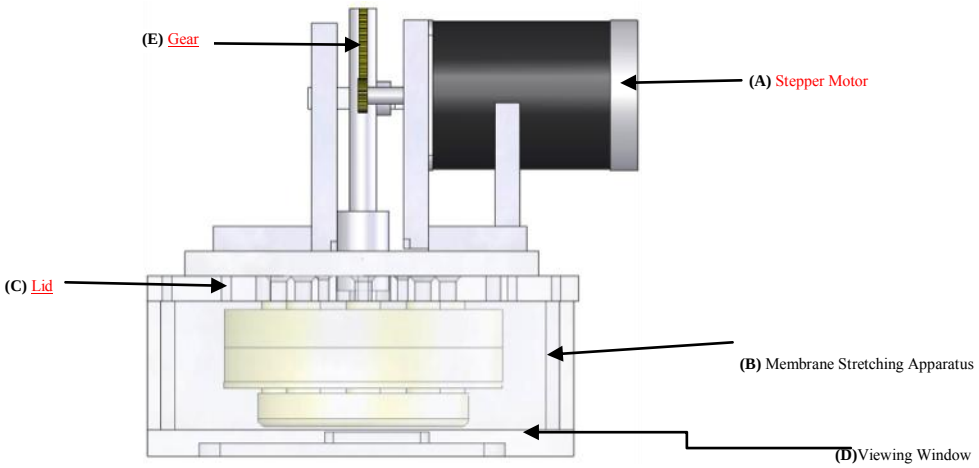

b. Side view of equibiaxial stretch device. Movement of (E) gear by stepper motor creates the equibiaxial stretch.

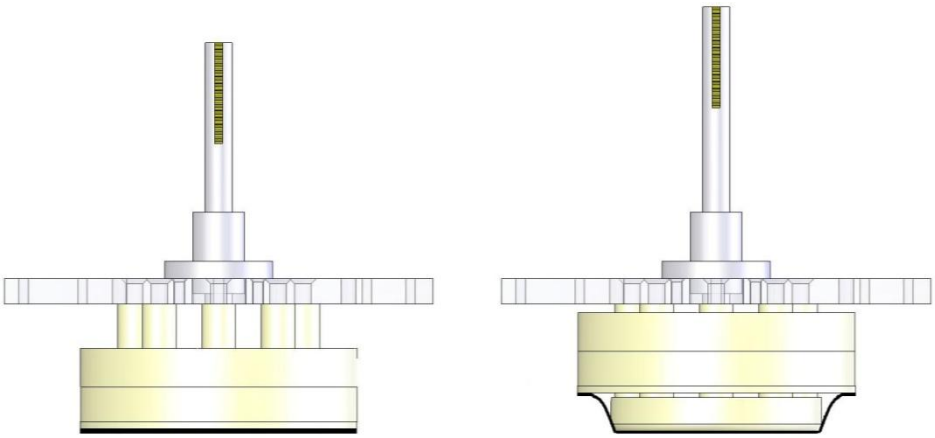

A) Relaxed Elastomer Membrane **B)** Stretched Elastomer Membrane

Fig 2. Side view of membrane in relaxed and stretched configuration. A) Elastomer membrane attached to the cell stretching mechanism on the left would maintain a relaxed conformation which is considered 0% stretch. B) Elastomer membrane attached to the cell stretching mechanism on the right would be stretched over the fixed center-piece by programming the device to apply a physiological stretch

The cell-stretching device was composed of a box containing growth media illustrated in isometric view in Figure 1a, and the actual stretching apparatus as shown in Figure 1b (Appendix A). The box was made of Lexan® with an abrasion resistant coating (Small Parts, Miramar, FL), and made water tight with non-toxic silicone aquarium sealant. The box was sterilized by soaking it in alcohol for 1 hr. then exposing to UV light for 1 hr. in a laminar flow hood. All parts associated with the stretching apparatus itself were fabricated from Delrin®, and all screws used in assembly were biocompatible 316 stainless steel (MSC Industrial Supply Company, Melville, NY), these were all sterilized by autoclaving for 1 hr. at 121°C . The cell stretching device was assembled in the laminar flow hood.

Stretch was controlled by a stepper motor and could be static in which the membrane maintained a constant 6% applied stretch or dynamic in which case the membrane was subjected to 6% applied stretch with a frequency of 1Hz. The stepper motor was programmed using SMC50-Win software (Anaheim Automation, Anaheim, CA). The acquisition program controlled the rack and pinion configuration which in turn creates the vertical movement of the membrane over a Delrin® disk. This creates a

prescribed equibiaxial stretch of the membrane as illustrated in side view in Figure 2. The code within the software was such that static stretch could be created by running the loop once or running it continuously for cyclic stretch. The motor motion was measured and it was found that 80 steps of the motor were equivalent to 1 mm in vertical movement of the gear and thus 1 mm of upward motion of the membrane over the fixed Delrin® disk.

The cells were imaged at a slight stretch of 3 mm, which was called viewing stretch, this was to ensure there was no slack in the membrane and the cells were all in the same viewing plane while being imaged. The box was also designed in such a way that the imaging plane could be adjusted by turning screws in the four corners of the lid to adjust the distance between the membrane and the coverslip. These screws were also adjusted to act as a safeguard against cells damage caused by the membrane pressing against the bottom of the box during stretching. The viewing window was composed of a rectangular microscope cover glass with dimensions 50x24 mm and the thickness between 0.15 and 0.19 mm. However, the actual region of interest that could be viewed was had dimensions 27.3x8.68mm , which includes the edge of the center hole moving out radially toward the outer edge of the membrane as shown in Figure 3.

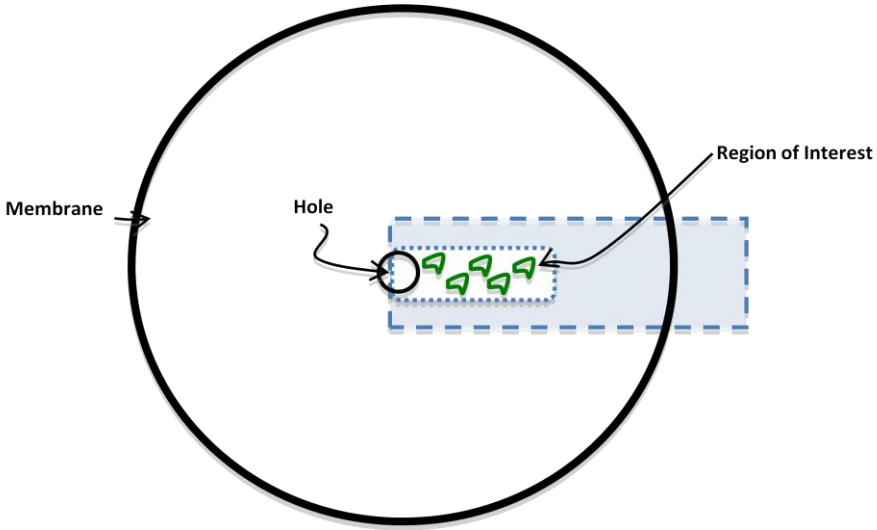

Fig. 3. Illustration of membrane and region of interest. Cells contained within the region of interest were imaged at each time point and radial displacement was calculated with respect to the center of the hole.

Cells were imaged at the 0 hour time point which is prior to stretch, and then 12, 24 and 48 hours after imposing stretch. The system was housed in a humidified, 5% CO_2, 37°C incubator during stretch. For each time point the box was moved to a zero position then the viewing stretch was imposed and cells were imaged. The box was placed at the same position on the stage for each imaging time point by being placed within the confines of two L-shaped pieces of Lexan®, which were attached to the stage. This adaptation allows for accurate live cell imaging with the box being at the same position for each set of images and the cells could be tracked by identifying their unique morphology from the membrane stain. Cells were adherent and identifiable beyond 48 hours, but for our purposes were only analyzed from 0 to 48 hours.

2.3 Microscopic Imaging

Cells were observed with a Nikon TE-2000 Inverted microscope equipped with confocal capability, a 543 nm HeNe laser, and a Nikon C-FL TRITC HYQ filter set (Nikon Instruments Inc., Melville, NY), which also included a motorized stage. The accompanying software, Metavue V6.2r4 by MetaMorph (Universal Immaging Corp., Downington, PA), had a stage memory feature. At each time point, the membrane was stretched to a viewing position to ensure that cells were in the correct viewing plane. To ensure consistency of the viewing plane the membrane was placed in the unstretched configuration and then moved to "viewing stretch" configuration. Though measures were taken to view cells at the same position each time, there was some error introduced as a result. This error was accounted for in our data analysis.

For each image the stage position was memorized and referenced to some origin that was set by the user and the same origin was used in all subsequent time points. Ten images of the edge of the center hole were captured and the origin was set. The stage was moved an arbitrary distance outward towards the edge of the membrane from the origin, and images of cell groups were captured and their stage locations memorized within the software for use at later time points. By setting the same origin at each time point, the stage position and the same grouping of cells could be easily located and imaged for each time point. The cells were imaged at 0, 12, 24, and 48 hour time points

at 40X magnification, and the same groupings were imaged by using the memorized stage positions to locate the cell groups and track their movement. The current image was aligned with the image at the previous time point and this stage position was saved along with image information in Metavue. The differences in stage position and uncertainties associated with membrane deformation are taken into account during data analysis.

3. DATA ANALYSIS

3.1 Image Analysis

Images captured via fluorescence microscopy allowed for both quantitative and qualitative understanding of cell migration patterns and morphology changes. Images were analyzed using ImageJ software (National Institutes of Health, Bethesda, MD), and identical cells were numbered at each time point and within each grouping of cells to ensure the same cell was being compared, as shown in Figure 4. Up to nine cells per image were analyzed. Cells with clearly defined nuclei were chosen. Images had dimensions of 1392x1040 pixels with the origin (0,0) being at the top left corner. The center coordinates of each cell with reference to the image origin were measured in pixels using the ImageJ software and then those coordinates were correlated to the (x,y) coordinates of each cell with reference to the center of the hole through a series of coordinate transforms (Appendix D), and vector calculations using the stage coordinates previously identified within the Metavue software for each image as described in more detail below. Calibration for the 40x magnification was 6.2 pixels per micron. This conversion factor was used to convert the cell center coordinates from pixels to microns.

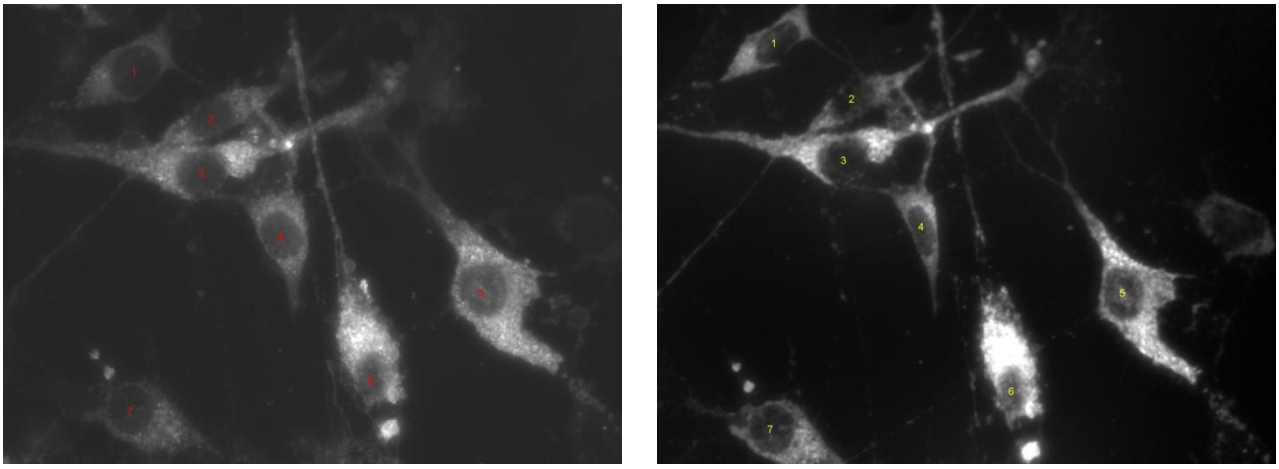

Fig. 4. Images of cells at 0 hour time point and 48 hour time point. The Images were analyzed at A) 0 hours and B) 48 hours, the cells were numbered for tracking purposes to ensure the nuclei of the same cells were measured at each time point. Images were converted to black and white images for analysis cells were

3.2 Determining Cell Displacement

Finding the radial position of the cell on the membrane with reference to the center of the hole was the first step in finding the cell displacement in order to determine migration. Once the cell coordinates relative to the center hole were found for each cell, the radial position along the membrane for each time point as well as the radial displacement of cells between time points were calculated.

3.3 Vector Analysis

Origin coordinates for the center of the hole were estimated, and stage positions and cell radial positions were found relative to this origin. Using stage coordinates acquired from Metavue and a series of vector transforms shown in Figure 5, the stage position with respect to the center of the hole was calculated, and represented by the vector ***R(x,y).*** Stage coordinates for the 0, 12, 24 and 48 hour time periods were obtained.

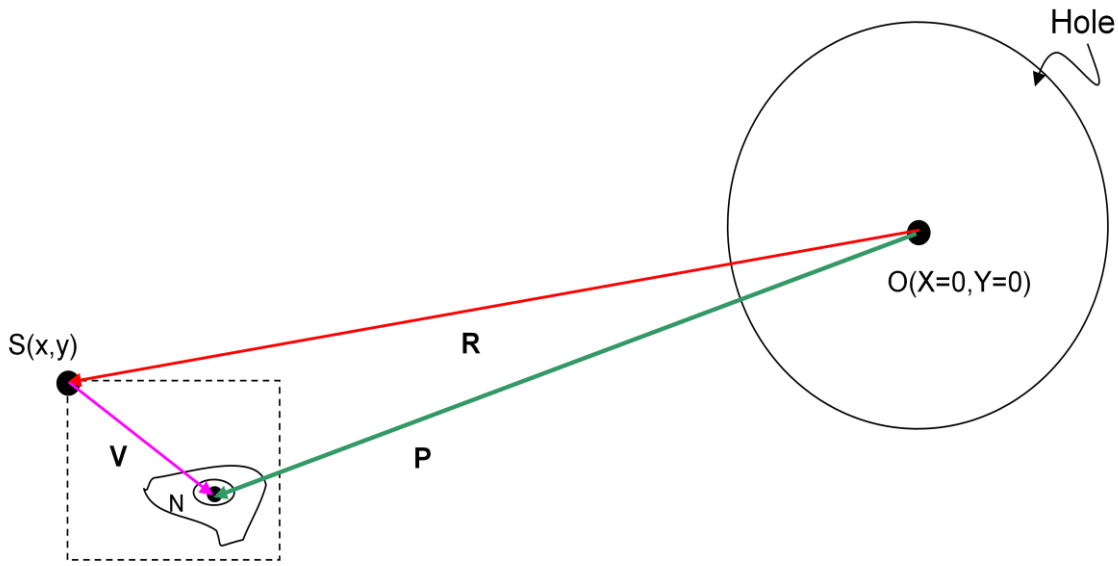

Fig. 5. Illustration of vector analysis to determine cell radial position. Vector analysis of cell radial position with respect to the origin at the center of the hole. Radial position (P) is the summation of the stage position (R) and the cell nucleus with respect to the stage position (V)

In order to find the radial position of a given cell of interest consider an image anchored at its upper left corner at ***S(x,y).*** Coordinates of the center of the cell with respect to ***S(x,y)*** are found using ImageJ, and represented by the vector ***V(x,y).*** Therefore, radial position of the cell nucleus with respect to the origin, ***P(x,y),*** is found via simple vector addition

$$\boldsymbol{P(X,Y) = R(X,Y) + V(x,y)} \quad (1)$$

Knowing the radial position at each time point allows for calculation of D^{t_n,t_o}, the apparent radial displacement.

3.4 Radial Displacement Taking into Account Membrane Displacement

Finding the radial position allowed for the calculation of the apparent cell displacement ***D***. This, however, does not take into account the membrane displacement, ***M***, which is needed to ensure that the migration we measure is true migration and not merely the cell moving with the membrane. The membrane displacement is needed to determine the value of "true" cell displacement ***C***.

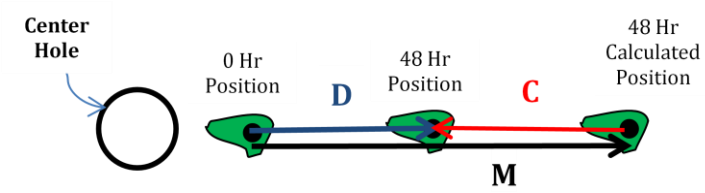

Fig. 6. Illustration of cell displacement and membrane displacement. The illustration above is a representation of apparent cell displacement, ***D*** and membrane displacement, ***M*** based on a comparison of measured radial position and calculated radial position which was found using either kinematics or the NeoHookean constitutive equation. ***C*** is considered to be true cell displacement.

It is necessary to calculate ***M***, the stretch state of the membrane for each time point, to do so we estimated the radius of the defect at each time point, $\boldsymbol{R_i}$. Calculating ***M***, corrects for inconsistencies in the "viewing stretch" at each time point. Images of the edge of the hole were collected at each time point then used to locate points along the edge found with the ImageJ software. A total of 66 points were collected and a least squares method was used to fit a circle along the edge of the hole, the radius of this circle is the hole radius. This estimation was made for each time point as shown in Figure 6.

Using the estimate of hole radius, the stretch state of the membrane, ***M*** was determined in two ways. The first is based on the NeoHookean constitutive equation and the second is based on kinematics. The models differ in that the NeoHookean model utilizes the material parameter **c** to estimate the mapped radial position, and the kinematic model requires a known value of $\boldsymbol{\lambda_z}$ the stretch in the z-direction. Displacement of the membrane was calculated using a method established by David and Humphrey (2004) applied to the NeoHookean strain energy function

$$W = c(\lambda_r^2 + \lambda_\theta^2 + \lambda_z^2 - 3) \tag{2}$$

where **c** is the material constant with units of kPa and $\boldsymbol{\lambda}$ is the stretch ratio (Appendix B). The kinematic equation

$$P_{48}^{est} = \sqrt{\left(r_{inner}^{48}\right)^2 - \frac{1}{\lambda_z}\left((P_0)^2 - \left(R_{inner}^{0}\right)^2\right)} \tag{3}$$

was based on the incompressibility assumption and is independent of the material parameter **c** and was the also used to estimate ***M*** (Appendix C). Each model has unknowns that are needed to determine membrane displacement; both require an estimate of $\boldsymbol{R_i}$ and $\boldsymbol{r_i}$. Once ***M*** was known, this value was then subtracted from the apparent displacement of the cells, ***D***. This value represents ***C***, the estimated displacement of the cells and represents the cell migration.

$$C^{est}_{t_n,t_o} = D^{t_n,t_o} - M^{est}_{t_n,t_o} \quad (4)$$

3.5 NeoHookean Model

Once the deformed and undeformed radii had been estimated it was neccessary to find material parameter **c** in order to use the NeoHookean model. To do so we conducted a uniaxial strain test for the silicone membrane material. This was done by marking a strain rosette on a membrane of known length and width dimensions and imaging the membrane with incrementally increasing force applied. Using ImageJ we measured coordinates of the strain rosette with the centerpoint being the center of the strain rosette. This method is illustrated in Figure 7. A calculation method established by Heistand et al. (2005) was used to create a stress stretch curve. A curve was then fit to the stress stretch data using the NeoHookean model. The material parameter **c** in the NeoHookean model that generated the best fit curve was the value that was used in further calculations. The value of **c** was estimated to be 438kPa.

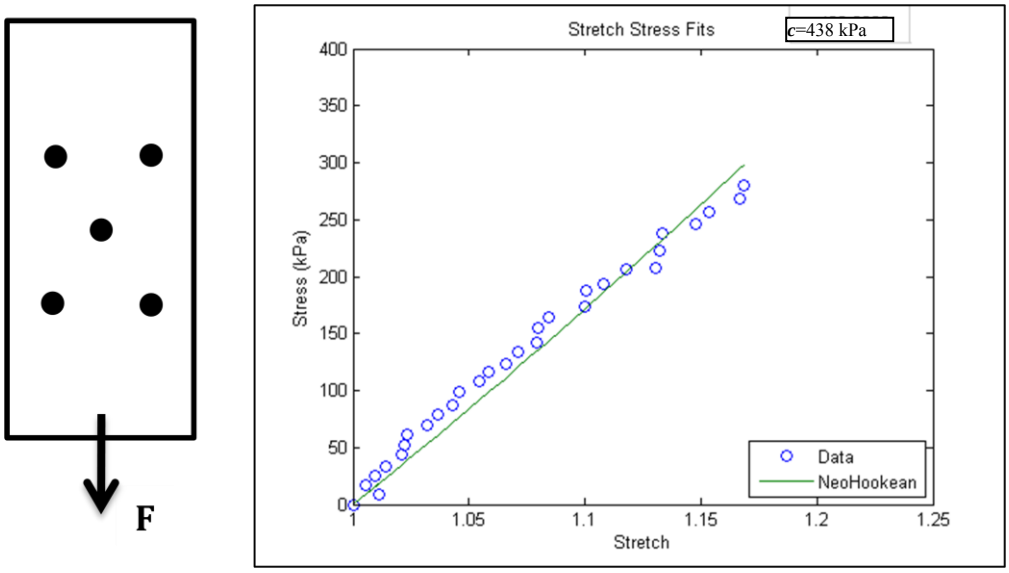

Fig. 7. Stress vs. Stretch curve for membrane material with NeoHookean fit. Downward force is applied to a membrane with fixed markers in a strain rosette configuration. From there a Stress vs. Stretch plot was created and the NeoHookean model with a material constant of 408.3636 kPa fitted to the data.

3.6 The Kinematic Model

In addition to the NeoHookean model described above, the kinematic model could also be used to calculate membrane displacement and generally does not require material constants. It does however require a known value of $\boldsymbol{\lambda_z}$. For incompressibility $\boldsymbol{\lambda_r}*\boldsymbol{\lambda_\theta}*\boldsymbol{\lambda_z}=1$, therefore

$$\boldsymbol{\lambda_z} = \frac{\mathbf{1}}{\boldsymbol{\lambda_r}*\boldsymbol{\lambda_\theta}} \tag{5}$$

We solved for $\boldsymbol{\lambda_z}$ using two methods; the first utilized the idea of incompressibility and volume conservation and allowed us to calculate $\boldsymbol{\lambda_z}$ by solving for the ratio of the area of the membrane at $\boldsymbol{t_0}$ and $\boldsymbol{t_{48}}$ (Appendix D). The other used the NeoHookean constitutive equation to solve for $\boldsymbol{\lambda_r}$ which is $\frac{\boldsymbol{dr}}{\boldsymbol{dR}}$ and $\boldsymbol{\lambda_\theta}$ which is $\frac{\boldsymbol{r}}{\boldsymbol{R}}$. Knowing these we can calculate $\boldsymbol{\lambda_z}$ and use it in the kinematic equation.

3.7 Uncertainty Percentages

Because both the NeoHookean and kinematic models are dependent on the radius measurement of the hole it was necessary to calculate the error in the estimation of the hole diameter and observe its effects on our calculation of cell migration. This was very important in determining how the error affects our measurement of cell migration. The radius is estimated using a best fit method of points along the edge of the membrane. This estimation is limited because we can only image a small arc along the edge of the hole due to viewing limitations. Determining the error in the estimation involved imaging membrane edges along the perimeter of the entire hole in a relaxed configuration and measuring the diameter of the center hole with a micrometer. Multiple measurements of hole diameter were done using the micrometer and the average of those was used as the "measured value" in the error calculation for the hole diameter. To obtain the calculated value, we used ImageJ and found the x,y coordinates of multiple points along the edge in each image were measured. Since experimentally edge data for a certain arc length along the edge of the circle could be obtained, the center coordinates and radius of the hole were calculated using the best fit method for multiple arcs around the perimeter of the entire hole. These calculated values of the radius were then compared to diameter measurements obtained with the micrometer. The maximum error was found to be 8.7% of the measured radius and the average error was found to be 4.1% of the measured radius.

Cell migration was determined based on whether or not the measured cell displacement was within the bounds of the maximum and minimum uncertainties which were calculated using the radius measurement errors. To do determine the upper and lower bounds of uncertainty, we calculated membrane displacement by comparing minimum and maximum possible radii at 0 and 48 hours. For example, to use the NeoHookean model we needed a $\boldsymbol{r_i}$ and $\boldsymbol{R_i}$ radius estimation as input. To determine minimum and maximum uncertainties we calculated the $\boldsymbol{r_i^0}$ and the $\boldsymbol{R_i^{48}}$ with ±8.7% error, and compared the minimum at $\boldsymbol{t_0}$ to the maximum at $\boldsymbol{t_{48}}$ and vice versa. The calculation of membrane displacement using these comparisons established the

minimum and maximum bounds of uncertainty. The uncertainty comparisons were also done using 4.1% error. Comparisons were not only made between the average and maximum percent error, but also between the NeoHookean method of calculating membrane displacement and the Kinematic method of calculating membrane displacement.

In summary, cell displacement and membrane displacement uncertainties were calculated taking into account the maximum (8.7%) and average (4.1%) error in the calculation of the center hole radius. This was done using the kinematics as well as the NeoHookean constitutive equation. The kinematic model was evaluated with $\boldsymbol{\lambda_z}$ being calculated in two ways, one found from volume conservation and another using the NeoHookean model. Comparisons were made between the cell displacement $\boldsymbol{D}$ and the membrane displacement $\boldsymbol{M}$. Uncertainty comparisons of true cell displacement $\boldsymbol{C}$ were also made. $\boldsymbol{C}$ takes into account membrane displacement and thus is a simpler and more direct way of determining if cell migration occurred. The kinematic model was evaluated with $\boldsymbol{\lambda_z}$ being calculated in two ways, one found from volume conservation and another using the NeoHookean model.

4. RESULTS

Cells were successfully cultured on the membrane in the custom cell culture device and transferred and mounted to the stretch system. Cells survived static and dynamic stretch environments for 48 hours. Live cell imaging capabilities also proved successful, cells were clearly identifiable and the alignment of images and ability to monitor the same cells at each time point was successful.

4.1 Static Stretch

Cells were exposed to a 6% applied static stretch and displacements were calculated to determine if cells migrated in reaction to stretch gradients. Though it may appear that cells have moved outward due to migration it can be seen in Figure 8 that, while the cells did show outward movement the hole radius was also stretch outward.

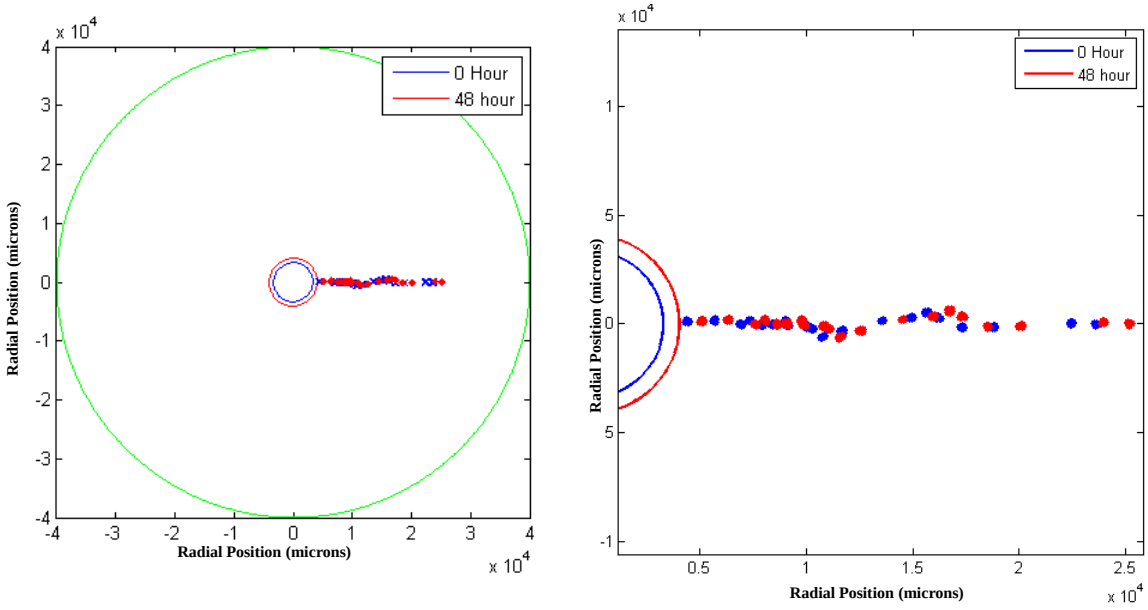

Fig. 8. Cell radial position at 0 hours and 48 hours for static stretch case. The illustration above plots the radial positions of the cells at each time point for the static stretch case. Though it appears the cells have moved, it must also be noted that the radius of the center hole has been stretched.

4.2 Results Using Kinematic Model with λ_z Evaluated via Volume Conservation

Considering the maximum error of 8.7% in measuring the hole radius, and an average value of λ_z was estimated using the idea of volume conservation Figures 9 and 10 illustrate there was no conclusive evidence of cell migration. Though migration may have occurred, it can be seen in Figure 8 that apparent cell displacement ***D*** falls within the bounds of the uncertainty in membrane displacement ***M***. The illustration true cell displacement ***C***, is shown in Figure 10 in which the range of uncertainties for ***C*** are from -9783.2μm to 1175.5μm. Based on the fact that the range of uncertainty includes both positive and negative data points, we cannot say whether cells moved inward, outward, or not at all. The maximum and minimum limits not only encompass the measured values of ***C***, but also contain values for zero displacement. This is evidence that though there may have been migration there is no conclusive evidence within the bounds of 8.7% error.

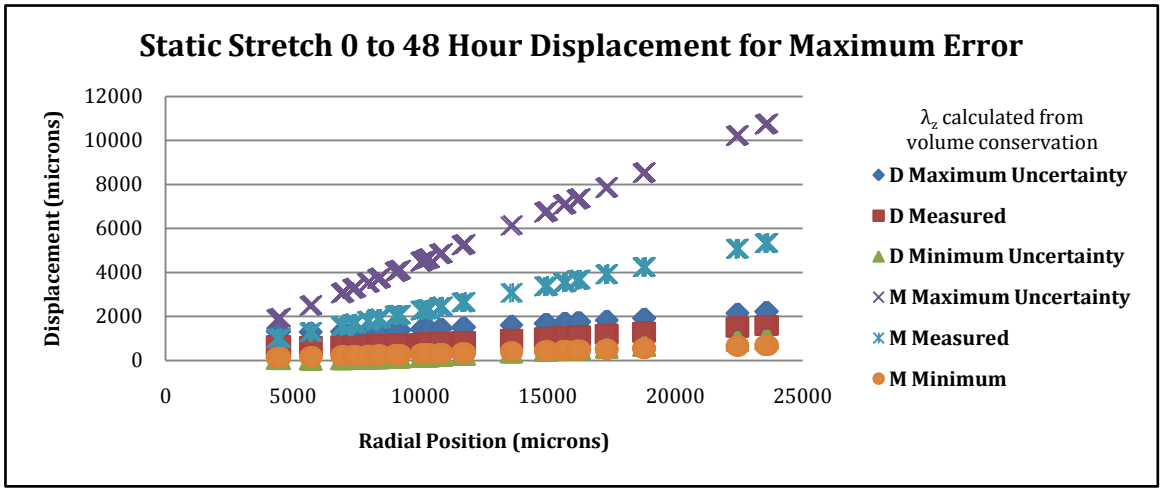

Fig. 9. Plot of uncertainties in ***D*** and ***M*** for static stretch, maximum error, kinematic model using λ_z found via volume conservation. Apparent cell and membrane displacement for 8.7% error, for this data λ_z was found using the volume conservation method. Overlap between the range of uncertainty for ***D*** and the range of uncertainty for ***M*** indicates that there is no definitive evidence that cell migration occurred.

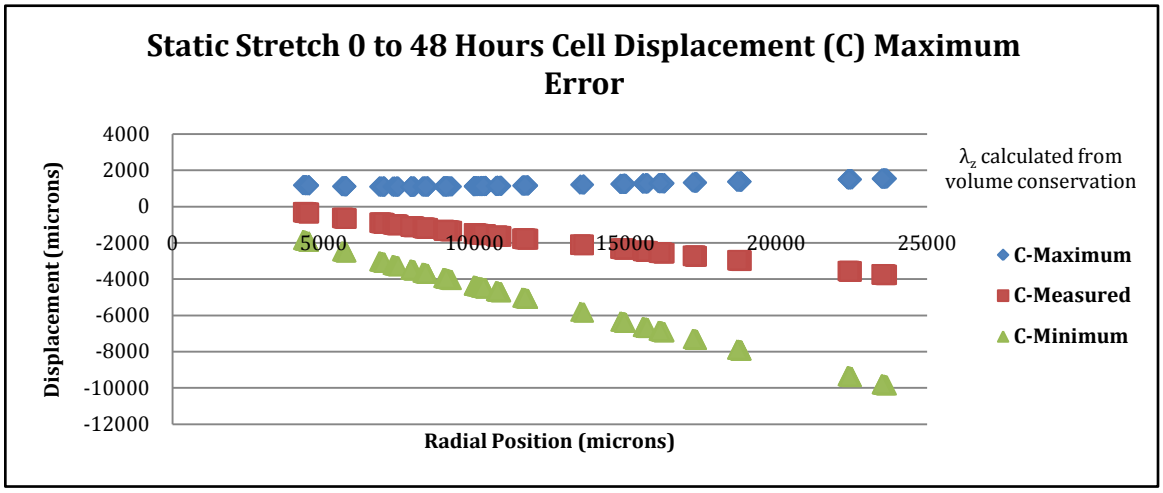

Fig. 10.Plot of uncertainties in ***C*** for static stretch, maximum error, kinematic model using λ_z found via volume conservation. Cell displacement ***C***, which takes into account membrane displacement for the case in which there was 8.7% error in the measurement of the cell radius. This was calculated using the maximum error and λ_z was found using the volume conservation method. Since the range of uncertainty includes 0µm displacement, it cannot be said conclusively that cell migration occurred.

Given that the maximum error provides the most conservative range, we also considered using the average error from the hole radius measurement. Using the average error of 4.1% from calculating the hole radius Figures 11 and 12 suggests that cell migration is evident beginning at a radial position of 7000µm and increases by 24% as we observe cells closer to the outer edge of the membrane. Apparent cell displacement is in the range of approximately 350-18200µm and shows no indication of overlap with the region of membrane displacement, suggesting cell migration. There is some overlap in the region towards the center hole of the cell displacement and membrane; therefore, there is no conclusive evidence of cell migration. In Figure 2, the plot of cell displacement ***C*** indicates that cell migration from 7000µm outward has occurred and the range of the displacement is anywhere from -186µm to -6510µm at the outer edge. The negative direction indicates that movement is occurring inward toward the center hole, and that there is greater movement inward at the outer edge of the membrane than closer in towards the center hole.

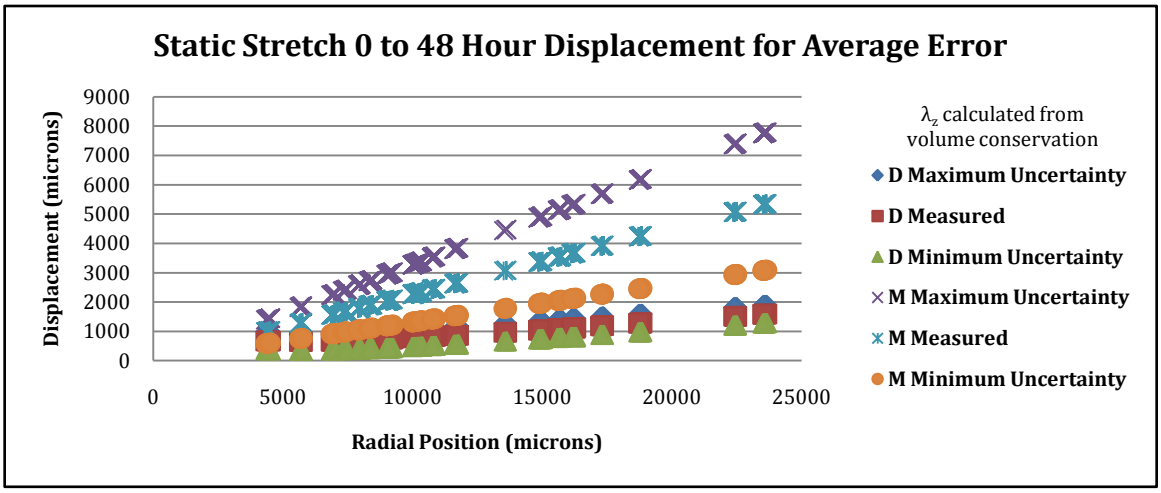

Fig. 11. Plot of uncertainties in ***D*** and ***M*** for static stretch, average error, kinematic model using λ_z found via volume conservation. Apparent cell displacement and membrane displacement for the 4.1% error in the hole radius estimation. There is no overlap between the ranges of uncertainty for ***D*** and ***M*** from a radial position of ~7000µm outward along the membrane, indicating that there was migration for the average percent error case.

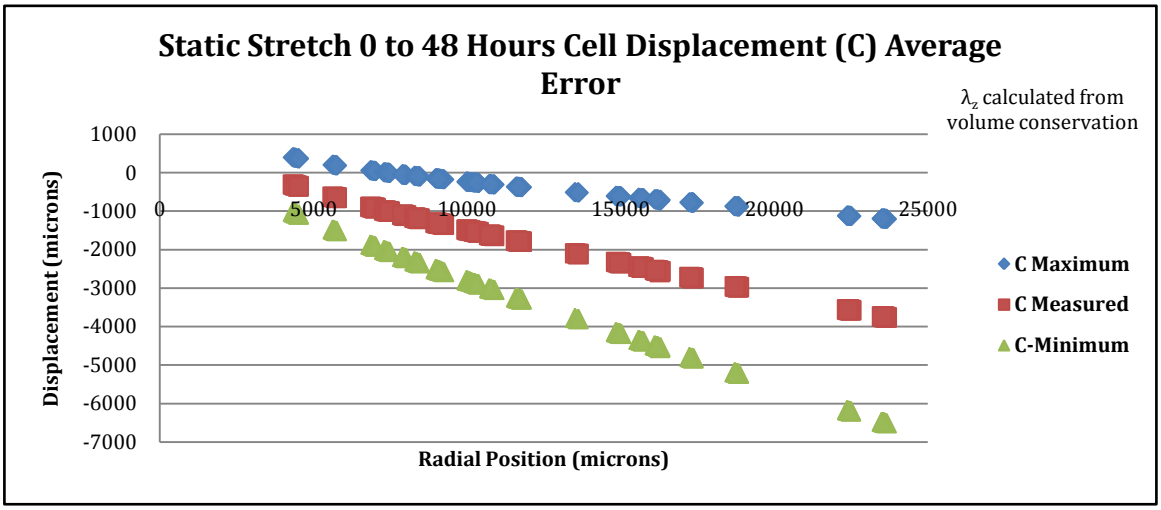

Fig. 12. Plot of uncertainties in ***C*** for static stretch, average error, kinematic model using λ_z found via volume conservation. The plot above illustrates cell migration ***C*** for 4.1% in hole radius measurement and $\boldsymbol{\lambda_z}$ was calculated using volume conservation. Based on the plot above migration occurred inward toward the center hole, and cell displacement ranges from -7µm nearer to the center hole and -6510µ closer to the outer edge.

4.3 Results Using Kinematic Model with $\boldsymbol{\lambda_z}$ Evaluated via NeoHookean Model

Stretch in the z-direction was also evaluated via the NeoHookean constitutive equation (Appendix E). Results from this approach with the maximum error of 8.7%

provide no conclusive evidence of cell migration. Though migration may have occurred, it can be seen in Figure 13 that cell displacement falls within the bounds of the membrane displacement. This can also be seen in Figure 14 in which the range of ***C*** minimum to ***C*** maximum values -4316μm to 1825μm contains values for zero displacement. This is evidence that though there may have been true cell migration there is no conclusive evidence within the bounds of 8.7% error. Though in the average error case illustrated in Figure 15, there is less overlap of the boundaries of ***M*** and ***D*** and the range is narrower, it still cannot be said definitively that there was cell migration. This is further illustrated in Figure 16 where the range of uncertainty for the cell displacement contains a value of 0μm indicating that cell migration may not have occurred.

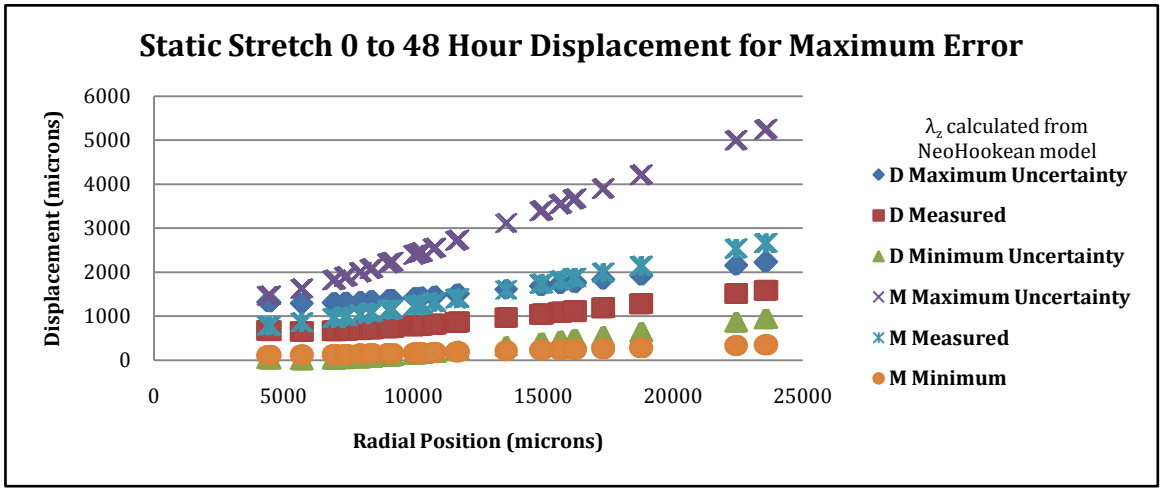

Fig. 13. Plot of uncertainties in ***D*** and ***M*** for static stretch, maximum error, kinematic model using λ_z found via NeoHookean constitutive equation. Range of uncertainty in apparent cell displacement and membrane displacement, ***D*** and ***M*** respectively, for 8.7% error of the hole radius calculation, $\boldsymbol{\lambda_z}$ was found via the NeoHookean model. Overlap in the maximum and minimum ranges of ***D*** and ***M*** indicates that we cannot say conclusively that cell migration occurred in response to 6% applied static stretch.

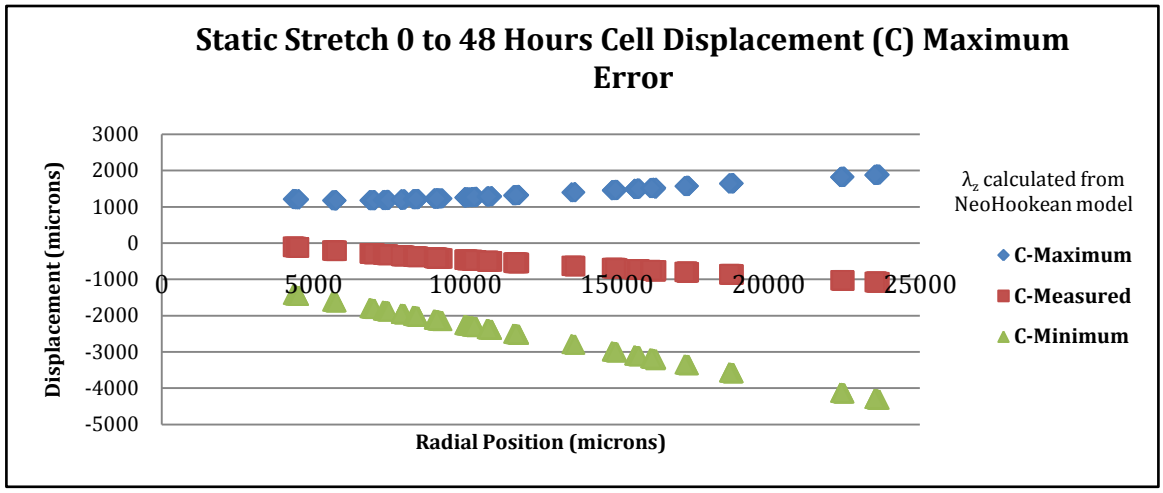

Fig. 14. Plot of uncertainties in ***C*** for static stretch, maximum error, kinematic model using λ_z found via NeoHookean constitutive equation. Cell displacement ***C***, for the 8.7% error in hole radius estimation and $\boldsymbol{\lambda_z}$ was calculated using the NeoHookean model. Though cell migration may have occurred we cannot say so conclusively because the range of uncertainty encompasses 0μm displacement.

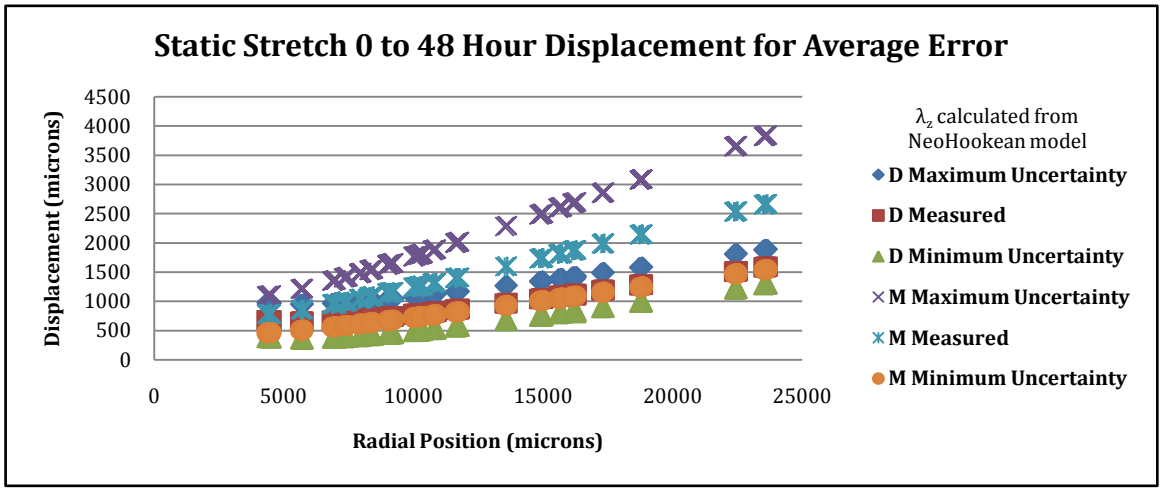

Fig. 15. Plot of uncertainties in ***D*** and ***M*** for static stretch, average error, kinematic model using λ_z found via NeoHookean constitutive equation. Apparent cell displacement and membrane displacement, for 4.1% error of the hole radius measurement and $\boldsymbol{\lambda_z}$ was calculated from the NeoHookean model. Overlap in the ranges of uncertainty is an indicator that we cannot say definitively that cell migration occurred in response to 6% applied static stretch.

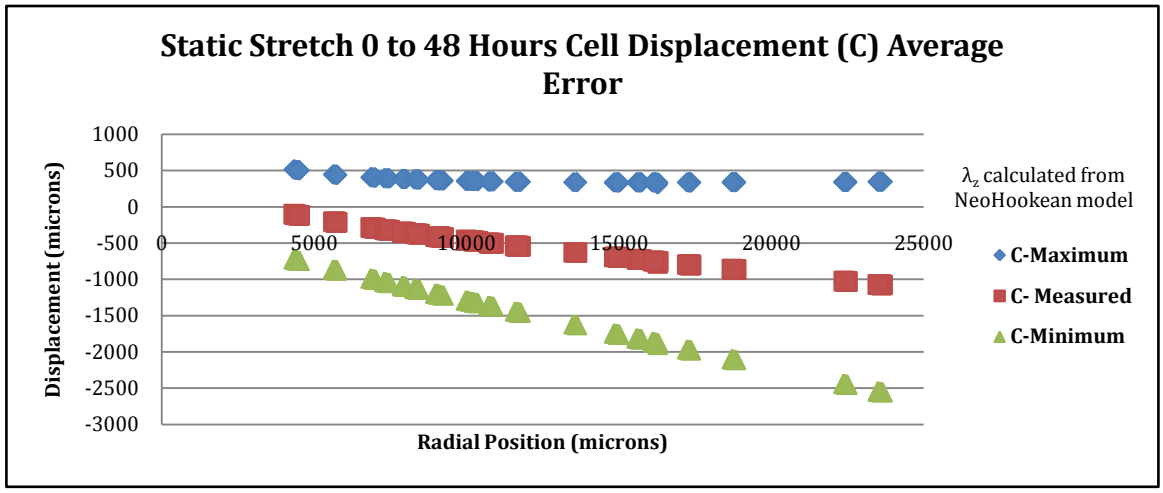

Fig. 16. Plot of uncertatinties in ***C*** for static stretch, average error, kinematic model found using λ_z found via NeoHooken constitutive equation. The above illustrates a plot of ***C***, cell displacement for 4.1% error and $\boldsymbol{\lambda_z}$ was calculated using the NeoHookean model. The range of uncertainty in cell displacement contains values for 0μm displacement along the membrane, therefore it cannot be said conclusively that cell movement occurred.

4.4 Results Using NeoHookean Constitutive Equation

As was the case for the kinematic model in which $\boldsymbol{\lambda_z}$ was calculated using the NeoHookean model, results found using the NeoHokean constitutive equation were similar. For both the maximum and average error cases it cannot be said conclusively that cell migration occurred. In the maximum error case, there is overlap in the uncertainty ranges of ***D*** and ***M***, and the range between the maximum ***C*** and the minimum ***C*** encompasses zero displacement values as illustrated in Figures 17 and 18. The same trend in the range of uncertainties can be seen in Figures 19 and 20 for the average error case. Because of these uncertainties we cannot conclude that there was cell migration.

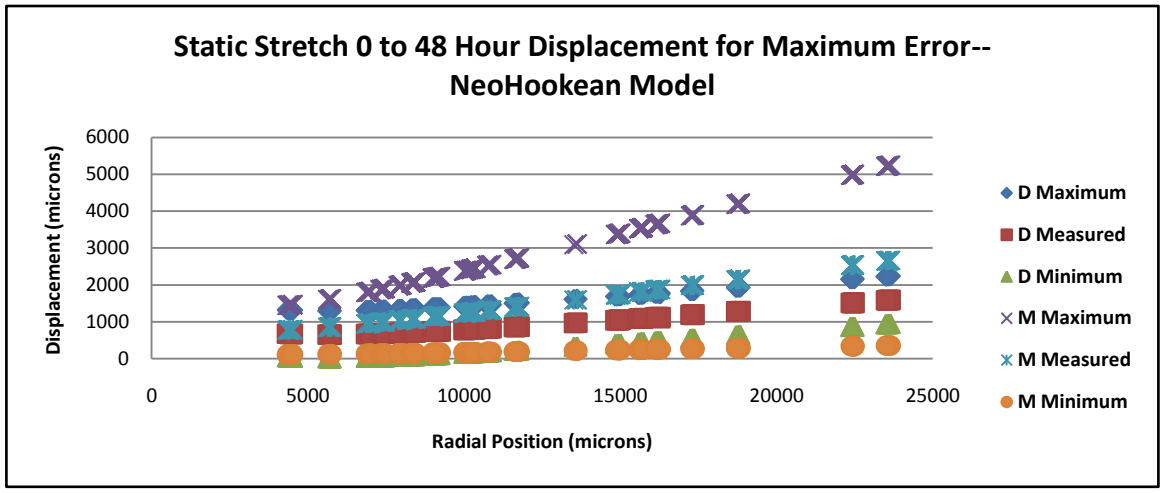

Fig. 17. Plot of uncertainties in ***D*** and ***M*** for static stretch, maximum error using the NeoHookean model. Because of the overlap in the range of uncertainty for ***D*** and the range of uncertainty M cell migration may not have occurred.

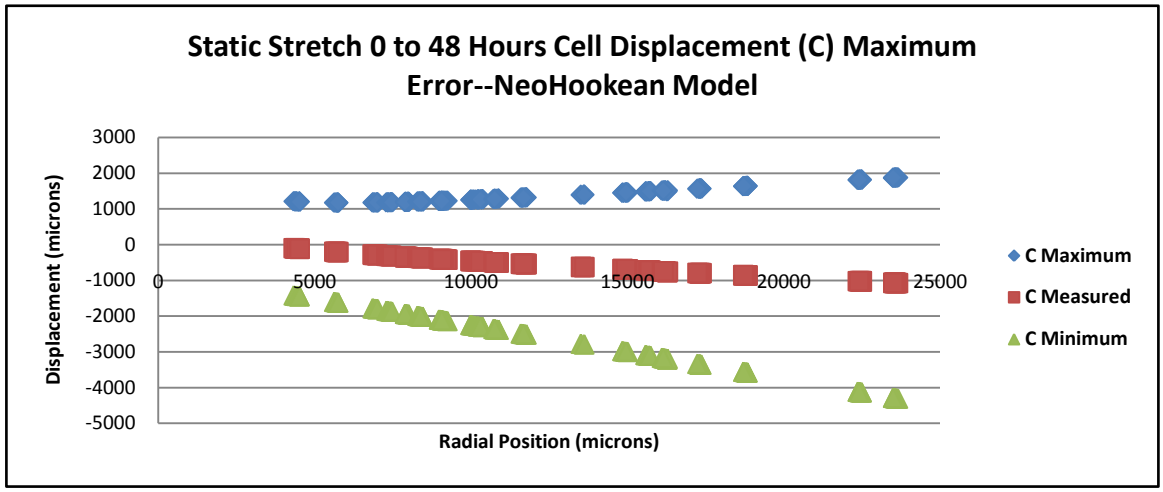

Fig. 18. Plot of uncertainties in ***C*** for static stretch, maximum error using the NeoHookean model. Because 0 displacement is within the limits of uncertainty we cannot say conclusively that cells migrated in response to static stretch.

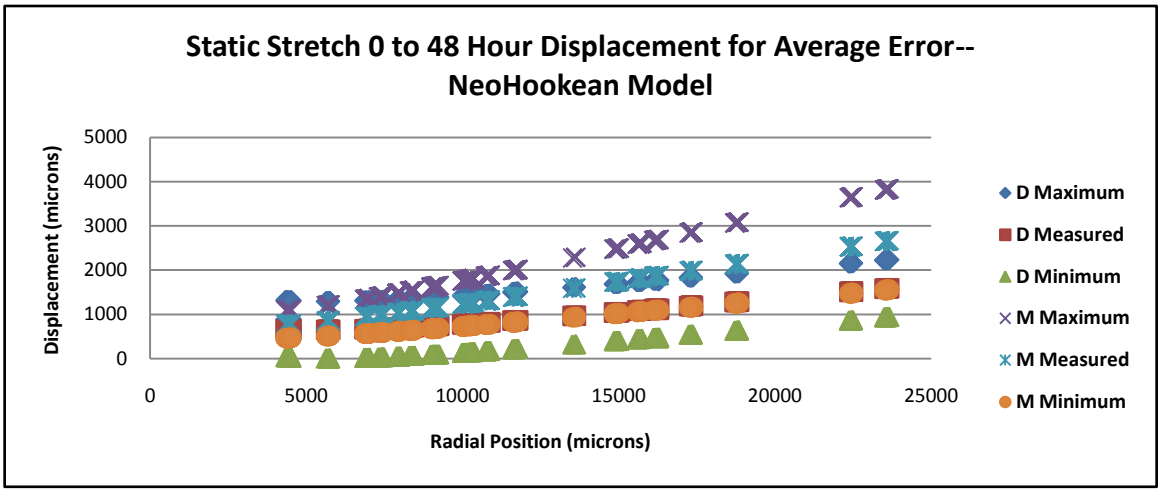

Fig. 19. Plot of uncertainties in ***D*** and ***M*** for static stretch, average error using the NeoHookean model. Together these plots indicate that we cannot say conclusively that cell migration occurred within the bounds of our uncertainty.

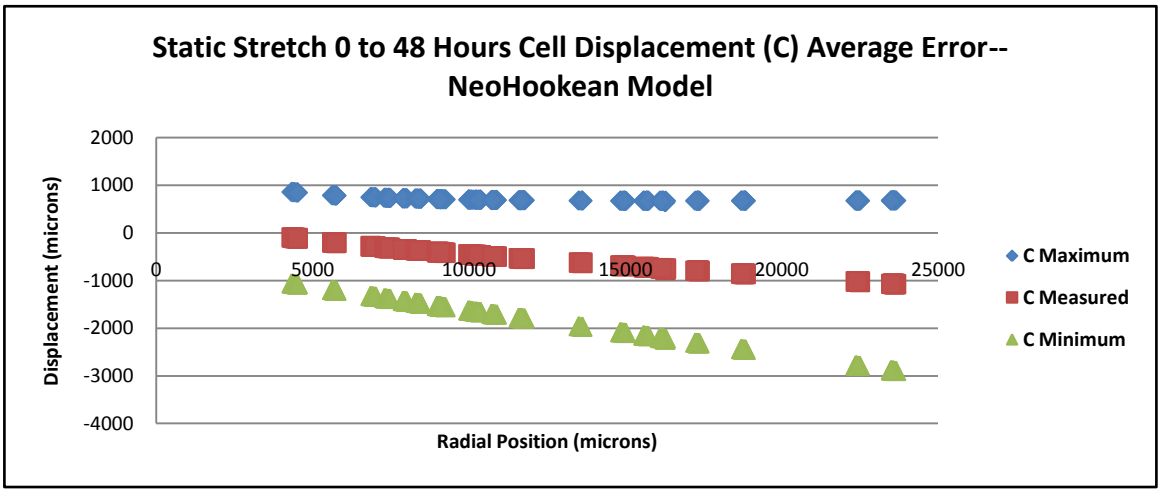

Fig. 20. Plot of uncertainties in ***C*** for static stretch, average error using the NeoHookean model. The plot above illustrates the range of uncertainty of cell displacement ***C*** for the NeoHookean model taking into account the average error in hole radius measurement.

4.5 Dynamic Stretch

Cells were exposed to 6% applied cyclic stretch with a frequency of 1Hz, and the cell response was observed to determine if migration occurred. Figure 21 illustrates that

though it appears cells migrated inward over the course of 48 hours, it must be noted that the hole radius has also been estimated to be smaller.

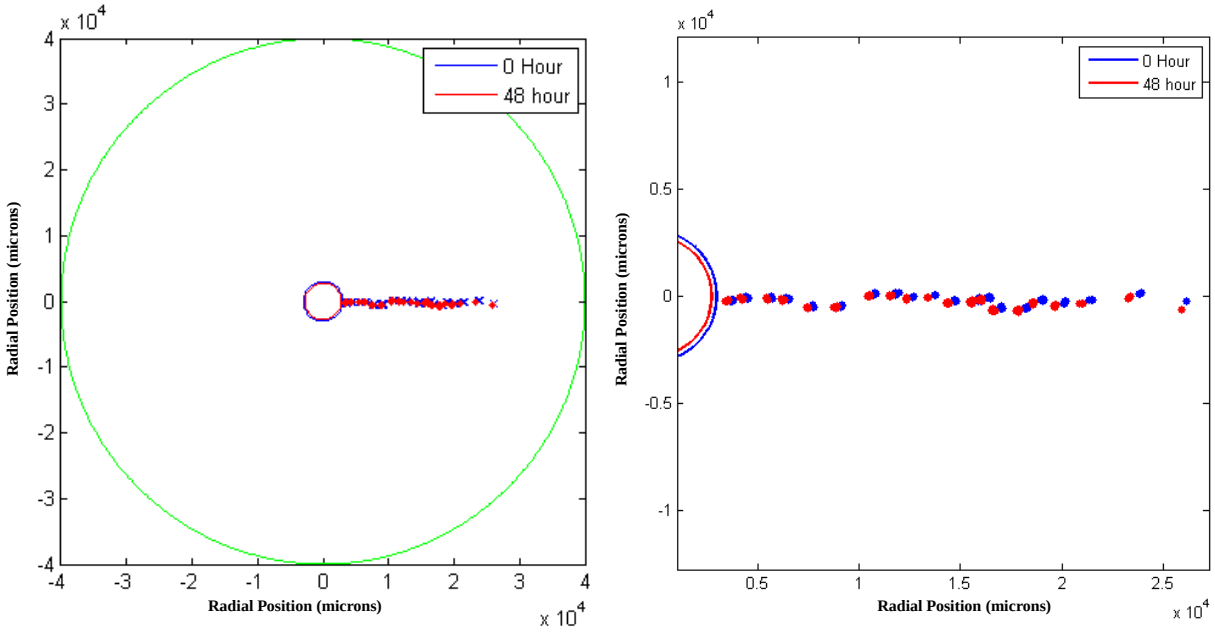

Fig. 21. Cell radial position at 0 hours and 48 hours for dynamics stretch case. Illustration of radial positions of cells at each time point though it appears cells have moved, it must also be noted that the radius of the center hole has been compressed in the dynamic stretch case.

4.6 Results Using Kinematic Model with λ_z Evaluated via Volume Conservation

For the purposes of assessing cell migration we solved for the range of uncertainty for apparent cell displacement and membrane displacement, ***D*** and ***M*** respectively using the kinematic model with λ_z found via volume conservation for both the maximum error in estimating hole radius (8.7%) and the average error (4.1%). In both Figures 22 and 23, which take into account the maximum error in estimating the hole radius, it was noted that the maximum and minimum bounds of ***D*** are well within the limits of uncertainty of ***M*** and for cell migration ***C***, the upper and lower limits contain a displacement value of 0μm. For the average error case, Figures 24 and 25 depict the upper and lower limits of uncertainty for ***D*** and ***M*** as well as ***C***. In the average error case, the values of ***D*** are within the range of ***M*** and the maximum and minimum bounds of ***C*** contain a 0μm. value of displacement. For this reason, we

cannot say with certainty that cell migration occurred, although cell movement may have occurred we cannot say within the boundaries of our uncertainty that it was migration.

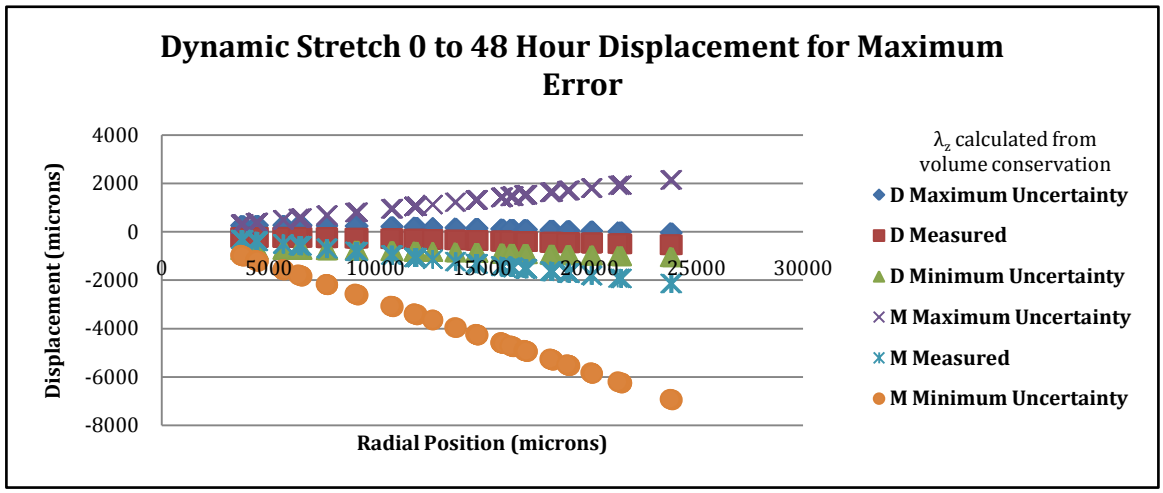

Fig. 22. Plot of uncertainties in ***D*** and ***M*** for dynamic stretch, maximum error, kinematic model using λz found via volume conservation. Apparent cell displacement and membrane displacement, ***D*** and ***M*** respectively for the maximum (8.7%) error in calculating the hole radius and λ_z was calculated using volume conservation. Since maximum and minimum bounds of ***D*** are within the maximum and minimum bounds of ***M***, we cannot say conclusively that cell migration occurred as a result of cyclic stretch with a frequency of 1Hz.

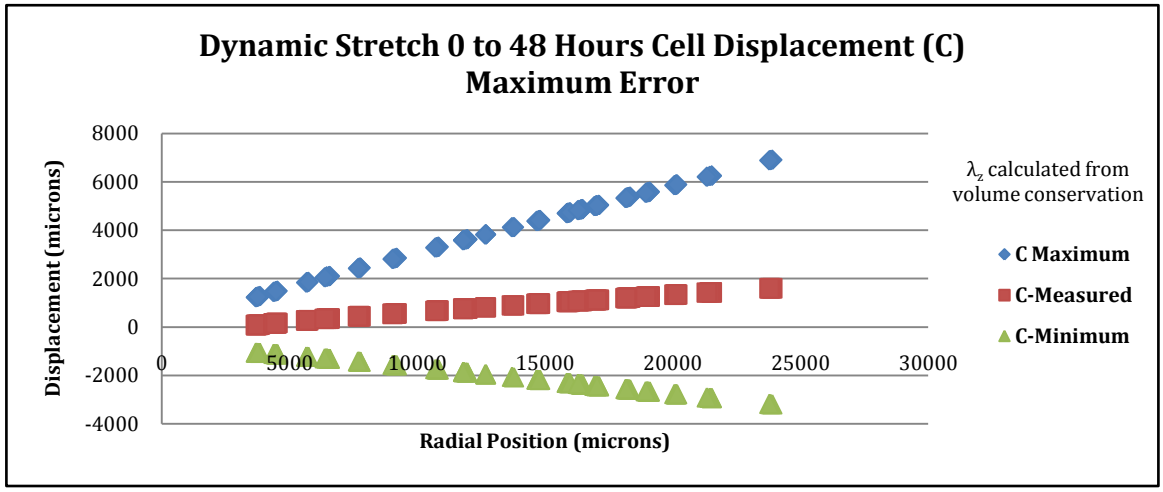

Fig. 23. Plot of uncertainties in ***C*** for dynamic stretch, maximum error, kinematic model using λz found via volume conservation. The plot above illustrates cell displacement ***C*** for 8.7% error in hole radius measurement, since the upper and lower limits of contain a zero value of displacement it cannot be said that cell migration occurred.

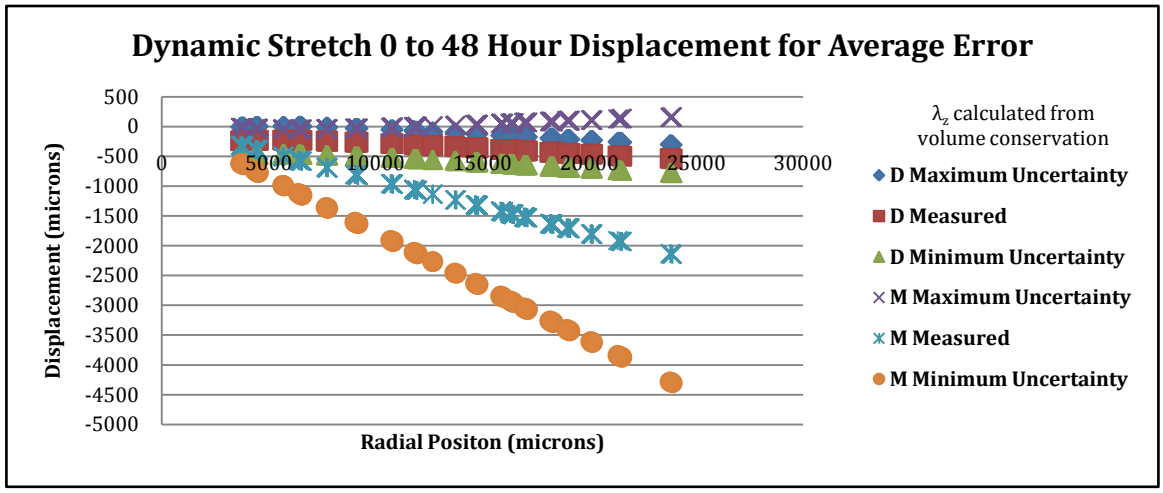

Fig. 24. Plot of uncertainties in ***D*** and ***M*** for dynamic stretch, average error, kinematic model using λz found via volume conservation. Observing the boundaries of uncertainty we cannot say absolutely that cell migration occurred.

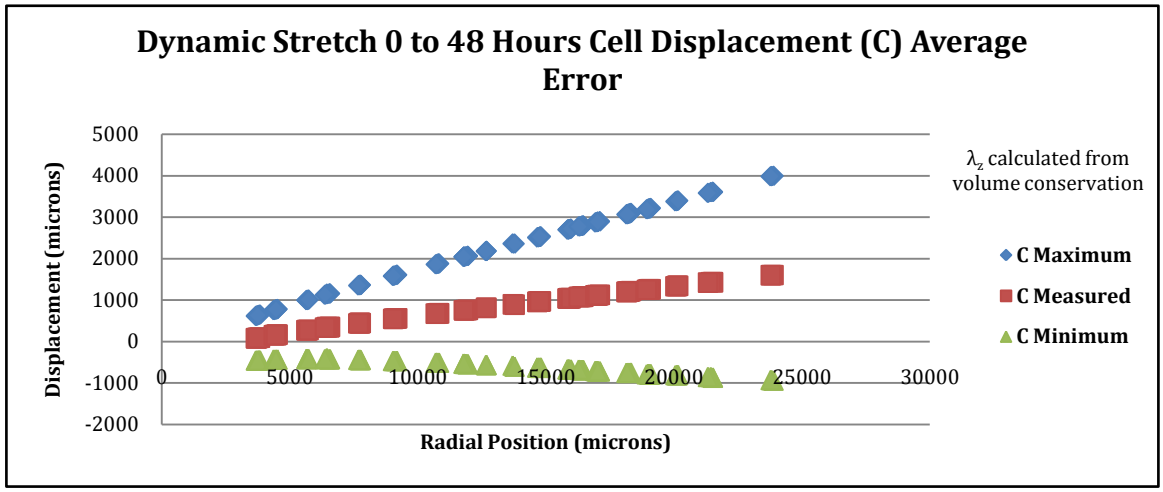

Fig. 25 Plot of uncertainties in ***C*** for dynamic stretch, average error, kinematic model using λz found via volume conservation. Cell displacement ***C***, which takes into account membrane displacement, for 4.1% error in calculation of the hole radius. Because the upper and lower limits of uncertainty include a zero value of displacement we cannot say conclusively that cells responded to 6% applied cyclic stretch with a frequency of 1Hz by migrating.

4.7 Results Using Kinematic Model with λ_z Evaluated via NeoHookean Model

When evaluating the cellular response to dynamic stretch it was observed that for both maximum and average error in measuring the hole radius we cannot say within the bounds of uncertainty that cell migration occurred. When using the kinematic equation

with λ_z evaluated from the NeoHookean model for the maximum error Figure 26 illustrates that the range of uncertainty for ***D*** was -1035μm to 276μm and the range of uncertainty for ***M*** was -3410μm to 1074μm, since the range of ***D*** is within the bounds of uncertainty of ***M*** we cannot say conclusively whether cell migration occurred. Another way of evaluating cell displacement is observing ***C***, the cell displacement taking into account membrane displacement as shown in Figure 27. For the maximum error case the lower and upper limits of ***C*** are -2118μm and 3371μm respectively, though cell displacement due to migration may have occurred, 0μm displacement is also within this range of ***C*** values indicating that there may not have been any cell displacement within the bounds of our uncertainty. Figures 28 and 29 illustrate that the same is true for the average error in calculating hole radius, but the ranges of uncertainty are narrower as is to be expected.

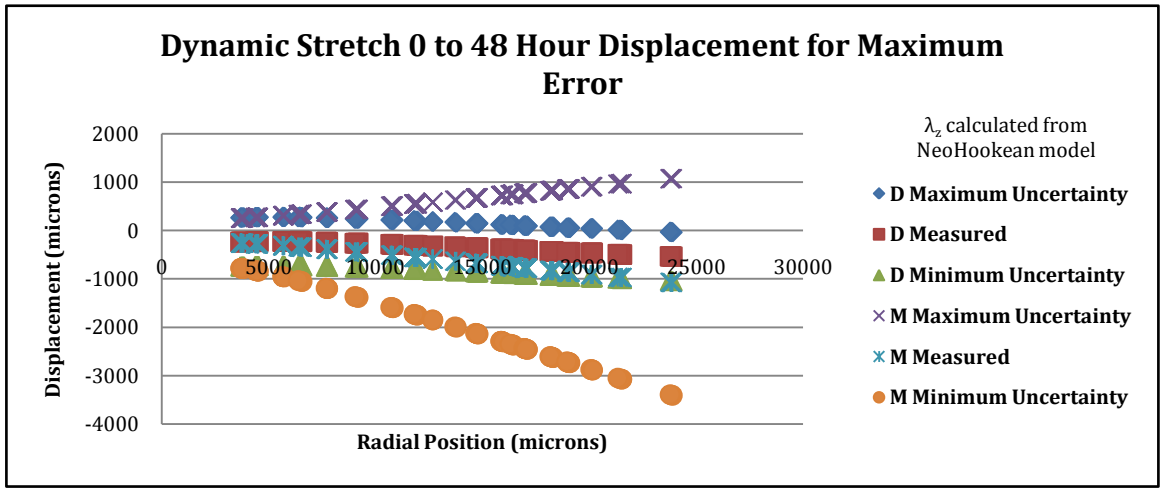

Fig. 26. Plot of uncertainties in ***D*** and ***M*** for dynamics stretch, maximum error, kinematic model using λz found via NeoHookean constitutive equation. The plot above illustrates apparent cell displacement ***D*** and membrane displacement M for 8.7% error in calculation of the hole radius. The range limits of uncertainty for ***D*** are within the upper and lower limits of ***M*** and so we cannot reasonably conclude that there was cell migration.

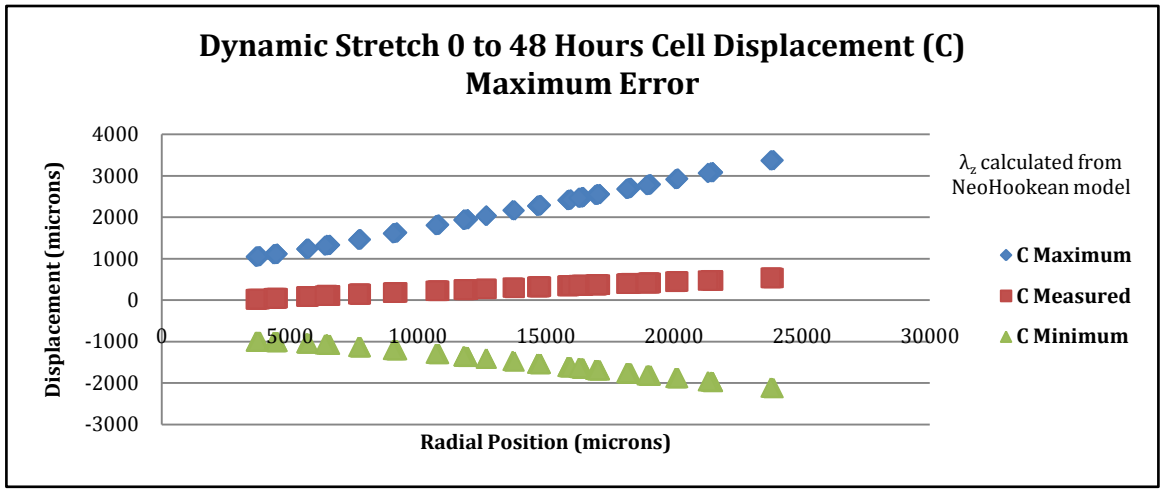

Fig. 27. Plot of uncertainties in ***C*** for dynamic stretch, maximum error, kinematic model using λz found via NeoHookean constitutive equation. Range of uncertainty in cell displacement, ***C*** which takes into account membrane displacement for the case in which hole measurement error was 8.7% and λ_z was calculated via the NeoHookean model. Though there may have been migration in response to 1Hz dynamic stretch we cannot say conclusively within the bounds of our error that there was cell migration.

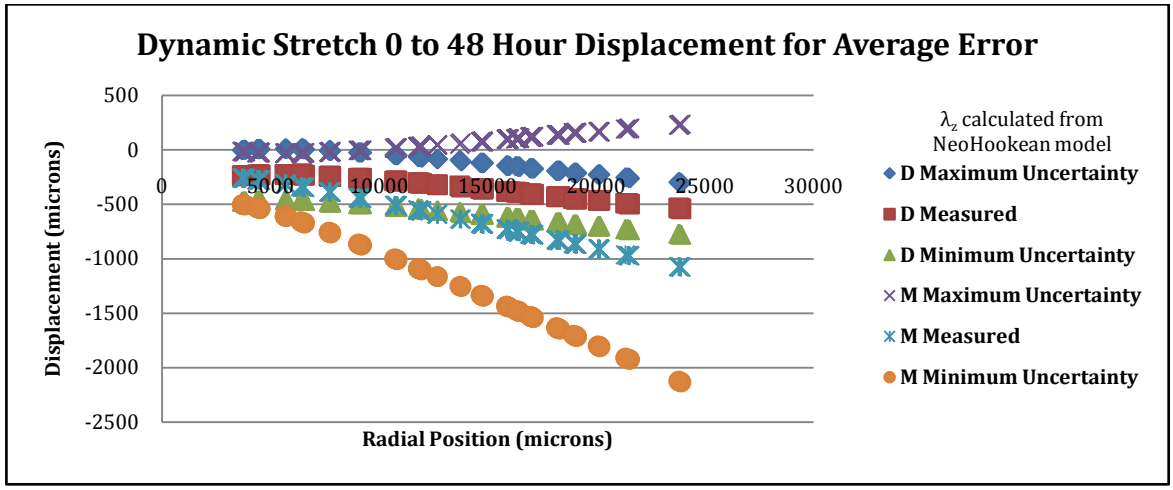

Fig. 28. Plot of uncertainties in ***D*** and ***M*** for dynamic stretch, average error using the NeoHookean model. Apparent cell displacement ***D*** and membrane displacement ***M*** for the average (4.1%) error in hole radius measurement case. Because of the overlap in the range of displacement for ***D*** and the range of displacement for ***M*** we cannot say conclusively that there was cell migration.

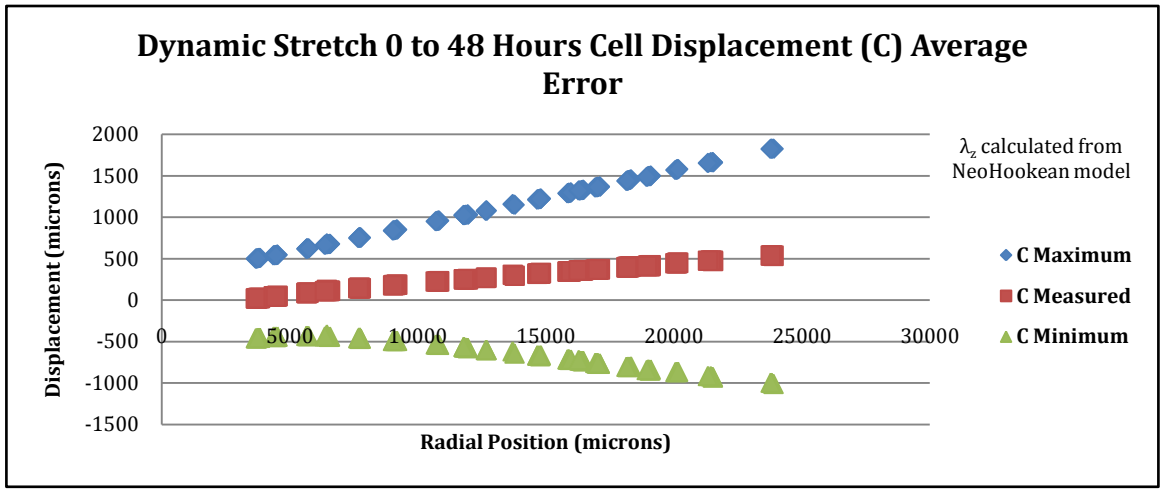

Fig. 29. Plot of uncertainties in ***C*** for dynamics stretch, average error, kinematic model using λz found via NeoHookean constitutive equation. Because the upper and lower limits of uncertainty include a 0μm value of displacement, cells may have migrated, but we cannot be certain.

4.8 Results Using NeoHookean Constitutive Equation

Using the NeoHookean constitutive equation with material parameter ***c*** equal to 408 kPa we were able to calculate displacements ***D***, ***M***, and ***C*** for the 0 to 48 hour time period. For the case that used the maximum error in estimating hole radius shown in figures to calculate the bounds of uncertainty shown in Figures 30 and 31and the case that used average error, Figures 32 and 33 indicate that the upper and lower limits of uncertainty contain 0μm displacement value and so we cannot say conclusively within the bounds of our uncertainty that migration occurred.

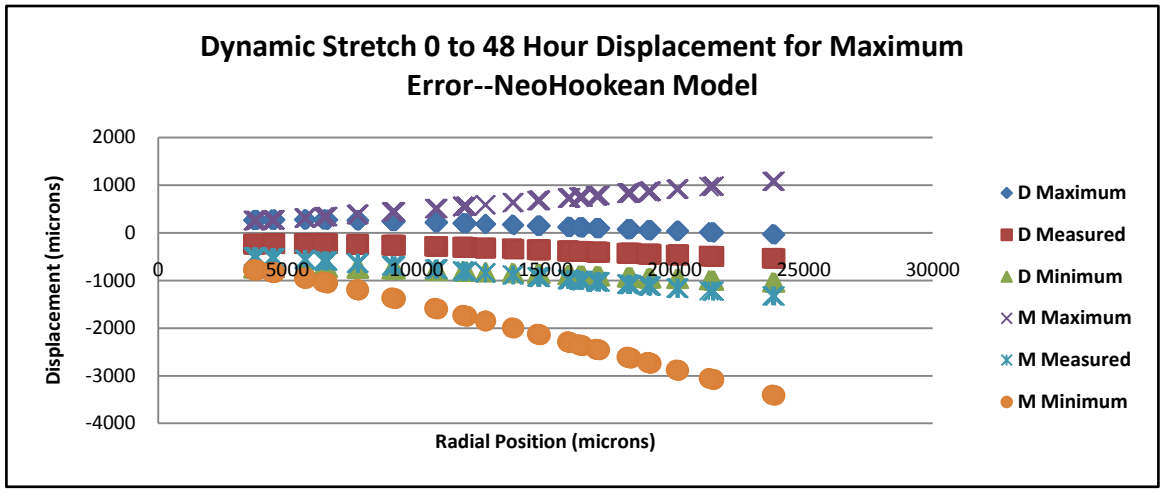

Fig. 30. Plot of uncertainties in ***D*** and ***M*** for dynamic stretch, maximum error using the NeoHookean model. The range of ***D*** is well within the limits of ***M*** and so we cannot say with ceratainty that cell migration occurred.

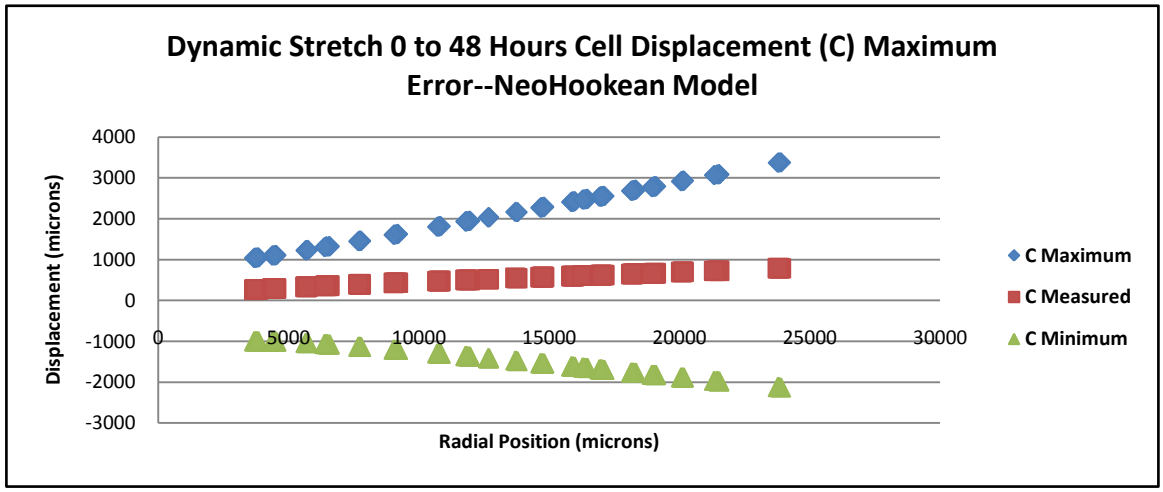

Fig. 31. Plot of uncertainties in ***C*** for dynamic stretch, maximum error using the NeoHookean model. Range in uncertainty of cell displacement ***C*** for the NeoHookean model ecompasses 0μm displacement.

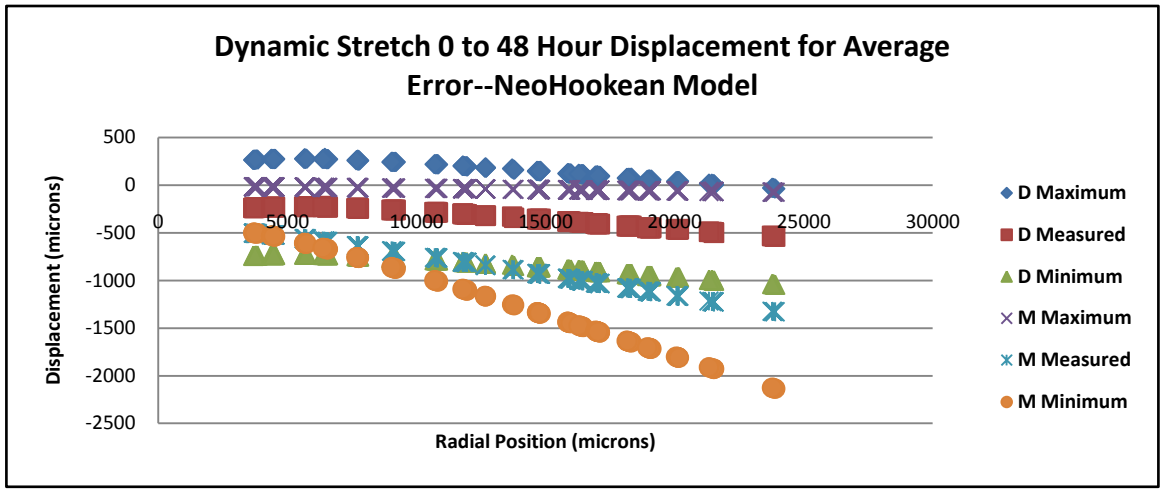

Fig. 32. Plot of uncertainties in ***D*** and ***M*** for dynamic stretch, average error using the NeoHookean model. The plot above illustrates uncertainties for cell displacement ***D*** and membrane displacement ***M*** for the NeoHookean model for the average error in hole radius calculation.

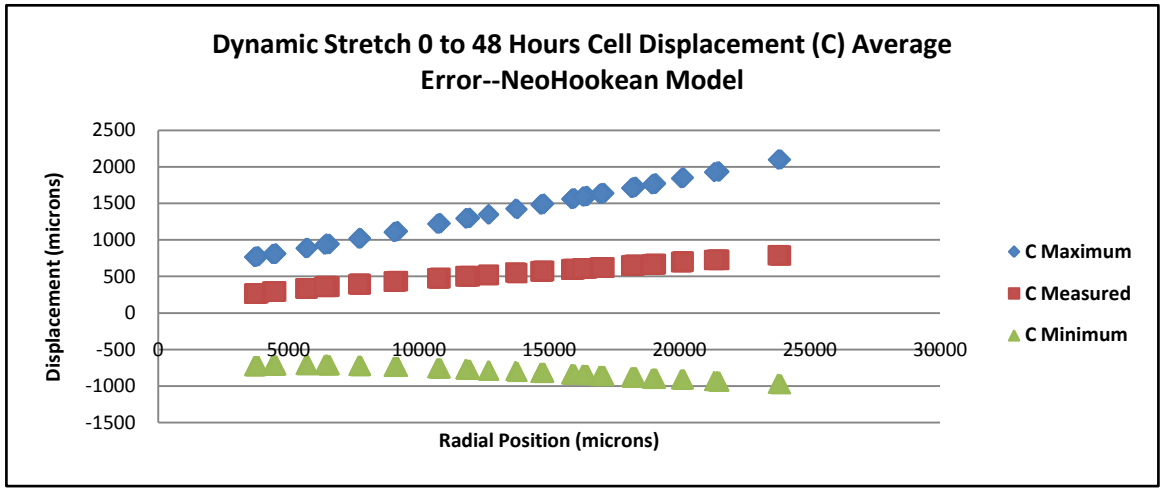

Fig. 33. Plot of uncertainties in ***C*** for dynamic stretch, average error using the NeoHookean model. Cell displacement ***C*** for the NeoHookean model could have been 0 μm and it is not certain that there was cell migration in response to 1Hz dynamic stretch,

5. DISCUSSION

Mechanobiology plays a key role in numerous pathologies, particularly in understanding wound healing and atherogenesis. One component of this involves understanding the cellular response to complex stretch environments like those that occur in vivo. The cell response to these mechanical conditions is the first step in determining specific pathogenic mechanisms and improving implantable device design.

Cells were successfully cultured on the fibronectin-coated membrane in the specially designed culture apparatus and mounted to the cell-stretching device. The device effectively subjected cells to static 6% applied stretch and 6% applied dynamic stretch at 1 Hz for 48 hours. Imaging of cells post-experimentation revealed that they remained adherent and could have remained stretched and intact beyond 48 hours. Live cell imaging was accomplished using fluorescent microscopy, and visualizing identical cell groups across the surface of the membrane at each time point was straightforward using the memorized stage position capability in the Metavue software.

For the static stretch case, there was no evidence of cell migration. The range of uncertainty in true cell migration, $\boldsymbol{C}$ includes both positive and negative values of displacement thus encompassing 0μm displacement. Because of this we cannot be certain of whether cells migrated inward, outward, or if there was any cell migration. There was also no significant cell migration exhibited for cells stretched at dynamic stretch at 1 Hz for 48 hours.

Our method of calculation allowed us to evaluate whether or not migration occurred as well as the direction that migration occurred, that is whether cells migrated inward toward the center hole, or outward toward the edge of the membrane. Though it was hypothesized that cell migration would occur in the both static and dynamic stretch cases, we could not determine conclusively whether or not migration occurred. We believe that this is in part due to the low value of stretch; greater cell migration would be observed at higher frequencies or higher percentages of stretch. For both stretch regimes, there was no discernible cell migration. This could be due to the fact that cell migration as a result of stretch was below the range of accuracy required for this measurement

technique. The cell displacements amongst cells that were imaged initially and at the 48 hour time point were not greater than the limits of uncertainty. This was the case for cells exposed to stretch near the center hole as well as cells exposed to stretch near the outer edge of the membrane.

Raeber and Hubbell (2007) found greater cell migration in response to 20% static stretch than 5% dynamic stretch in the short term. However, as the amount of time cells were exposed to stretch increased the migrational response increased as well. In our case, cells may not have been exposed to enough stretch to produce a definitive migration response or the experiment should have been continued beyond 48 hours to observe a response. The fact that cells underwent a small percentage of stretch and a relatively small stretch gradient is created from this sized center hole may have contributed to the minimal observed cell migration. Though greater stretch gradients could have been produced using the device for this feasibility study we maintained a 6% applied static and dynamic stretch. Fibroblasts are a very robust cell line that may need greater variation in their mechanical stress environment to induce them to migrate to maintain a homeostatic state. In order to increase the stretch gradient the diameter of the center hole in relation to the diameter of the entire membrane could be increased; also, increasing the percentage of stretch and/or the frequency in the dynamics case could lead to more observable migration. The formation of cell contacts may have also inhibited cell movement. According to Lo, C-M. et al.,(2000) cells migrate if there are limited cell-to-cell contacts and they have space to move.

Additionally, the determination of cell movement is dependent on the curve fit of the center hole radius. This creates a range of uncertainty and limits the accuracy of cell migration. To accommodate this uncertainty, measured cell displacements were compared to the minimum and maximum cell displacements for their respective cases. This uncertainty is based on the error in the measurement of the center hole radius which could not be imaged in its entirety due to imaging limitations. Though there may have been some movement it cannot be said conclusively that there was cell migration. A more accurate method of measuring cell displacement would be the addition of fixed

marker points on the membrane that could be imaged using fluorescence microscopy. Having fixed points would aid in a more accurate determination of cell movement. Each image would then have a stationary marker and the cell location could be measured with reference to a known stationary point thereby increasing the accuracy of measured cell migration.

The model used to determine the membrane movement $\boldsymbol{M}$ and in turn the cell movement $\boldsymbol{C}$ also has limitations. The NeoHookean model which was used is dependent on material parameters which were arrived at experimentally, in addition both the NeoHookean model and the kinematic model are reliant upon accurate measurement of the center hole radius, which we have already established introduces some error into the calculation. The kinematic model also has its own set of limitations because it is dependent upon $\boldsymbol{\lambda_z}$, which could not be measured directly, but had to be calculated indirectly. Calculation of $\boldsymbol{\lambda_z}$ in this way also relies on accurately measuring the hole radius at each time point, and yields only an average $\boldsymbol{\lambda_z}$ for the entire membrane.

6. FUTURE WORK

This work provides a basis for further exploration into the concepts of cellular reaction to stretch gradients. Cellular migration and morphology changes could be more pronounced if a larger center hole is incorporated into the membrane thus creating a larger stretch gradient or if greater static and dynamic stretch is produced. These changes can be clearly and accurately measured using the current staining and confocal microscopy techniques. Accuracy could be increased in future, by marking the membrane so that cell migration can be observed relative to a fixed marker at a known radial position on the membrane.

Another adaptation would be the use of a 3-D matrix that allows for greater insight into morphological changes and cell-to-cell interactions. This would also provide a more realistic environment for changes occurring within the body during wound healing or atherosclerosis. Moreover, this device could be used to study additional cell types. Live imaging of the cell-cell interaction between two different cell types, such as smooth muscle cells and endothelial cells would more accurately depict physiologic conditions. This is primarily important in the study of atherosclerosis, when trying to emulate an arterial wall which is composed of many cell and tissue types. Morphological changes and migratory patterns are the more visible reactions to stretch gradients, the study of protein expression and gene regulation would greatly enhance the understanding of various disease states and tissue processes in response to stretch gradients. The use of microarray analysis to evaluate such changes would be a great step towards evaluating possible methods of prevention and treatment of disease at the cellular level.

7. CONCLUSION

In conclusion, we have proven feasibility of a novel system for exposing cells to stretch gradients while maintaining viability for 48 hours. Our device was successfully used to image and monitor cells over the entire 48 hour process. Though our preliminary studies could not demonstrate large cell migrations, the groundwork has been laid for future work that can move beyond the simple 2-D single cell type environment presented here to more complicated 3-D co-culture experiments that more accurately represent the in vivo environment. Such future work will be crucial to the understanding and development of improved treatments for wound healing, atherosclerosis and heart disease.

REFERENCES

Balestrini, J.L., and Billiar, K.L., 2006. Equibiaxial stretch stimulates fibroblasts to rapidly remodel fibrin. Journal of Biomechamics 39. 2983-2990.

Bedoya, J., Meyer, C.A., Timmins, L.H., Moreno, M.R., Moore, J.E. 2006. Effects of stent design parameters on normal artery wall mechanics. Journal of Biomechanical Engineering 128. 757-765.

Beningo, K.A., and Wang, Y-L., 2007. Double-hydrogel substrate as a model system for three-dimensional cell culture. Methods in molecular biology, vol. 370: Adhesion Protein Protocols. 203-211

Bischofs, I.B., Schwarz, U.S., 2003. Cell organizationin soft media due to active mechanosensing. Proceedings of the National Academy of Sciences 100. 9274-9279.

Brown, R.A., Prajapati, R., McGrouther, D.A., Yannas, I.V., Eastwood, M., 1998. Tensional homeostasis in dermal fibroblasts: mechanical responses to mechanical loading in three-dimensional substrates. Journal of Cellular Physiology 175. 323-332.

Bush, J.A., Ferguson, M.W.J., Mason, T., McGrouther, D.A., 2007. Skin tension or skin compression? Small circular wounds are likely to shrink, not gape. Journal of Plastic, Reconstructive, and Aesthetic Surgery xx. 1-6.

Chuong, C.J., Fung, Y.C., 1986. On Residual Stress in Arteries. Journal of Biomechanical Engineering 108. 189-192.

Clark, R.A.F., 1996. Molecular and cellular biology of wound repair. Plenum Press; New York. pp.13-27.

David, G., and Humphrey, J.D., 2004. Redistribution of stress due to a circular hole in a nonlinear anisotropic membrane. Journal of Biomechanics 37. 1197-1203.

Delfino, A., Moore, J.E., Stergiopulos, N., Vaclavik, V., Genton, C.Y., Meister, J.J., 1998. Wall stresses in the carotid bifurcation: effects of wal non-homogeneity and correlation with intimal thickness. Journal of Vascular Investigations 4. 61-71.

DiPietro, L.A., and Burns, A.L., 2003. Wound healing: methods and protocols. Humana Press; Totowa, NJ, pp. 37-41.

Grymes, R.A., and Sawyer, C., 1997. A novel culture morphology resulting from applied mechaical strain. In Vitro Cellular Developmental Biology 33. 392-297.

Guo, W., Frey, M.T., Burnham, N.A., Wang, Y., 2006. Substrate rigidity regulates the formation and maintenance of tissues. Biophysical Journal 90. 2213-2220.

Heistand, M.R., Pedrigi, R.M., Delange, S.L., Dziezyc, J., Humphrey, J.D., 2005. Multiaxial mechanical behavior of the porcine anterior lens capsule. Biomechanics and Modeling in Mechanobiology 4. 168-177.

Hinz, B., and Gabbiani, G., 2003. Mechanisms of force generation and transmission by myofibroblasts. Current Opinion in Biotechnology 14. 538-546.

Li, S., Butler, B., Wang, Y., Hu, Y., Han, D.C., Usami, S., Guan, J-L., Chien, S. 2002. The role of the dynamics of focal adhesion kinase in the mechanotaxis of endothelial cells. Proceedings of the National Academy of Science 99. 3546-3551.

Lo, C-M., Wang, H-B., Dembo, M., Wang, Y-L., 2000. Cell movement is guided by the rigidity of the substrate. Biophysical Journal 79. 144-152.

Loesberg, W.A., Walboomers, X.F., van Loon, J.J.W.A., Jansen, J.A. 2005. The effect of combined cyclic mechanical stretching and microgrooved surface topography on the behavior of fibroblasts. Journal of Biomedical Materials Research 75A. 723-732.

Martin, P. 1997. Wound healing—aiming for perfect skin regeneration. Science 276. 75-81.

Ohashi, T., Masuda, M., Matsumoto, T., Sato, M., 2007. Nonuniform strain of substrate induces local development of stress fibers in endothelial cells under uniaxial cyclic stretch. Clinical Hemorheology and Microcirculation 37(1-2). 37-46.

Pelham Jr., R.J., and Wang, Y-L, 1997. Cell locomotion and focal adhesions are regulated by substrate flexibility. Proceedings of the National Academy of Sciences 94. 13661-13665

Pickett, B.P., Lawrence, P.A., Burgess, M.C., Livermore, G.H., Tzikas, T.L., Vossoughi, J., 1996. Tensile strength vs healing time for wounds closed under tension. Archives of Otolaryngology-Head and Neck Surgery 122. 565-568.

Raeber, G.P., Lutolf, M.P., Hubbell, J.A., 2007. Part II: Fibroblasts preferentially migrate in the direction of principal strain. Biomechanics and Modeling in Mechanobiology 7. 215-225.

Raeber, G.P., Mayer, J., Hubbell, J.A., 2008. Part I: A novel in-vitro system for simultaneous mechanical stimulation and time-lapse microscopy in 3D. Biomechanics and Modeling in Mechanobiology 7(3). 203-214.

Sheetz, M.P., Felsenfeld, D.P., Galbraith, C.G., 1998. Cell migration: regulation of force on extracellular-matrix-integrin complexes. Trends in Cell Biology 8(2). 51-54.

Silver, F.H., Siperko, L.M., Seehra, G.P., 2003. Mechanobiology of force transmission in dermal tissue. Skin Research and Technology 9. 3-23.

Thampatty, B.P., and Wang, J.H.-C., 2007. An new approach to study fibroblast migration. Cell Motility and the Cytoskeleton 64. 1-5.

Vande Geest, J.P., Di Martino, E.S., Vorp, D.A., 2004. An analysis of the complete strain field within Flexercell^{TM} membranes. Journal of Biomechanics 37. 1923-1928.

Zuber, T.J., 2002. Punch biopsy of the skin. American Family Physician 65. 1155-1158

APPENDIX A

Cell Stretch Device Drawings and Assembly

All units are in centimeters.

Box Assembly

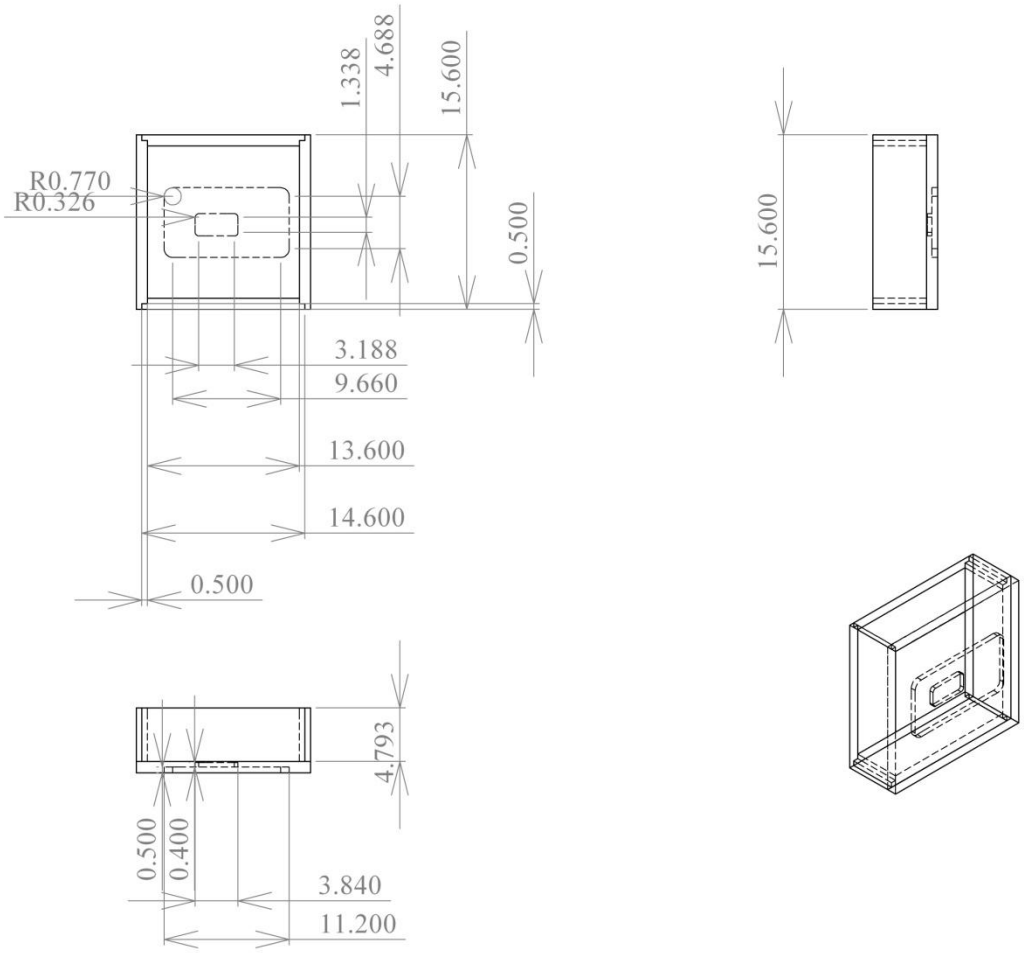

Bottom Box Assembly

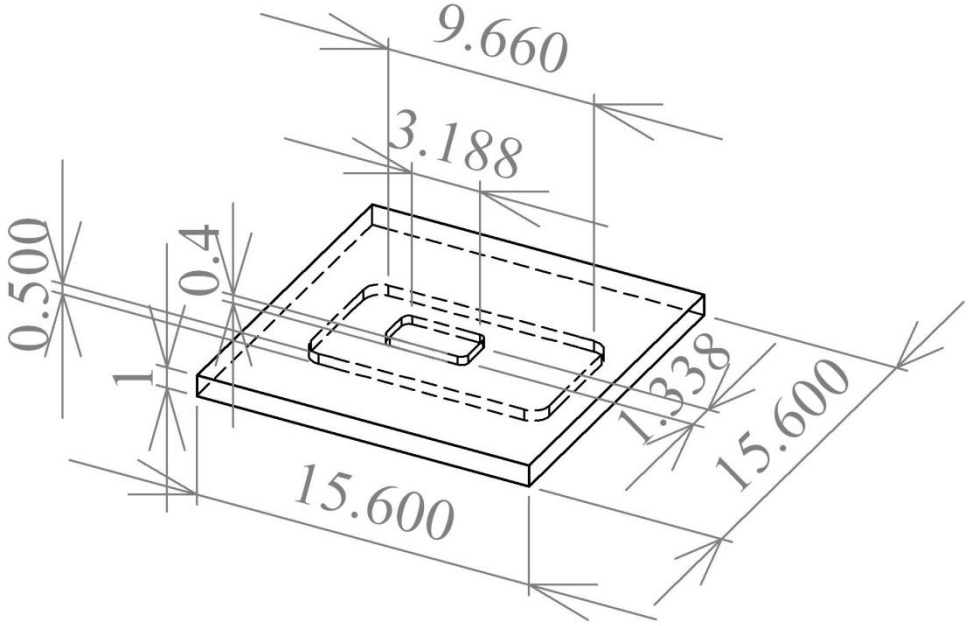

Box-Bottom Plate

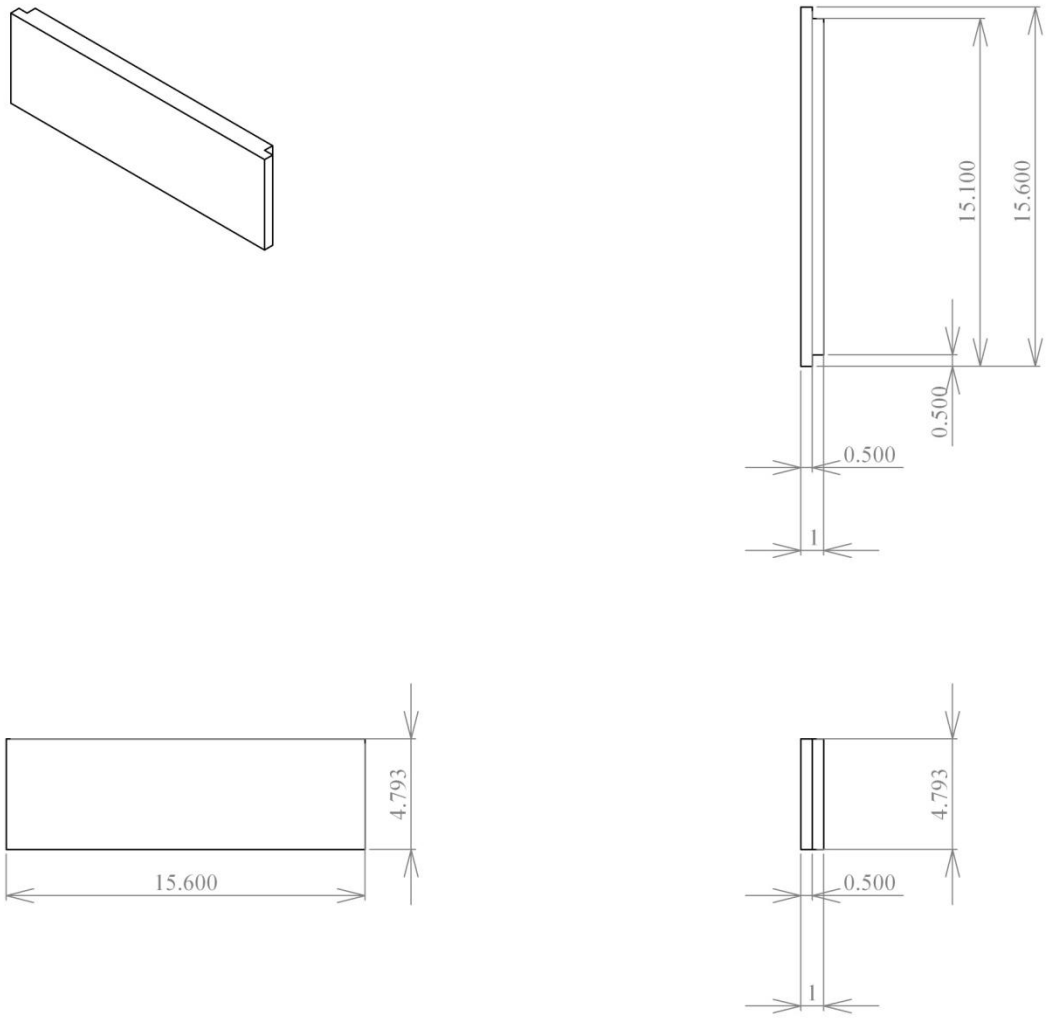

Box-Side Plate A

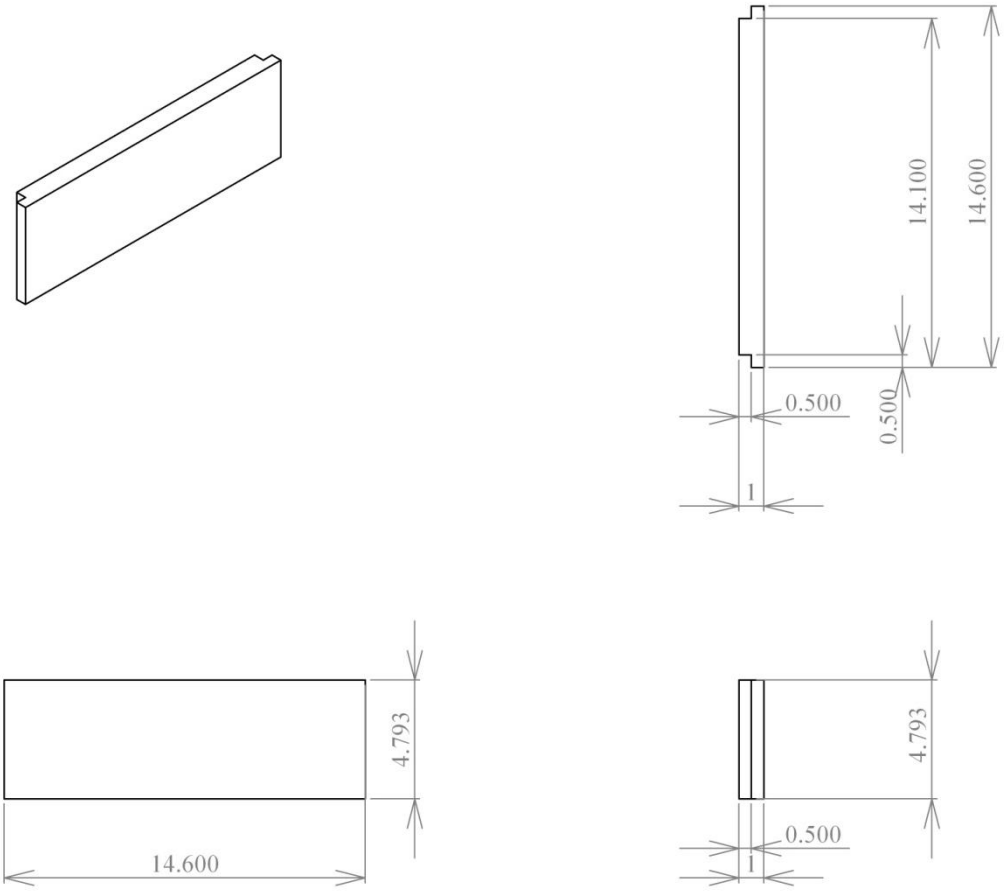

Box-Side Plate B

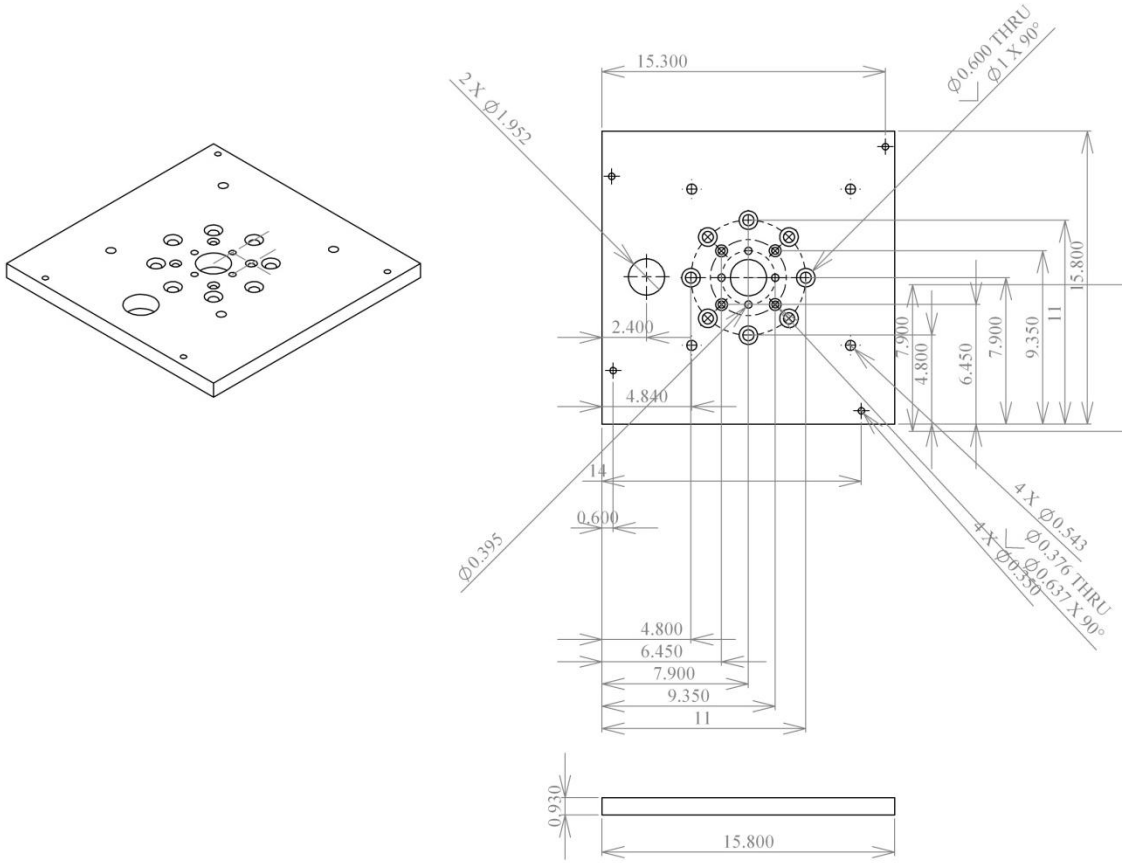
15.300
2 X Ø1.952
Ø0.600 THRU
Ø1 X 90°
15.800
11
9.350
7.900
6.450
4.800
7.900
2.400
4.840
14
0.600
Ø0.395
4 X Ø0.543
Ø0.376 THRU
4 X Ø0.350
Ø0.637 X 90°
4.800
6.450
7.900
9.350
11
0.930
15.800

Box-Lid

Motor Assembly

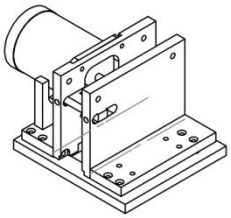

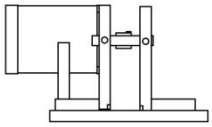

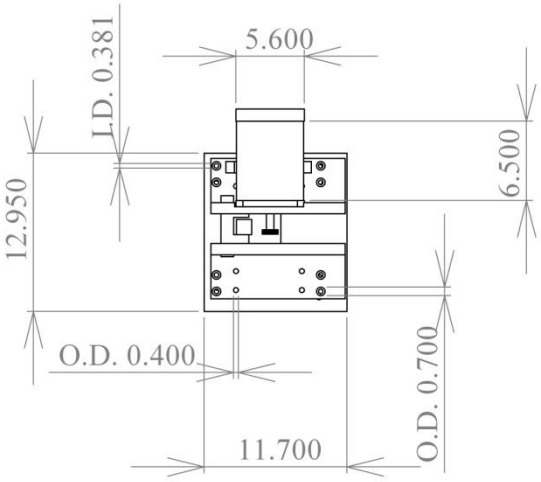

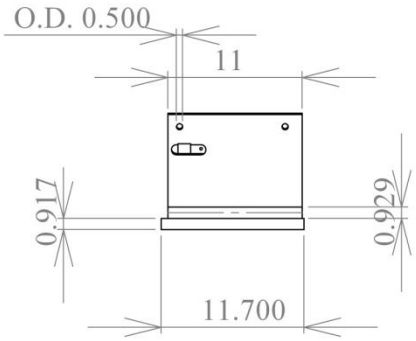

Motor Assembly

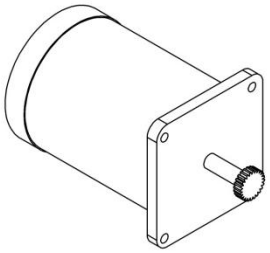

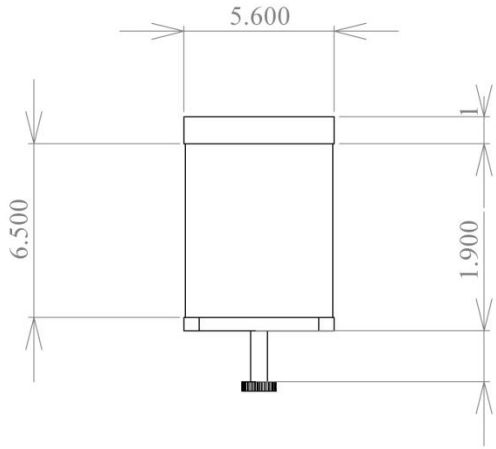

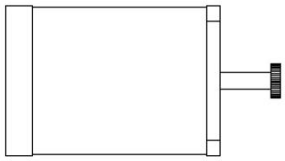

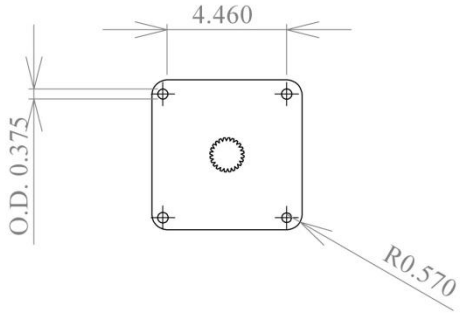

Motor

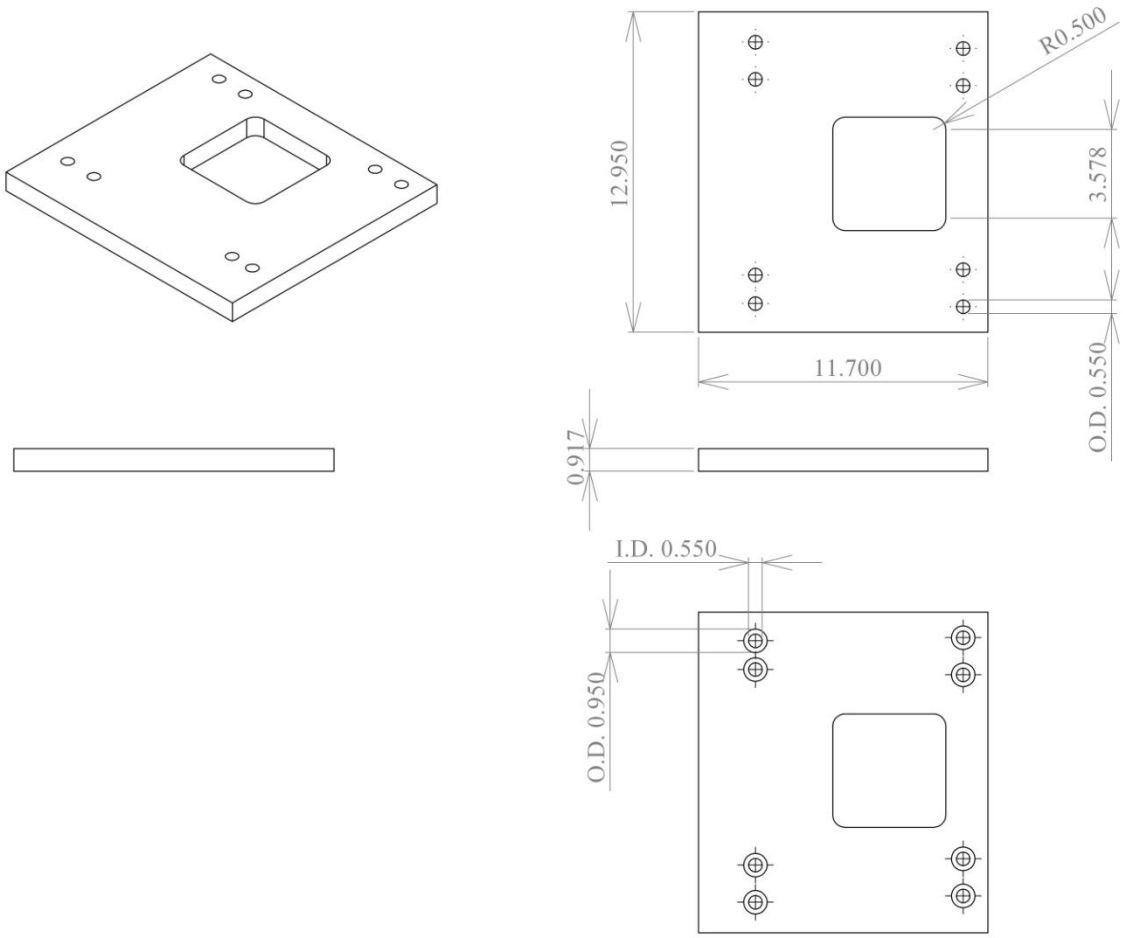

Motor Support-Bottom Plate

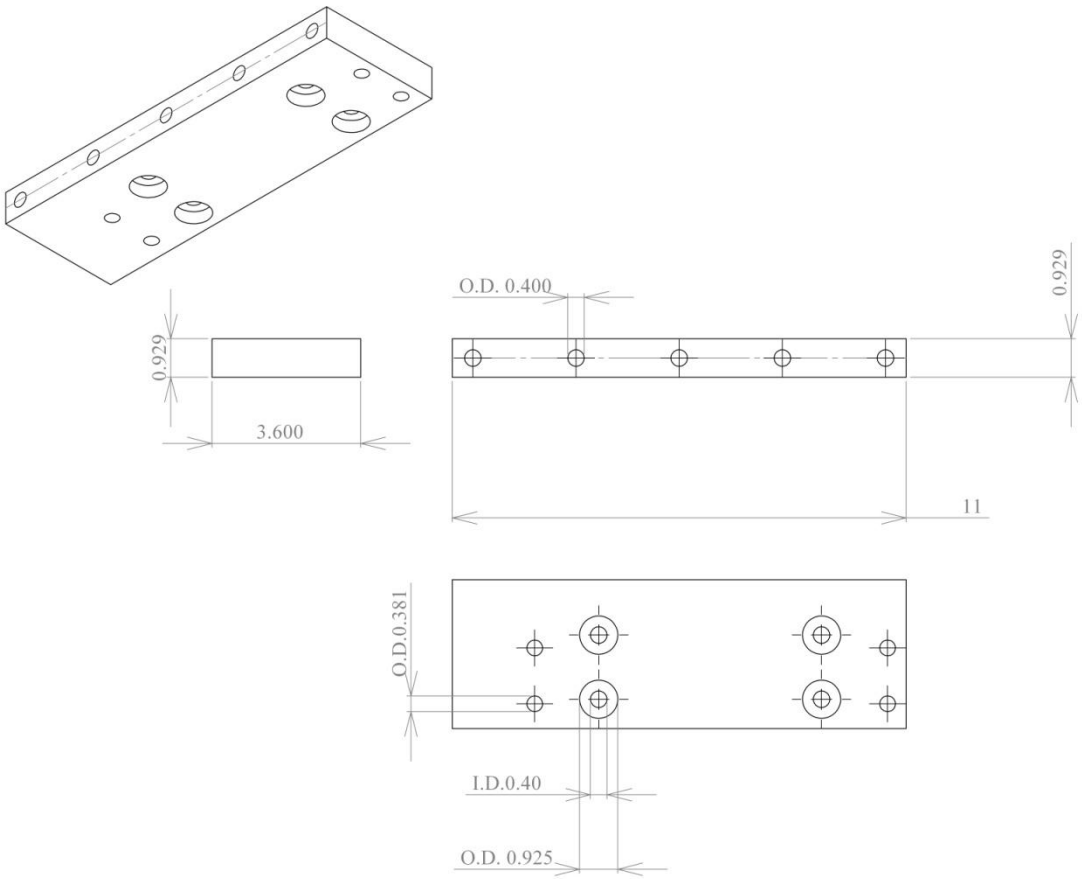

Motor Support Base Plate-A

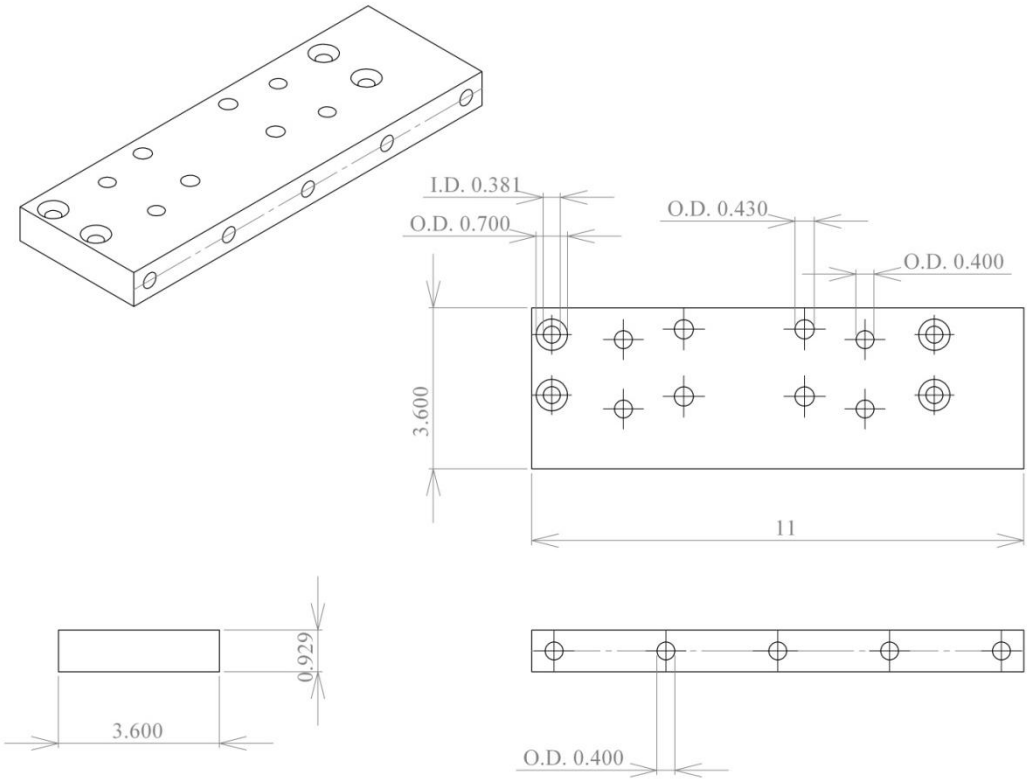

Motor Support-Base Plate B (Motor Side)

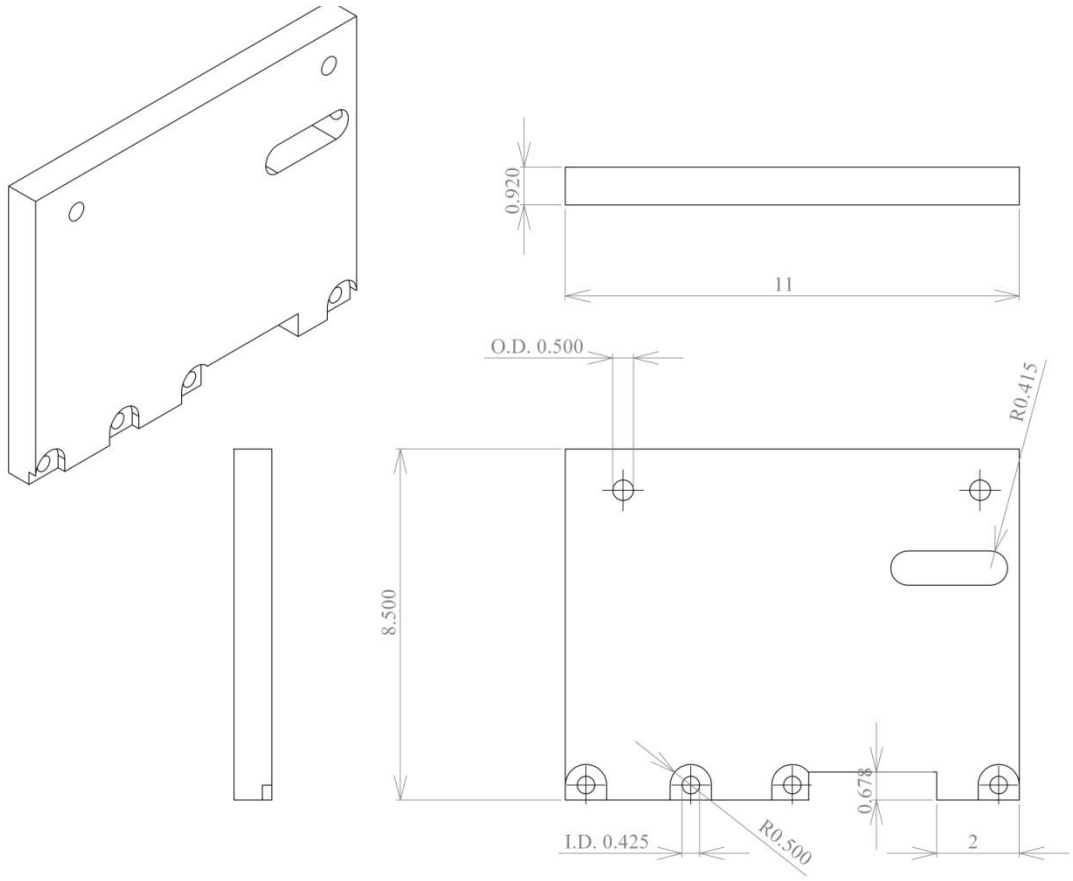

Motor Support- Side Support A

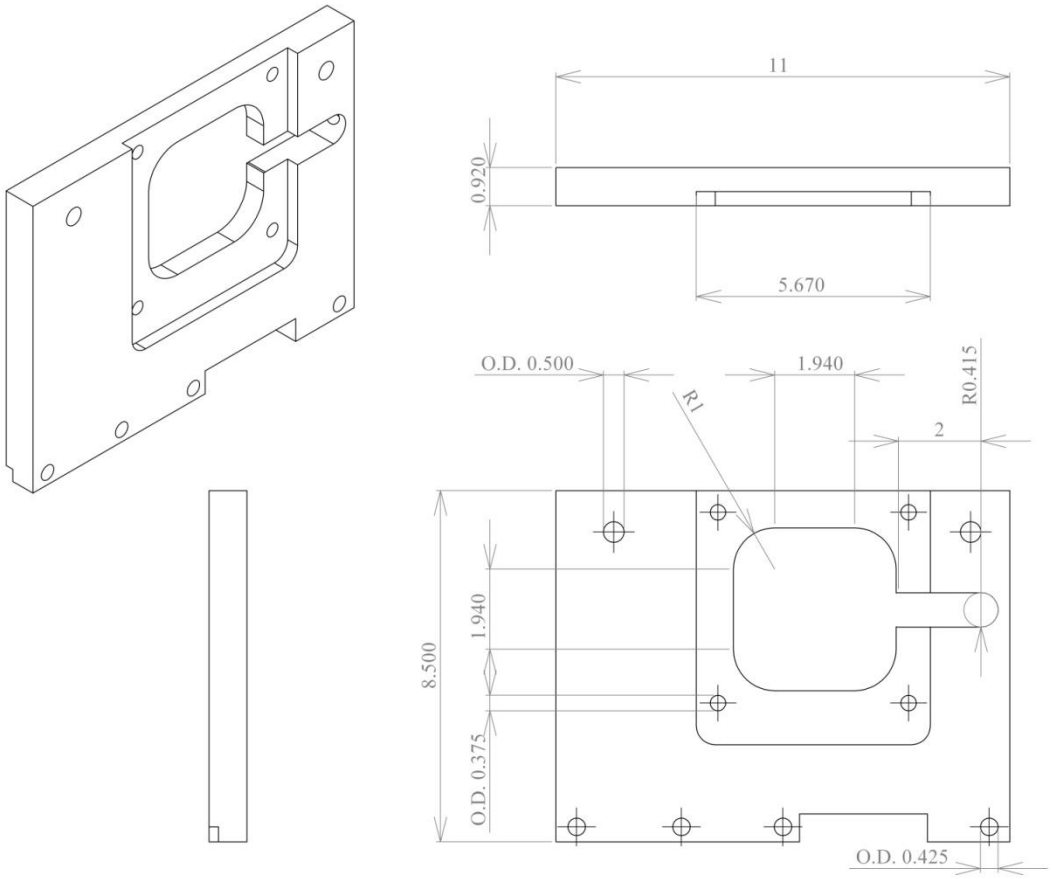

Motor Support-Side Support B (Motor Side)

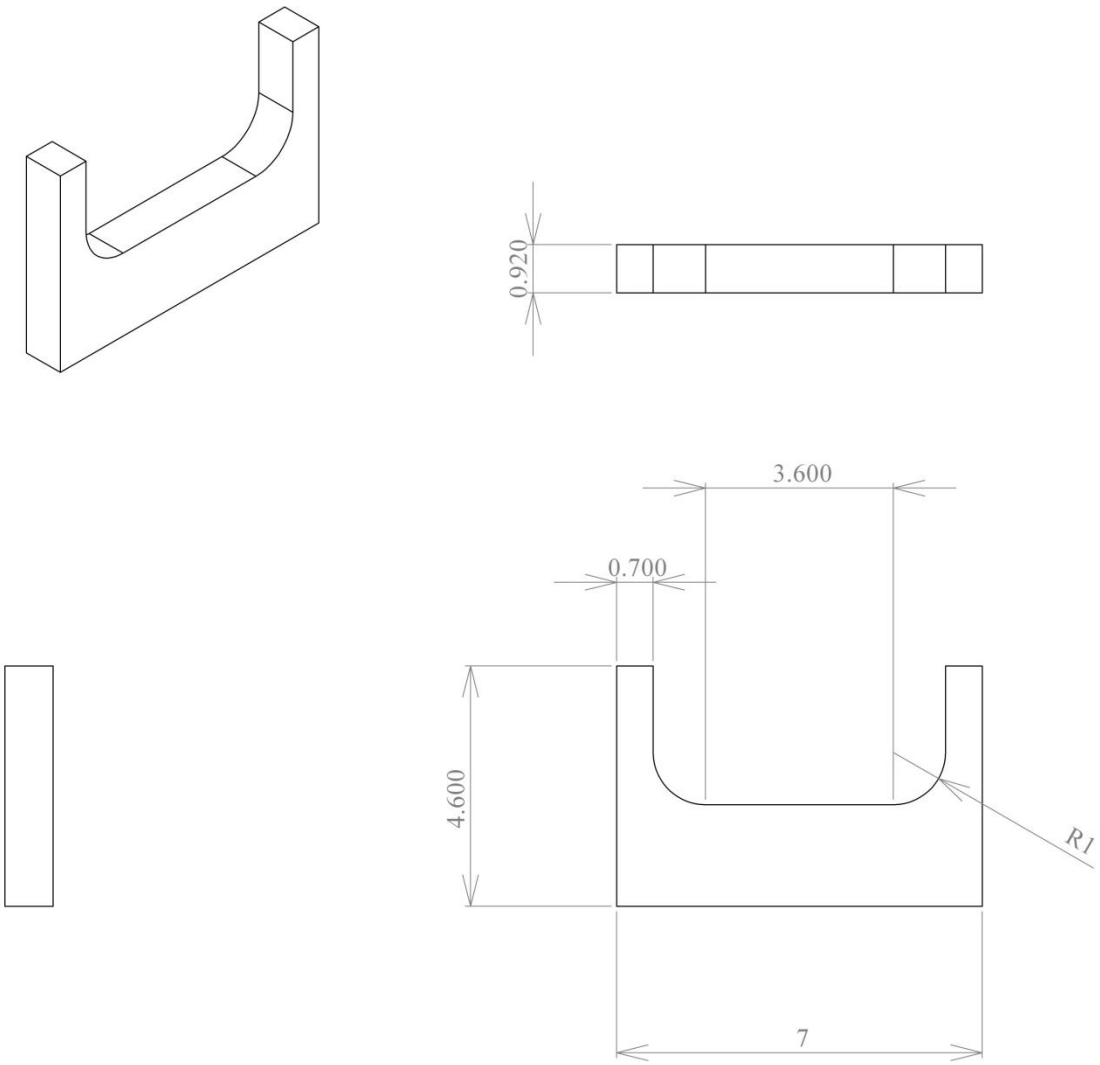

Motor Support Plate

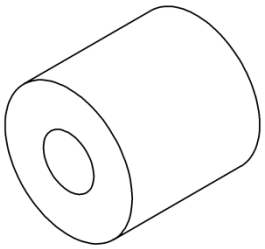

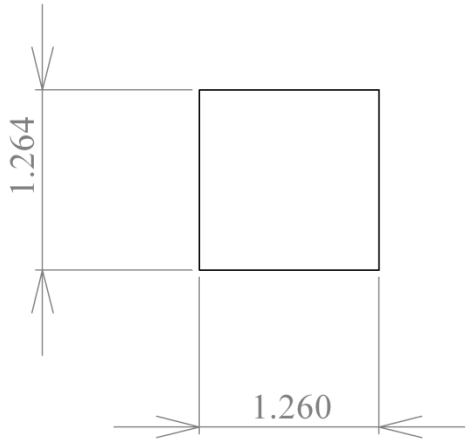

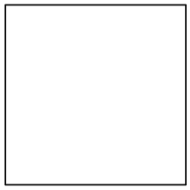

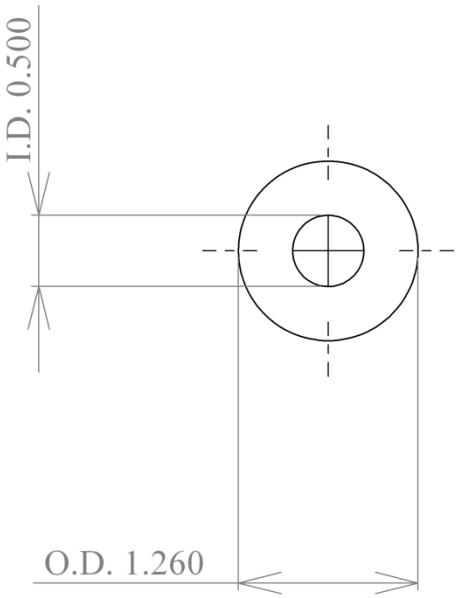

Cylinder Insert

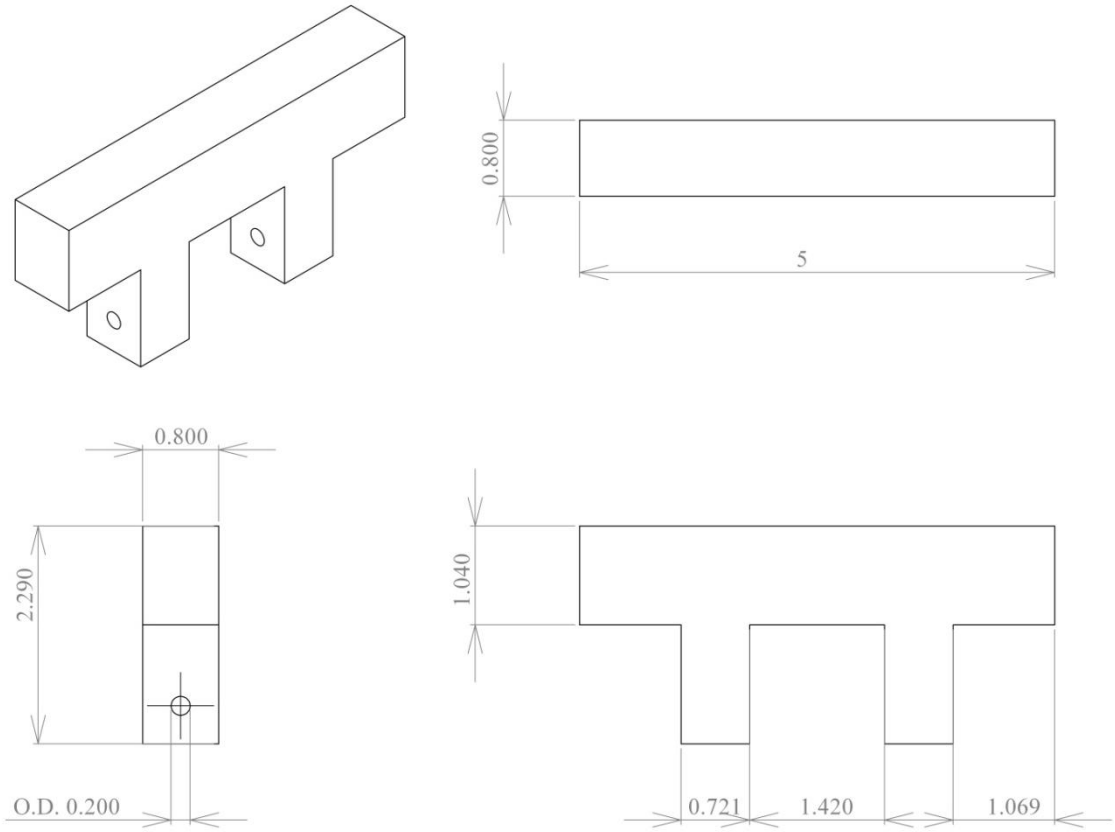

Cylinder Insert Support

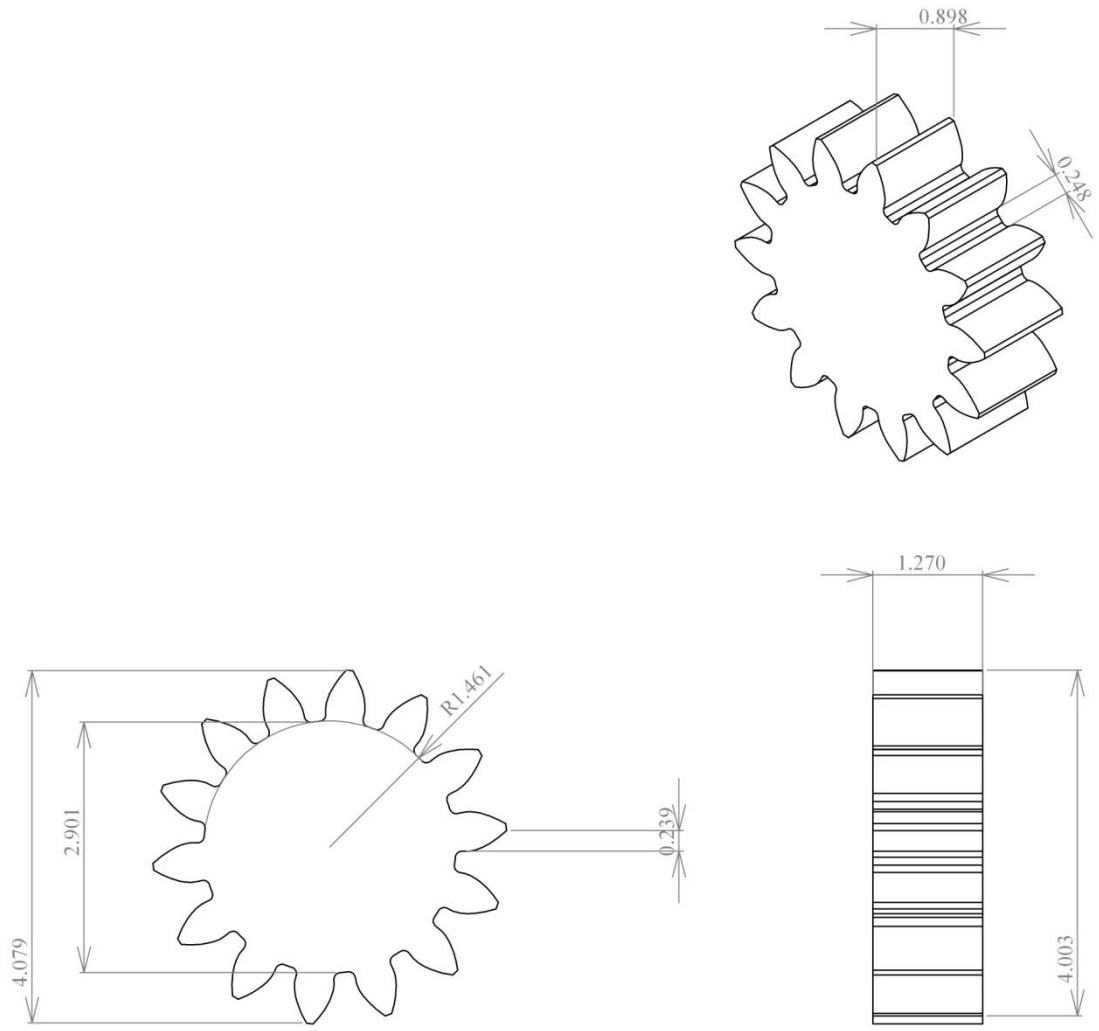

Gear

Cell Stretcher Assembly

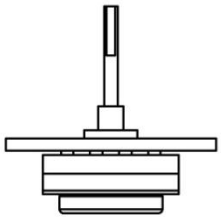

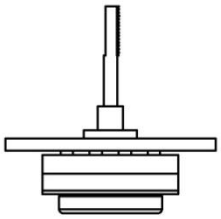

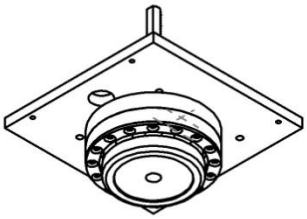

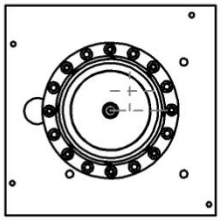

Cell Stretcher Assembly

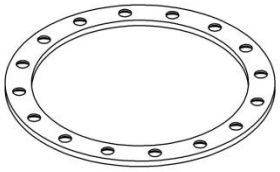

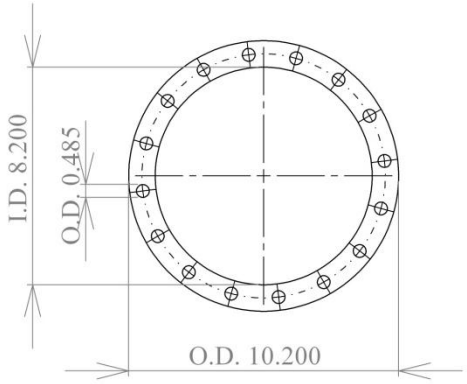

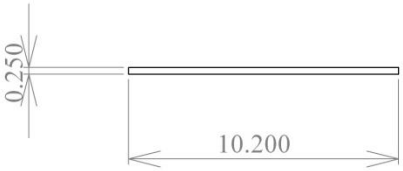

16 Hole Thin Ring

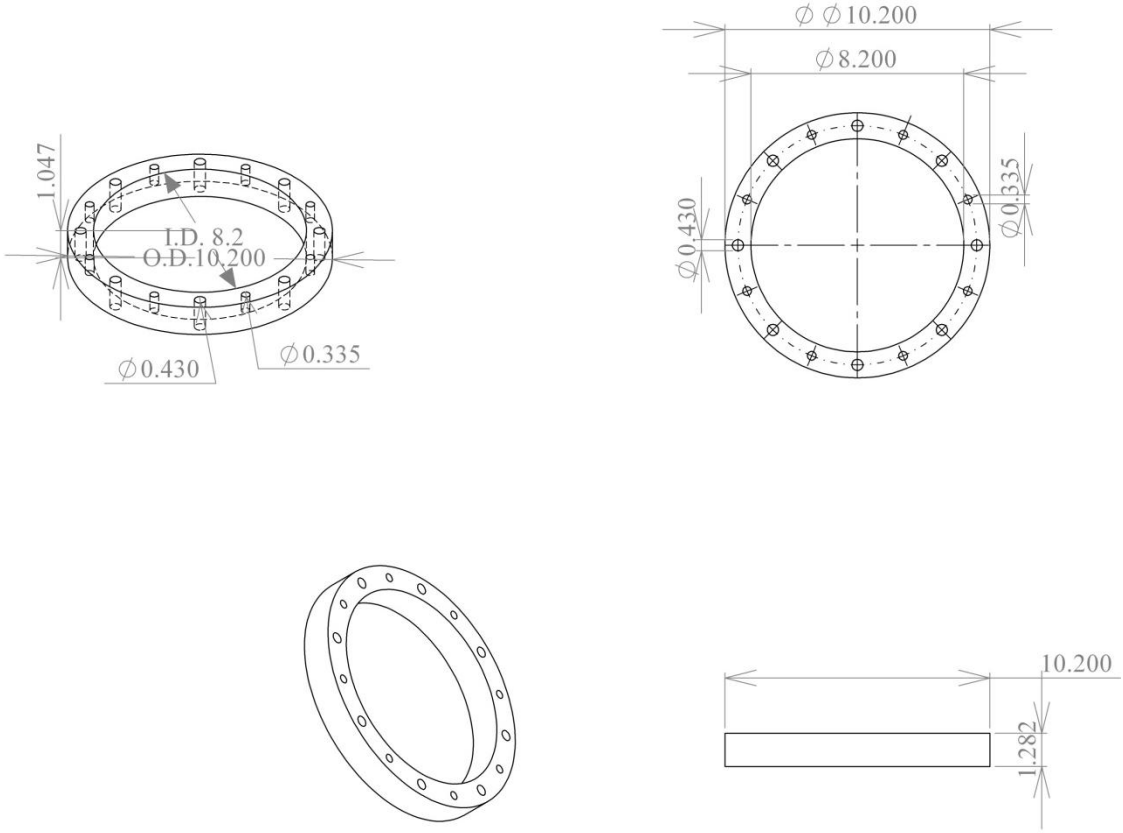

16 Hole Thick Ring

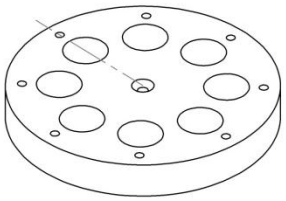

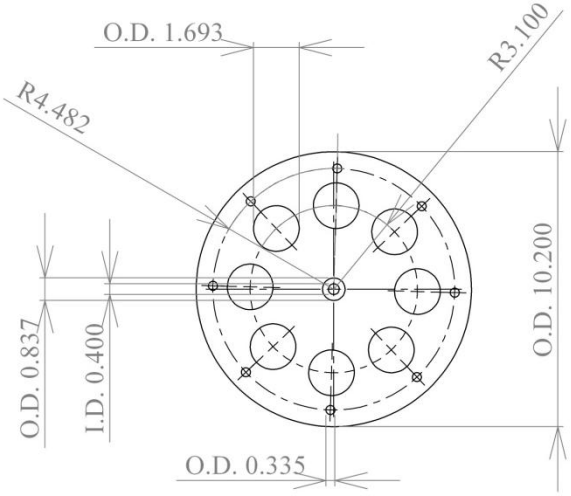
O.D. 1.693
R3.100
R4.482
O.D. 10.200
O.D. 0.837
I.D. 0.400
O.D. 0.335

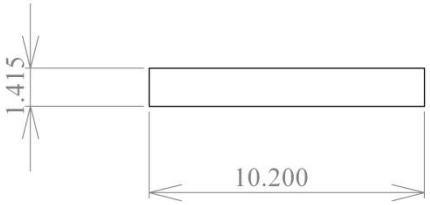
1.415
10.200

8 Hole Disk

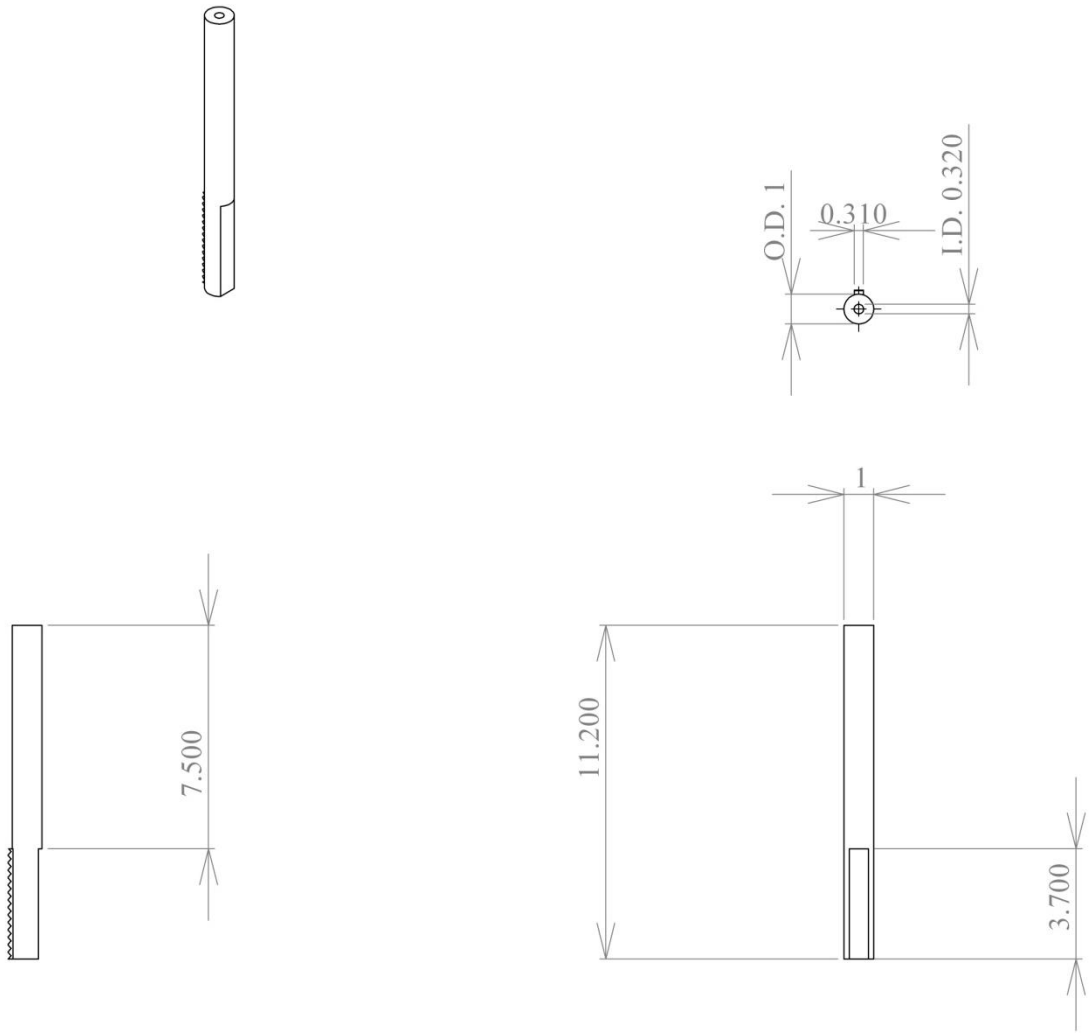

Gear Shaft

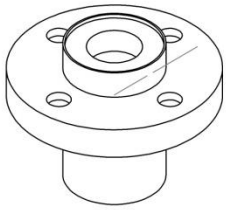

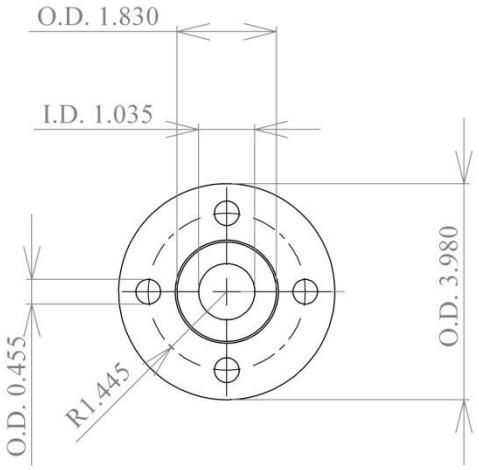

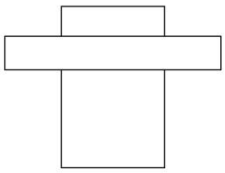

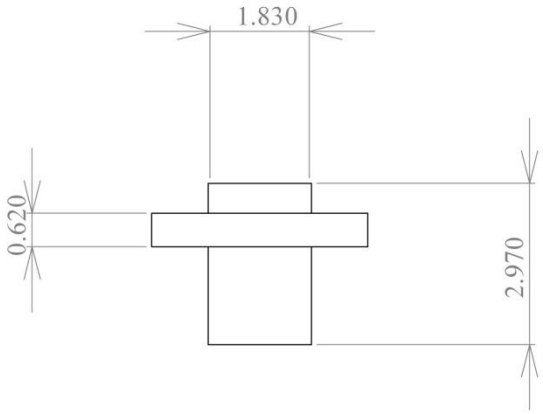

Bushing

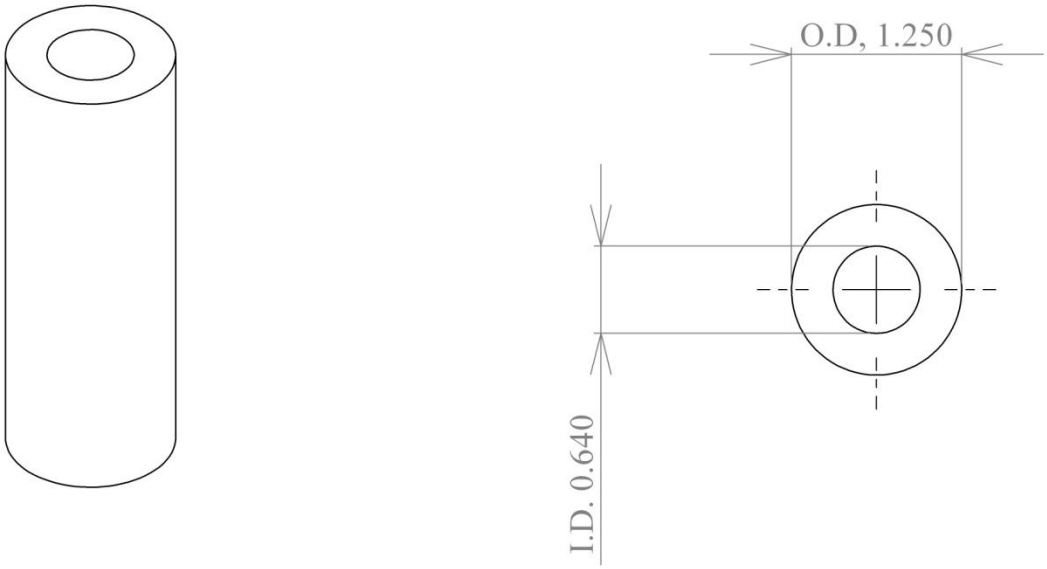

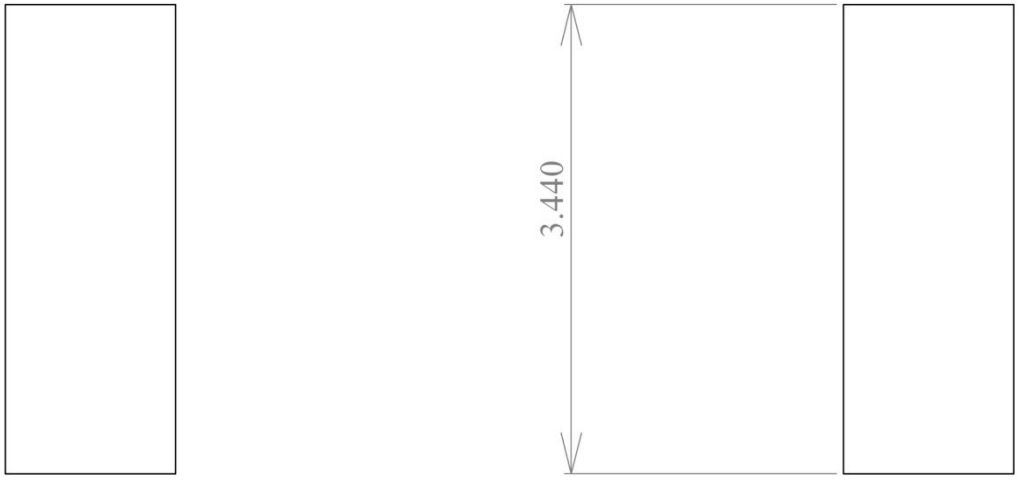

Short Tube

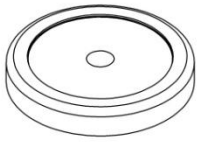

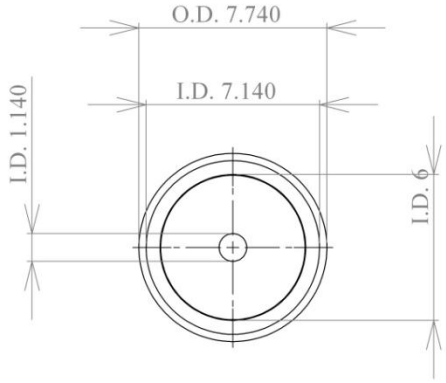

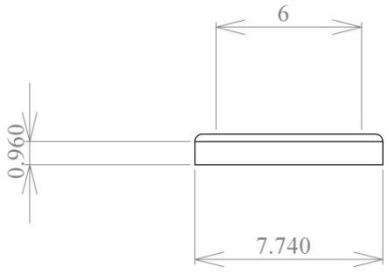

Solid Disk

Cell Culture Portion of the Device

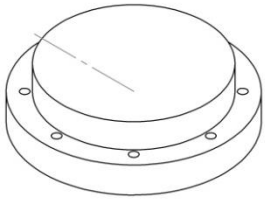

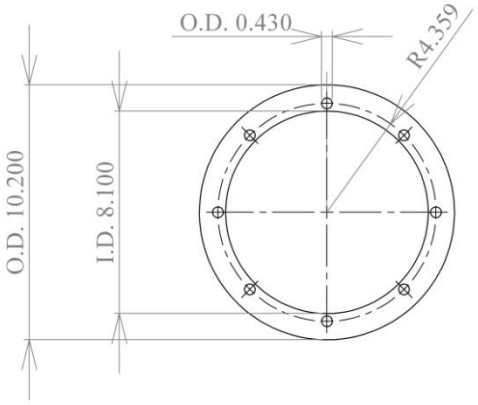

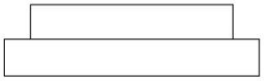

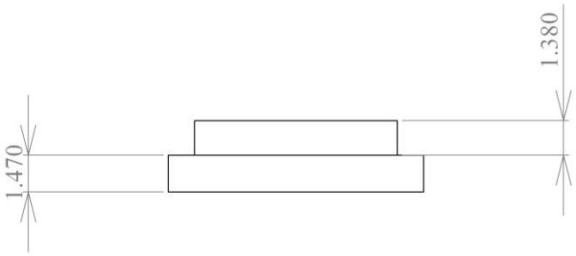

Cell Culture Platform

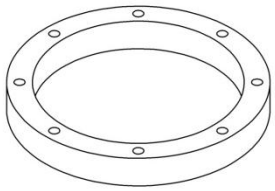

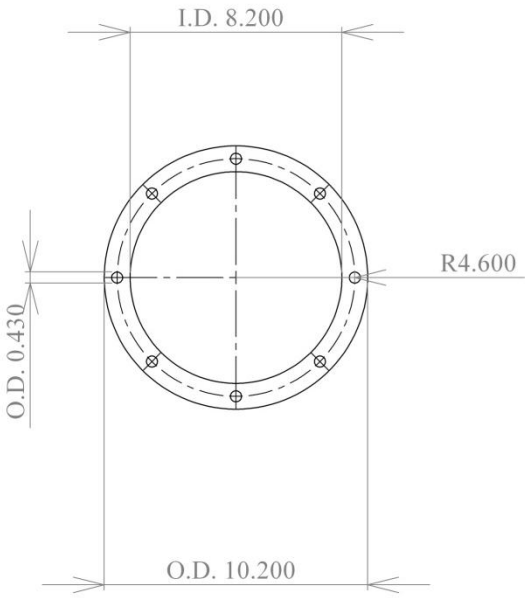

Pre-Stretch Thick Ring

APPENDIX B

NeoHookean Constitutive Equation

David & Humphrey 2004 Solved the following equation

$$r'' = \frac{(t_{\theta\theta} - t_{rr})\left(\frac{\lambda_R}{r}\right) + \frac{\partial t_{rr}}{\partial \lambda_\theta} * (\lambda_\theta - \lambda_R)\frac{1}{R}}{\frac{\partial t_{rr}}{\partial \lambda_R}}$$

Where
R:undeformed radius
r: deformed radius
r': $\frac{dr}{dR} = \lambda_R$

$$F = \begin{bmatrix} \lambda_R & 0 \\ 0 & \lambda_\theta \end{bmatrix} = \begin{bmatrix} r' & 0 \\ 0 & \frac{r}{R} \end{bmatrix}$$

NeoHookean Model:
Where I is the 1st invariant of the strain tensor
II is 2nd invariant of the strain tensor

$$I = tr[C] = \lambda_1 + \lambda_2 + \lambda_3$$

$$II = \frac{1}{2}(tr[C])^2 - tr[C^2] = \lambda_1^2\lambda_2^2 + \lambda_2^2\lambda_3^2 + \lambda_3^2\lambda_1^2$$

$$C = F^T F$$

$$C = \begin{bmatrix} \lambda_1^2 & 0 & 0 \\ 0 & \lambda_2^2 & 0 \\ 0 & 0 & \lambda_3^2 \end{bmatrix}$$

Plug the 1st and 2nd invariants into the NeoHookean Constitutive Equation

$$W = c(I - 3)$$

$$W = c(\lambda_1^2 + \lambda_2^2 + \lambda_3^2 - 3)$$

where c is the material parameter with units of kPa found through material testing.

For Incompressibility $\lambda_1^2\lambda_2^2\lambda_3^2 = 1$

In our case NeoHookean model takes the form

$$W = c\left(\lambda_R^2 + \lambda_\theta^2 - 2\right)$$

In our case for incompressibility $\lambda_R^2\lambda_\theta^2\lambda_Z^2 = 1$

$$E = \begin{bmatrix} E_{RR} & 0 \\ 0 & E_{\theta\theta} \end{bmatrix} = \frac{1}{2}\begin{bmatrix} \lambda_R^2 - 1 & 0 \\ 0 & \lambda_\theta^2 - 1 \end{bmatrix}$$

$$t_{rr} = \lambda_r^2 \frac{\partial W}{\partial E_{rr}} = 2c\lambda_r^2$$

$$t_{\theta\theta} = \lambda_\theta^2 \frac{\partial W}{\partial E_{\theta\theta}} = 2c\lambda_\theta^2 - 1$$

Plug the $t_{RR}\ and\ t_{\theta\theta}$ into the equation for r'' from David and Humphrey and we can solve for membrane displacement using only material parameters c_1 and c_2 as well as r and R

λ_θ^{outer} is the circumferential stretch (load)applied to the outer edge to go from R_{inner} to r_{inner}

Boundary condition to solve the differential eqn that finds r'' is that t_{rr}=0 at the outer edge

$$\left.\frac{dr}{dR}\right|_{R_i} = 1 \Big\} B.C.\ to\ solve\ for\ r''$$

t_{RR} is greatest at outer edge-radial stress
$t_{\theta\theta}$ is greatest at the inner edge-circumferential stress

MATLAB CODE

MoonRiveEq12

$$\boldsymbol{y(1) = r}$$

$$\boldsymbol{y(2) = \frac{dr}{dR} = r' = \frac{dy(1)}{dR}}$$

$$\boldsymbol{dy(2) = r'' = \frac{\frac{\lambda_R}{r}(t_{\theta\theta} - t_{rr}) + \frac{\partial t_{rr}}{\partial \lambda_\theta}(\lambda_\theta - \lambda_R)\frac{1}{R}}{\frac{\partial t_{rr}}{\partial \lambda_R}}}$$

APPENDIX C

Kinematic Equation

The following illustrates how the kinematic equation used in our data analysis was derived, and gives a brief example of its use.

Finding Kinematic Equation

$$F = \begin{bmatrix} \frac{dr}{dR} & 0 & 0 \\ 0 & \frac{r}{R} & 0 \\ 0 & 0 & \lambda_z \end{bmatrix}$$

For Incompressibility

$$det[F] = 1$$

$$\frac{dr}{dR}\left(\frac{r}{R}\right)\lambda_z = 1$$

$$r\frac{dr}{dR} = \frac{R}{\lambda_z}$$

Integrate both sides

$$\int_{r_i}^{r} r\frac{dr}{dR}\,dR = \int_{R_i}^{R} \frac{R}{\lambda_z}\,dR$$

$$\frac{1}{2}r^2\Big|_{r_i}^{r} = \frac{1}{2\lambda_z}R^2\Big|_{R_i}^{R}$$

$$\frac{1}{2}(r^2 - r_i^2) = \frac{1}{2\lambda_z}(R^2 - R_i)$$

$$r^2 - r_i^2 = \frac{1}{\lambda_z}(R^2 - R_i^2)$$

$$r^2 = r_i^2 + \frac{1}{\lambda_z}(R^2 - R_i^2)$$

$$r = \sqrt{r_i^2 + \frac{1}{\lambda_z}(R^2 - R_i^2)}$$

Example of solving a kinematic model for Static Stretch 0-48 Hours and incompressibility

$$P_{48}^{est} = \sqrt{\left(r_{inner}^{48}\right)^2 - \frac{1}{\lambda_z}\left((P_0)^2 - \left(R_{inner}^{0}\right)^2\right)}$$

$$where\ P_0\ is\ the\ radial\ position\ at\ time\ 0$$

$$R_{inner}^{0} \; is \; the \; hole \; radius \; at \; time \; 0$$
$$r_{inner}^{48} \; is \; the \; hole \; radius \; at \; time \; 48$$
$$P_{48}^{est} \; is \; the \; estimated \; radial \; position \; from \; kinematics$$

Next to solve for the membrane displacement for 0 to 48 hours

$$M_{0,48} \; is \; the \; membrane \; displacement \; from \; 0 \; tot \; 48 \; hours \; for \; each \; point \; where \; a \; cell \; is \; located$$
$$M_{0,48} = P_{48}^{est} - P_0$$

APPENDIX D

Volume Conservation

Estimating an average λ_z for the kinematic model, from volume conservation based on incompressibility.

Where:
V=Volume
A=Area
t=Membrane Thickness

$$V = A * t$$
$$A_0 t_0 = A_{48} t_{48}$$
$$\frac{A_0}{A_{48}} = \frac{t_{48}}{t_0}$$
$$\frac{\pi R_{outer}^2 - \pi R_{inner}^2}{\pi r_{outer}^2 - \pi r_{inner}^2} = \frac{t_{48}}{t_0} = \lambda_z$$

$$\boldsymbol{\frac{R_{outer}^2 - R_{inner}^2}{r_{outer}^2 - r_{inner}^2} = \lambda_z}$$

APPENDIX E

Plots of λ_z

Supplemental Plots from using the NeoHookean Model to calculate $\boldsymbol{\lambda_z}$

Static Stretch

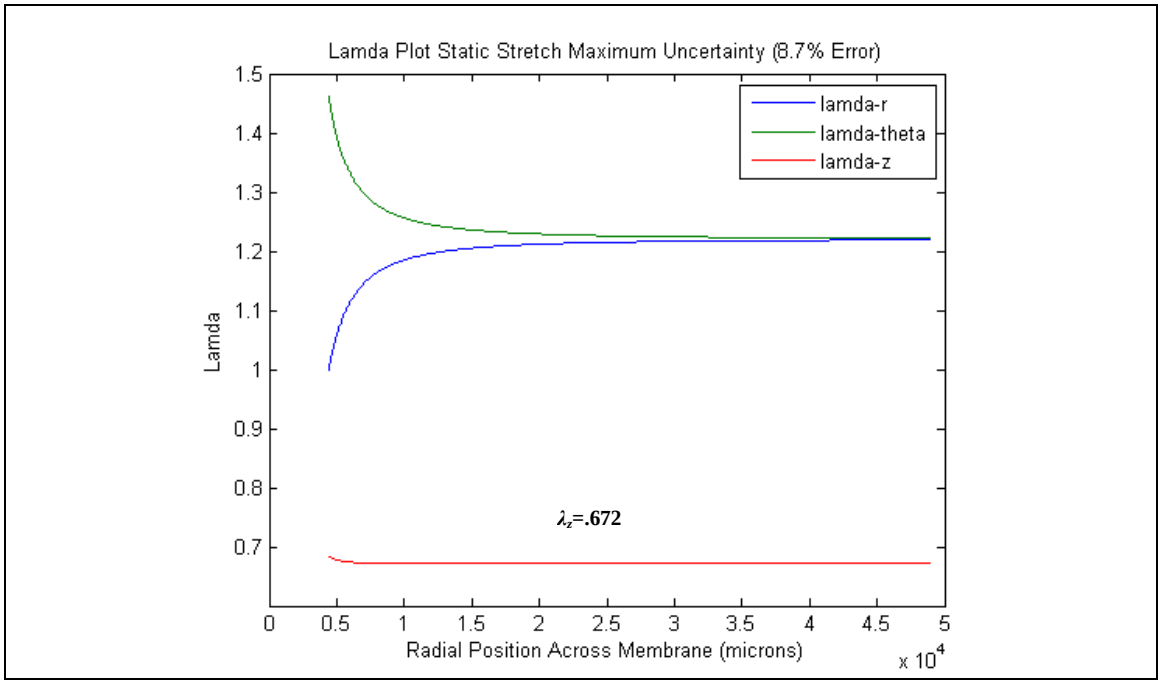

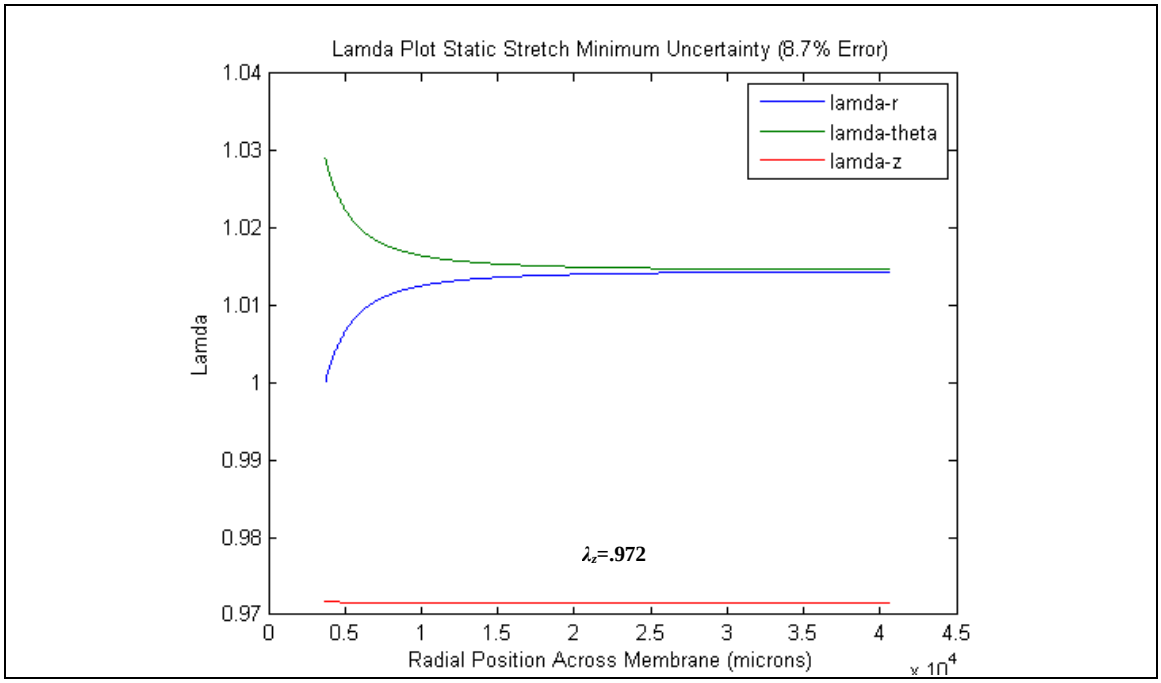
Lamda Plot Static Stretch Minimum Uncertainty (8.7% Error)
lamda-r
lamda-theta
lamda-z
Lamda
Radial Position Across Membrane (microns)
x 10^4
λz=.972

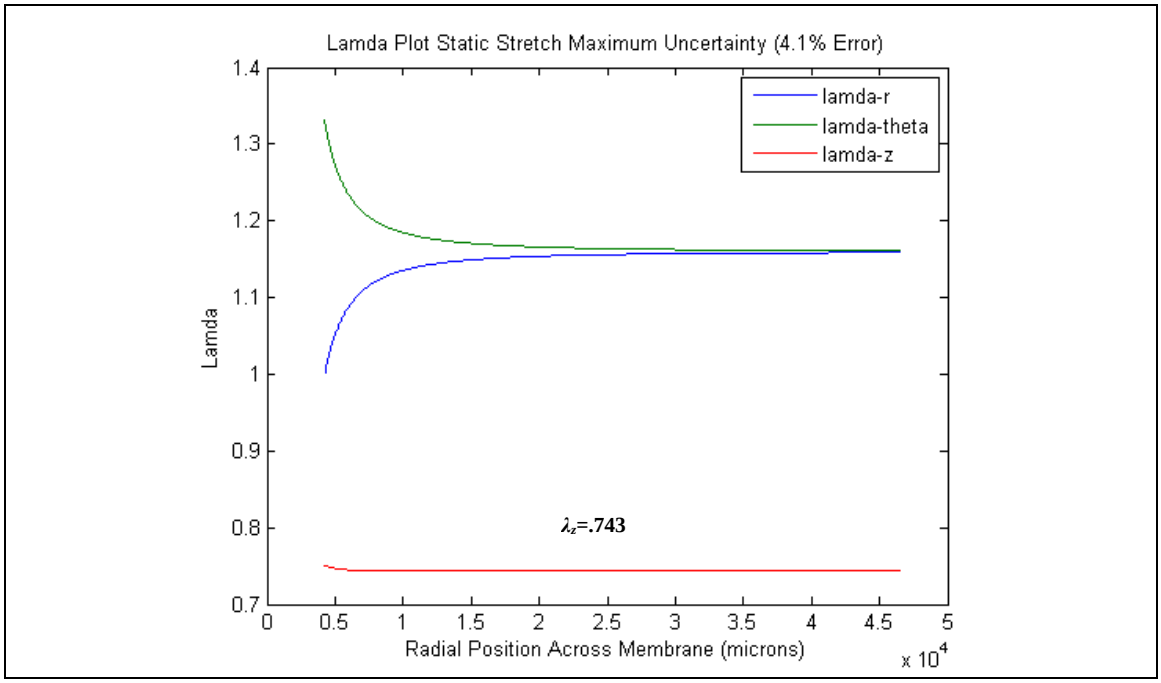
Lamda Plot Static Stretch Maximum Uncertainty (4.1% Error)
lamda-r
lamda-theta
lamda-z
Lamda
Radial Position Across Membrane (microns)
x 10^4
λz=.743

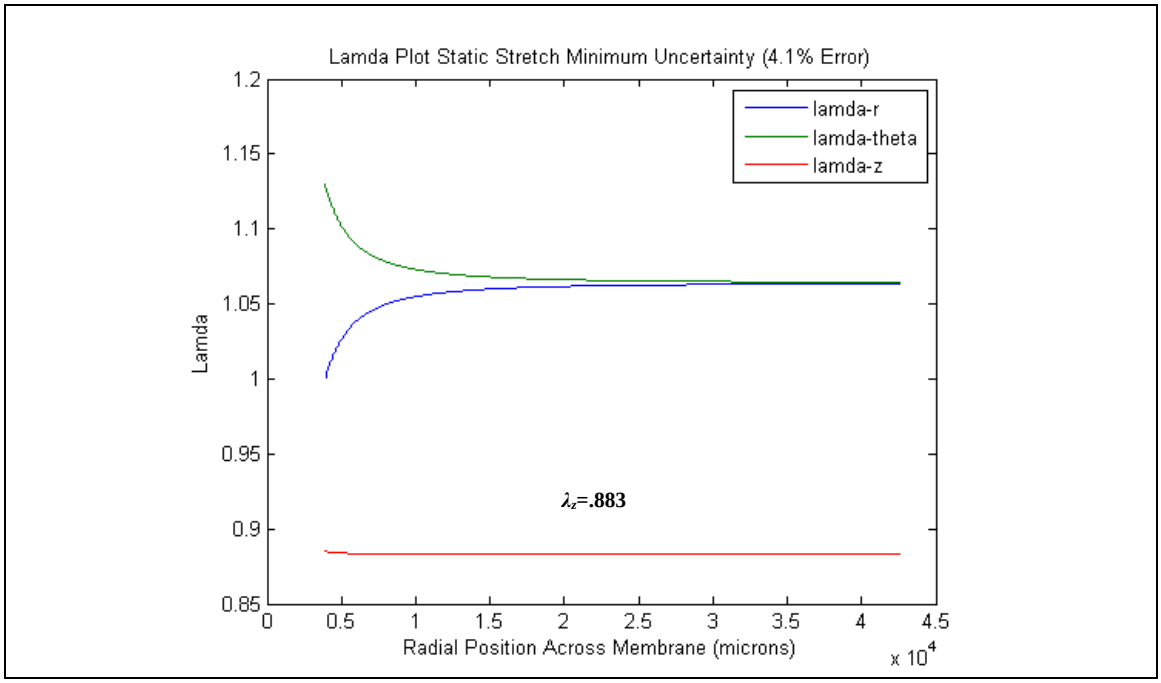
Lamda Plot Static Stretch Minimum Uncertainty (4.1% Error)
lamda-r
lamda-theta
lamda-z
Lamda
Radial Position Across Membrane (microns)
x 10^4
λz=.883

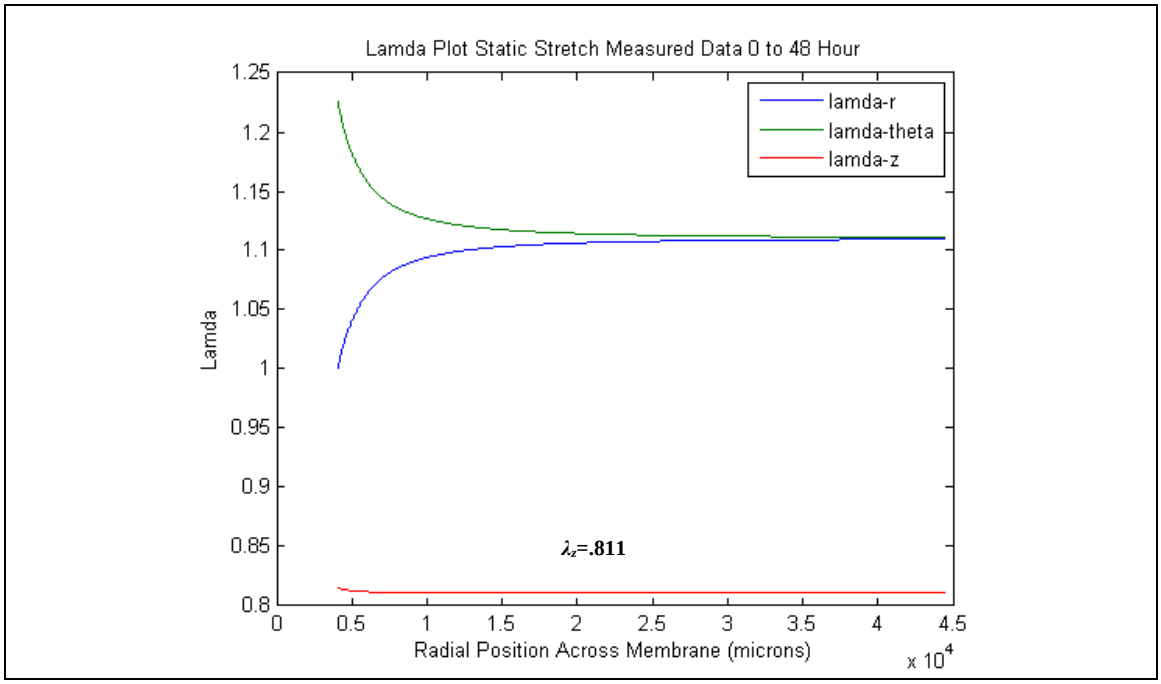
Lamda Plot Static Stretch Measured Data 0 to 48 Hour
lamda-r
lamda-theta
lamda-z
Lamda
Radial Position Across Membrane (microns)
x 10^4
λz=.811

Dynamic Stretch

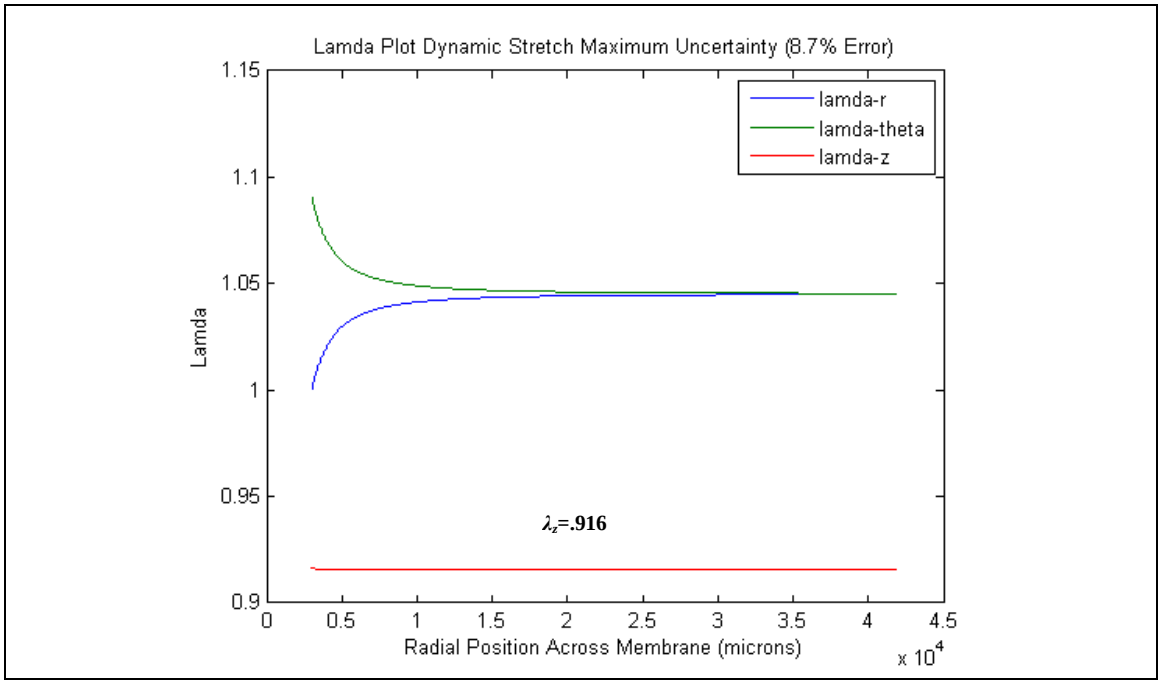

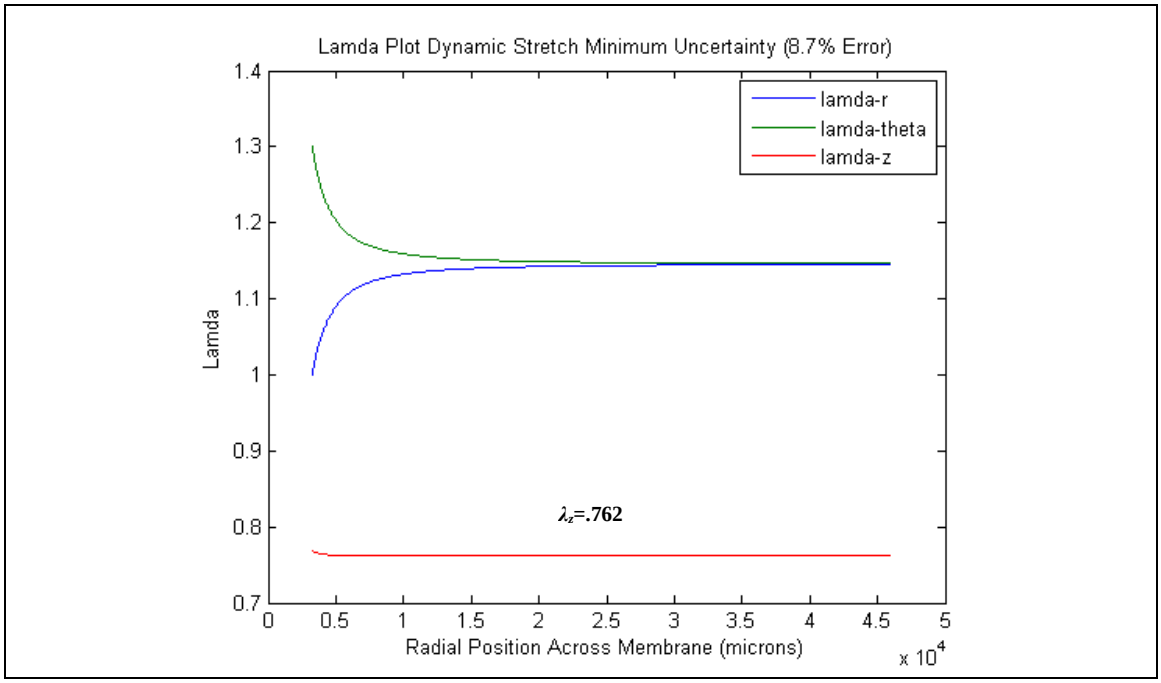
Lamda Plot Dynamic Stretch Minimum Uncertainty (8.7% Error)
lamda-r
lamda-theta
lamda-z
Lamda
Radial Position Across Membrane (microns)
x 10^4
λz=.762

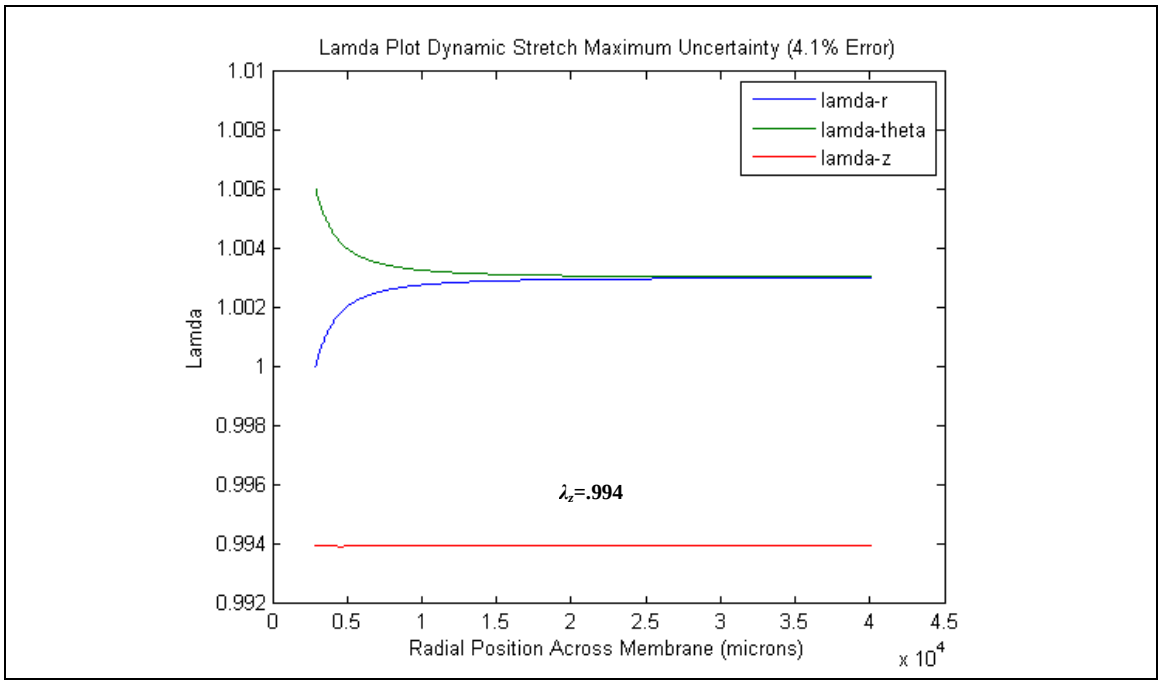
Lamda Plot Dynamic Stretch Maximum Uncertainty (4.1% Error)
lamda-r
lamda-theta
lamda-z
Lamda
Radial Position Across Membrane (microns)
x 10^4
λz=.994

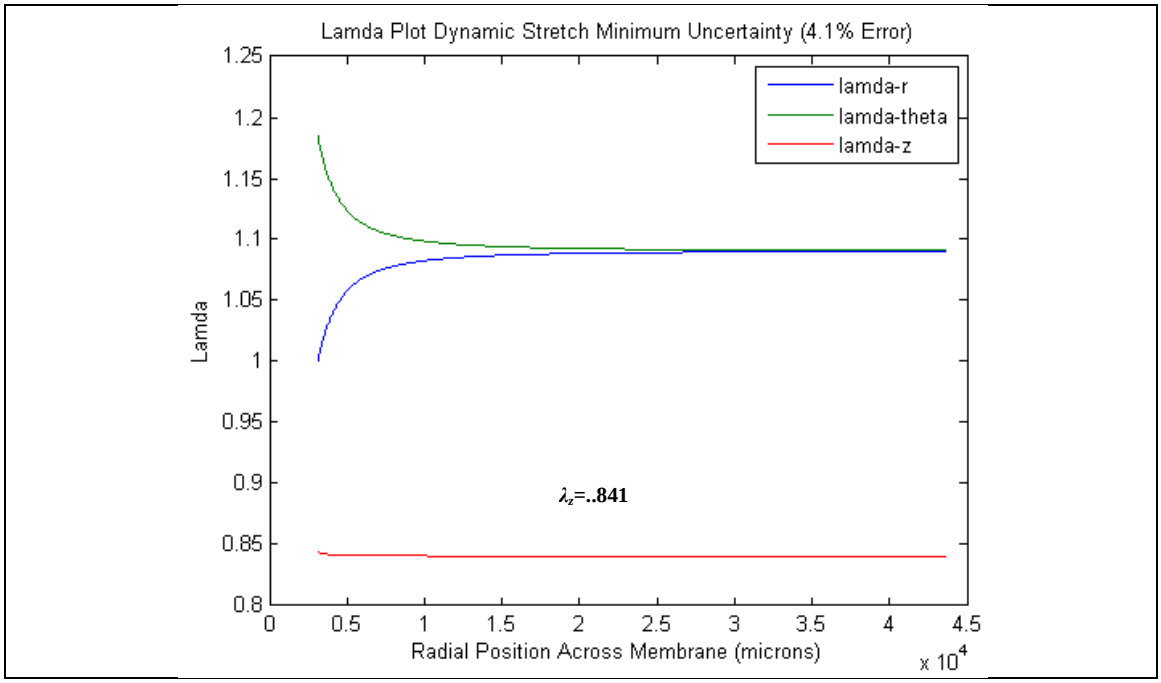
Lamda Plot Dynamic Stretch Minimum Uncertainty (4.1% Error)
lamda-r
lamda-theta
lamda-z
Lamda
Radial Position Across Membrane (microns)
x 10^4
λz=..841

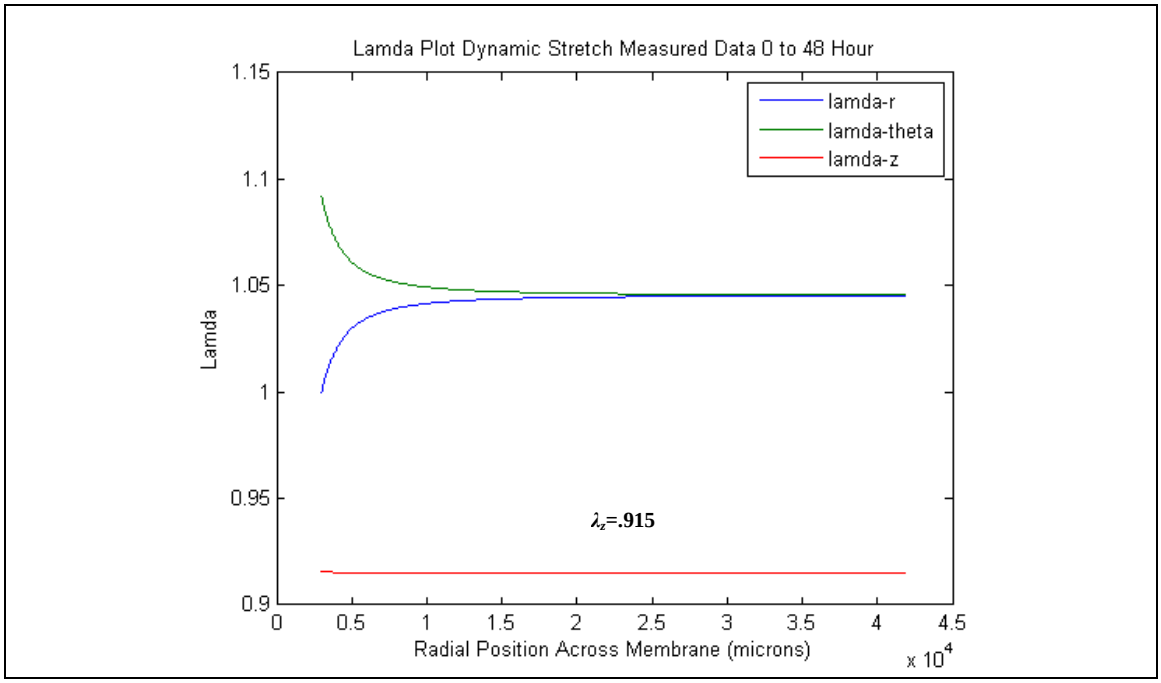
Lamda Plot Dynamic Stretch Measured Data 0 to 48 Hour
lamda-r
lamda-theta
lamda-z
Lamda
Radial Position Across Membrane (microns)
x 10^4
λz=.915

VITA

Name:	Shiva Yazdani-Beioky
Address:	Biomedical Engineering, 337 Zachry Engineering Center 3120 TAMU College Station, TX 77843-3120
Email Address:	shiva.yazdani@gmail.com
Education:	B.S., Biomedical Engineering, Texas A&M University, 2004 M.S., Biomedical Engineering, Texas A&M University, 2010